Performance of Nonlinear Mechanical, Resonant-Shunted Piezoelectric, and Electronic Vibration Absorbers for Multi-Degree-of-Freedom Structures

by

Gregory S. Agnes

Dissertation submitted to the faculty of the
Virginia Polytechnic Institute and State University
in partial fulfillment of the requirements for the degree of

DOCTOR OF PHILOSOPHY

in

Engineering Mechanics

Daniel J. Inman, Chairman
Ali H. Nayfeh
Scott Hendricks
Raymond Plaut
Ronald D. Kriz

Keywords: Nonlinear Dynamics, Vibration Absorbers, Smart Structures

Performance of Nonlinear Mechanical, Resonant-Shunted Piezoelectric, and Electronic Vibration Absorbers for Multi-Degree-of-Freedom Structures

Gregory S. Agnes

(ABSTRACT)

Linear vibration absorbers are a valuable tool used to suppress vibrations due to harmonic excitation in structural systems. Limited evaluation of the performance of nonlinear vibration absorbers for nonlinear structures exists in the current literature. The state of the art is extended in this work to vibration absorbers in their three major physical implementations: the mechanical vibration absorber, the inductive-resistive shunted piezoelectric vibration absorber, and the electronic vibration absorber (also denoted a positive position feedback controller). A single, consistent, physically similar model capable of examining the response of all three devices is developed.

The performance of vibration absorbers attached to single-degree-of-freedom structures is next examined for performance, robustness, and stability. Perturbation techniques and numerical analysis combine to yield insight into the tuning of nonlinear vibration absorbers for both linear and nonlinear structures. The results both clarify and validate the existing literature on mechanical vibration absorbers. Several new results, including an analytical expression for the suppression region's location and bandwidth and requirements for its robust performance, are derived.

Nonlinear multiple-degree-of-freedom structures are next evaluated. The theory of Nonlinear Normal Modes is extended to include consideration of modal damping, excitation, and small linear coupling, allowing estimation of vibration absorber performance. The dynamics of the N+1-degree-of-freedom system reduce to those of a two-degree-of-freedom system on a four-dimensional nonlinear modal manifold, thereby simplifying the analysis. Quantitative agreement is shown to require a higher order model which is recommended for future investigation.

Finally, experimental investigation on both single and multi-degree-of-freedom systems is performed since few experiments on this topic are reported in the literature. The experimental results qualitatively verify the analytical models derived in this work. The dissertation concludes with a discussion of future work which remains to allow nonlinear vibration absorbers, in all three physical implementations, to enter the engineer's toolbox.

Sponsorship provided by the USAF Institute of Technology, Civilian Institute Program.

Dedication

I dedicate this dissertation to my wife, Susan, and daughter, Courtney, whose love and support made it possible.

Acknowledgements

I wish to first and foremost acknowledge my wife, Susan. Its the second graduate degree we've struggled through together and although as we've laughed aplenty and cried a little these last three years I couldn't have finished without your love and support. Thank you.

My daughter, Courtney, was all of 8 weeks old when we moved to Blacksburg three years ago. I thank her for her understanding when Daddy had to work and for the joy she brought me when I needed a break. I'm glad you enjoyed helping in the lab.

Next, I would like to thank Dr. Inman, my advisor for these last three years. On short notice, I asked him if he would take me as a student and although I never had him for a class, his advice both on the research and professional matters was invaluable. I hope both our personal friendship and professional relationship will continue to grow over the years.

To the members of my committee, Drs. Nayfeh, Hendricks, Plaut, and Kriz I extend my gratitude for their suggestions and discussions. To Dr. Nayfeh for his help with all things nonlinear or perturbed and to Dr. Kriz for his help securing computing resources. Special thanks to Dr. Plaut for his careful review of the text. Thank you.

This dissertation would not be complete without the assistance of my friends and coworkers in the Mechanical Systems Lab. Thanks to Mauro, Dino, Clay, Eric, Debbie, Jens, and Marca for their discussions and assistance with classwork and research over the past three years. A special thanks to Eric, Liz, Maggie, and Ollie Austin for putting me up for the last month while I was homeless. Thanks also to John, Randy, and Dr. Chen of the Nonlinear Dynamics group for their insightful discussions.

Finally, I would like to thank my parents, teachers and mentors who, over the years, provided me with the opportunity to learn and instilled the discipline needed to reach today.

This work was supported by the Air Force Institute of Technology, Civilian Institution Program. Thanks to my various program managers especially Capt. James Ulman for their guidance and excellent support. Thanks also to VTAF whose officers and enlisted staff provided administrative support while I was stationed here.

Gregory S. Agnes

Contents

List of Figures

List of Tables

Chapter 1

Introduction

Suppression of vibration is increasingly demanded by modern structures. The drive to produce higher performance, lower cost structures and machines has resulted in reduced structural weight and hence increased compliance. Nowhere has this trend been more evident than the aerospace industry where the demand for smaller, lighter, cheaper aircraft and spacecraft systems drives the acquisition effort. The demand for performance exists in the face of ever harsher environments with increased disturbance levels. Meanwhile, the need for cleaner, more maintainable systems reduces the number of connectors, joints, wires, and other "dirty" components which contribute to structural damping. Modern systems thus face higher disturbances with lower damping and increased compliance, resulting in larger and often nonlinear vibrations. To achieve performance goals, the designer must address the suppression of nonlinear vibrations.

1.1 Review of the Vibration Suppression Literature

Techniques used to reduce structural vibrations can be classified with two criteria. First, one can either modify existing modes or add additional modes to the system. Secondly, the technique can be either active or passive. A technique is passive if it requires no external energy; otherwise, it is active. Differentiating between adding modes or altering existing

modes results in an important distinction in the response of the modified system. This is not well recognized in the literature or in practice and can lead to valuable insight into the design and implementation of vibration suppression systems. The purpose of this section is to review the relevant literature within this framework, motivating the subsequent research.

1.1.1 Modal Modification

Passive modal modification is perhaps the simplest and most commonly used technique. To reduce the vibrations, the mode shapes and modal parameters are altered until acceptable performance is achieved. For instance, if the rotation frequency of machinery is known to lie within a certain bandwidth, the support structure is designed such that no resonant frequencies lie within that bandwidth. Another example of passive modal modification is the use of passive damping treatments such as constrained layer damping treatments [1] or the addition of dashpot dampers to a structure. These modify the modal damping of various structural modes and reduce the vibration of the system. The performance of passive modal modification can be assessed for linear systems using techniques found in most vibration texts [2, 3]. First, the governing equations are transformed using modal analysis into a set of uncoupled single degree of freedom modal equations, assuming proportional damping. The response of each mode is then determined and compared to design criteria. Structural modifications can then be designed and the structure reanalyzed.

Nonlinearity complicates this approach since structural modes can respond to excitation far away from their resonant frequencies. For example:

> "von Karman observed that certain parts of an airplane can be violently excited by an engine running at an angular speed much larger than their natural frequencies, and Lefschetz described a commercial aircraft in which the propellers induced a subharmonic vibration in the wings which in turn induced a subharmonic vibration in the rudder. The oscillations were violent enough to cause tragic consequences." [4]

Nonlinear systems can also exhibit jump phenomena and either quasiperiodic or chaotic responses to harmonic disturbance. The effect of changes in various parameters can be examined to a limited extent using perturbation techniques for either weak nonlinearities or small motions. Nayfeh and Mook [4] discuss such techniques, but their applications are mostly limited to single-degree-of-freedom systems. Multiple-degree-of-freedom structures are treated, but not in a modal manner, thus limiting the analysis to systems with a limited number of degrees of freedom.

The concept of modal behavior for nonlinear systems was introduced by Rosenberg [5–7]. According to his definition, a nonlinear normal mode of a discrete conservative system must satisfy three conditions [8, 9]:

i. The masses execute periodic motions (not necessarily harmonic).

ii. The masses pass through static equilibrium simultaneously.

iii. Displacement of one mass uniquely defines the displacements of all masses.

These criteria are analogous to the synchronous motion criteria of linear normal modes. However, the nonlinear normal modes are also classified as similar (the relation of criterion three is linear) or non-similar (the relation is nonlinear) in contrast to linear normal modes which always have linear relationships represented by the mode shape. The number of nonlinear normal modes of a system under this definition is at least equal to the number of degrees of freedom, but can be greater.

Shaw and Pierre [10, 11] present an alternative definition of nonlinear normal modes, defined for both conservative and dissipative systems. Their definition is made in the phase space and the nonlinear normal modes are as follows [8]:

i. Motions (not necessarily periodic) exist on invariant manifolds of the system which are tangent to the linear normal modes at the equilibrium points.

ii. Motions pass through stable equilibrium.

iii. Displacement of one mass uniquely defines the displacements of all masses.

Thus the first criterion ensures there are exactly as many nonlinear normal modes as there are linear normal modes for infinitesimal nonlinearity or system energy. Again, both similar and nonsimilar modes are possible. This concept was later broadened by Slater and Inman [12] who removed the second constraint. This allows nonlinear normal modes to be the counterpart of linear complex modes for systems which are nonmodally damped. Such modes are designated nonequal phase. Using the invariant manifold concept, nonlinear normal modes can be used to define a nonlinear coordinate transformation from the physical to the modal system [11, 12]. In the modal space, however, nonlinear couplings between the modes can exist, but in the absence of internal resonance, are higher order effects near modal resonance. Thus, nonlinear normal modes can be used to examine the modal response of a system, and the results can be used to design passive modal modifications to the structure in a manner similar to linear normal modes.

The solution for nonlinear normal modes (as defined by Shaw and Pierre) can be performed using a number of techniques [8]. The original Real-Variable Invariant-Manifold method [10], while conceptually significant, is difficult to implement for large systems, especially in the presence of internal resonance. It can be simplified by solving the linear eigenvalue problem and transforming the equations to modal space. Two methods proposed in [13] are easier to implement: the Complex-Variable Invariant-Manifold approach and the Method of Multiple Scales. Solution of the manifold dynamics for any of these methods is limited to small nonlinearities except for special cases.

Active modal modification usually involves feedback control using measurements at one or more points on the structure. Through feedback control, the modal parameters of the closed loop system can be altered. For linear systems, the use of collocated velocity feedback to provide increased structural damping is an example. For multi-degree-of-freedom systems, any static gain feedback methodology such as eigenstructure assignment or LQG control also simply modifies the eigenstructure (modal structure) of the system. Many powerful techniques have been developed for linear systems control design. One of the sim-

plest theoretical methods is modal control which determines changes in the modal dynamics required and then uses the inverse modal transform to determine the physical controller. Perfect modal observability and controllability are required to implement this approach.

For nonlinear systems, Slater [12, 14] extended the approach of Shaw and Pierre [11] to include forcing and sensing. Thus nonlinear controllers could be designed in the nonlinear modal coordinate space and then transformed into physical coordinates. In a similar manner, individual modes could be linearized, creating a modal form of feedback linearization control. In contrast to linear theory, nonlinear theory lacks the tools for optimal design, requiring a trial and error approach. Whether active or passive modal modification is employed, the result is a physical structure with an improved modal structure capable of satisfying performance requirements.

1.1.2 Modal Addition

When modal modification is impractical, additional degrees of freedom can be placed into the structure in such a manner that vibration of critical components is reduced. Usually these new degrees of freedom will undergo large motions, absorbing the energy of the disturbance. For example, vibration isolation is often achieved by placing a soft spring in the energy transmission path. If a hard mount is replaced by a soft spring, a new degree of freedom is added to the structure. (If an existing flexible mount is modified, this would be modal modification instead.) This spring will undergo large deflection, but isolates the critical system components from the disturbance. Both passive and active vibration isolation are possible (see Sciulli [15] for a recent review of vibration isolation for both single and multiple degree of freedom systems). Nonlinear effects can be used to improve vibration isolation particularly the concept of mode localization [9].

When it is not possible to isolate a system from disturbances, vibration absorbers use modal addition to passively attenuate the response of a structure to external excitations. The mechanical vibration absorber was first introduced at the turn of the century. The theory of the classical device may be found in many standard vibrations textbooks. See for

instance den Hartog [16] or Inman [2]. In brief, a single-degree-of-freedom system is inertially coupled to a structure with its resonance tuned near that of the primary structure, creating a one-to-one frequency relationship. Properly tuned, the device can reduce the response of a structure to a narrowband harmonic excitation or, by adding damping to the absorber, to a broadband excitation.

A recent review of the theory and application of the linear vibration absorber [17] notes the mass and stroke length design limitations imposed by practical applications. Geometric considerations can limit the stroke length (the amount of travel) of the added mass. Since the mass added to a system must often be minimized, the tradeoff between mass and stroke is a crucial design constraint. Given a fixed mass and stroke length, an absorber is efficient for only a narrow range of driving force and frequency variations. Consequently, active and/or adaptive feedback control is topical [17, 18]. Using active control to minimize the response of the system, smaller absorber stroke lengths can be achieved, albeit with increased system complexity.

One solution to these limitations is the piezoelectric vibration absorber formed by coupling a resonant electrical shunt between the electrodes of piezoelectric materials attached or embedded in the structure. Tuning the shunt near a structural mode causes mechanical energy to be transformed into electrical energy and dissipated by the resistive element in the shunt in a manner analogous to a damped mechanical vibration absorber. Forward [19] experimentally demonstrated the use of both resistive and resonant electrical shunts. Hagood and Von Flotow [20] later presented an analytical model. Other researchers [21–23] have extended this device providing multimode and self- tuning shunts. Incorporation of a simultaneous active and passive signal is also possible [24].

The piezoelectric vibration absorber solves the stroke length problem by providing an unobtrusive energy dissipation mechanism, but creates new design challenges. The large inductances required to tune the electrical resonance are unreasonable for passive components. Consequently, active inductors are synthesized using op- amps making piezoelectric vibration absorbers semiactive (or powered) devices. A second design challenge presented

by the piezoelectric vibration absorber is the structural properties of available piezoelectric materials. Since piezoelectric materials transform strain energy into electrical energy, they must be located in areas of high strain energy to function efficiently. Since their structural properties are inferior to traditional load carrying materials, this poses a design challenge: maximize strain energy in the piezoelectric material while maintaining structural integrity. A final concern for the designers is the nonlinear behavior of piezoceramics [25]. To date, no study could be found on the effects of small nonlinearities on the performance of piezoelectric vibration absorbers.

Results have, however, been reported on nonlinear (mechanical) vibration absorbers. Early work [26–28] considered a linear system with a nonlinear absorber and neglected damping entirely. Most commonly, a nonlinear spring is used in place of the linear spring when designing the absorber. In 1952, Roberson [26] reported that a broadening of the suppression bandwidth was possible, and that the zero response frequency (design operational frequency in most cases) changed with force level and nonlinearity. References [27, 28] came to similar conclusions with slightly different systems. Miller [29] presented a nonlinear design using pneumatic springs, while Hunt and Nissen [30] used Belleville washers and reported that a broadening of the suppression bandwidth is possible. Several authors [31–33] have applied optimization methods to absorber design, but considered system damping of ten percent or more. This is unrealistic for many applications. Each pointed to bandwidth improvements and several claimed higher harmonic behavior improved the design.

However, Shaw [34] warned of the presence of quasiperiodic responses near the tuning frequency. Such motions were present in numerical simulations of lightly damped linear systems with nonlinear absorbers. These responses were also confirmed analytically in [35, 36]. Rice and McCraith [35] used the method of harmonic balance to numerically investigate the response of a linear system with a nonlinear absorber to narrowband excitation. Natsiavas [36] considered the case of the nonlinear system with a nonlinear absorber and demonstrated the adverse effects of system nonlinearity on absorber performance. Note that limited experimental work has been reported.

Alternately, the motion of the structure can serve as a parametric excitation to a nonlinear absorber [37]. Oueini, *et al.* [38] have experimentally implemented a similar system using nonlinear feedback control with piezoelectric actuators. This approach will not be considered in this work. Thus there appeared to be both some promise and some peril in using nonlinear mechanical vibration absorbers. The effect of nonlinearity on the response of the piezoelectric vibration absorber is currently unknown.

Active modal modification has also been pursued. For a linear system, any dynamic compensator designed via H_∞ , μ-synthesis, or other modern control algorithms uses a combination of modal modification and modal addition, but physical intuition into the inner workings of the control schemes is limited since they are designed for generic first order systems of the form $\dot{x} = Ax$ instead of second order dynamic systems.

In contrast, the Positive Position Feedback (PPF) algorithm developed by Goh and Caughey [39] and implemented by Fanson and Caughey [40, 41] uses the second order form, allowing better physical insight to vibration control by active modal addition. In this algorithm, a position signal is compensated by a second order filter for feedback control. For linear systems, the PPF controller is stable even in the presence of unmodelled actuator dynamics, unlike the often used direct velocity feedback (which is a form of modal modification). Baz, *et al.*, later combined PPF with Independent Modal Space Control [42, 43] to design independent second order feedback compensators for individual modes. Caughey later noted that positive position feedback was a generalization of the mechanical vibration absorber [44]. For this reason, PPF control can be denoted an electronic vibration absorber. Other significant contributions to the PPF literature include the work of Dosch [45], who derived stability conditions and applied PPF to an eight-ribbed space antenna. Many other numerical and experimental implementations of the PPF control scheme may be found in the literature. No reports on the influence of nonlinearity on the performance of PPF controllers could be found.

1.2 Objectives

The focus of this work will be on vibration suppression for nonlinear multi-degree-of-freedom discrete structures via vibration absorbers. The detailed objectives are as follows:

- Demonstrate the equivalence, to first-order nonlinear effects, of the mechanical vibration absorber, the piezoelectric vibration absorber, and positive position feedback.
- Utilize perturbation methods to find the general nonlinear response of the aforementioned systems.
- Develop design guidelines for tuning the linear and nonlinear parameters for vibration absorbers for nonlinear single-degree-of-freedom systems.
- Demonstrate the use of nonlinear normal modes to allow modal design of absorbers for N-degree-of-freedom nonlinear structures using these guidelines.
- Qualitatively verify the models through experimental investigations for both single and multiple degree-of-freedom systems.

Analytical, numerical, and experimental techniques will be used to demonstrate the performance of nonlinear absorbers for a variety of nonlinear systems.

1.3 Overview

To achieve the objectives presented in the previous section, nonlinear models for the mechanical, shunted piezoelectric and electronic (PPF) vibration absorbers are derived in Chapter 2. By proper choice of states and nondimensional parameters, these systems all reduce to a single set of identical nonlinear differential equations (to first order nonlinear effects) while maintaining consistent physical variables.

Chapter 3 is devoted to examining both the linear and nonlinear response of the unified model. Since there are many control parameters, a limited set of cases will be investigated: linear system/linear absorber (LSLA), nonlinear (cubic) system/ linear absorber

(NSLA) and linear system/nonlinear (cubic) absorber (LSNA). From the work cited above, quasiperiodic responses can result from the nonlinearities in the LSNA system. It will be shown analytically that they can also occur in the NSLA. Finally, a fourth system, nonlinear (cubic) system/nonlinear (cubic) absorber (NSNA), will be investigated. Tuning is accomplished by observing the effects of linear and nonlinear parameters from the previous three systems. Criteria for judging controller performance will also be addressed. Both numerical and analytical (perturbation) methods will be used to calculate the responses.

Once a design methodology for a single-degree-of-freedom structure has been established, N-degree-of-freedom discrete systems will be discussed in Chapter 4. The equations of motion will be placed into modal form using nonlinear normal modes, and an absorber designed for one of the modes. The procedure followed will be similar to Slater's, however dynamic compensation instead of static compensation will be used. Since the example of Shaw and Pierre [10] of a two-degree-of-freedom system has been used often in the literature as a benchmark problem, it will be used to illustrate the methodology for absorber design.

Experimental investigations will be used to verify the analytical and numerical analysis of the response of the single-degree-of-freedom system with a vibration absorber using an analog computer. These will be conducted for various combinations of parameters. Then the two-degree-of-freedom system of Shaw and Pierre will be similarly investigated. Finally, a vibration absorber will be implemented using nonlinear PPF on a beam to further verify the utility of the models in an experimental application.

The proposed work will meet the objectives outlined above. A single nonlinear model for a single-degree-of-freedom mechanical, piezoelectric, or electronic vibration absorber will be found. This model will be used to verify past research efforts for LSNA systems as well as providing novel investigation into NSLA and NSNA systems. The model will preserve physical intuition, unlike some past investigations. The discussion of nonlinear effects for the piezoelectric vibration absorbers is new to the literature and was recently published [46]. The derivation of a tuning strategy for the design of nonlinear absorbers will overcome shortcomings noted by previous research and provide some analytic results for design. The

state of the art will be further advanced by the use of nonlinear normal modes to design vibration absorbers for N-dof systems. Finally, experimental verification of the predicted quasiperiodic response will be accomplished. In summation, using nonlinear normal modes, a design methodology for second-order, nonlinear vibration absorbers will be developed to suppress the vibration of multiple- degree-of-freedom structures and machines which can be implemented in mechanical, shunted piezoelectric, or electronic (PPF) form.

Chapter 2

Single-Degree-of-Freedom System Models

System models for the mechanical vibration absorber, the piezoelectric vibration absorber, and the positive position feedback algorithm may be found in the various references cited. However, the common form of the models results in three different sets of equations. By careful selection of nondimensional parameters, and by enforcing the requirement that the degrees of freedom represent the motion of the base system and the stroke length of the absorber, a common set of equations can be formed.

2.1 Mechanical Vibration Absorber

A model of a single-degree-of-freedom structure with a mechanical vibration absorber is shown in Figure 2.1. A single-degree-of-freedom system of mass, M, stiffness, K, and viscous damping, C, is driven by an external excitation, F, and responds with displacement, X. By adding an absorber (with mass, stiffness, damping and displacement denoted M_a, K_a, C_a and X_a, respectively) the displacement of the original system can be reduced. The displacement of the absorber is also referred to as the stroke length in the literature.

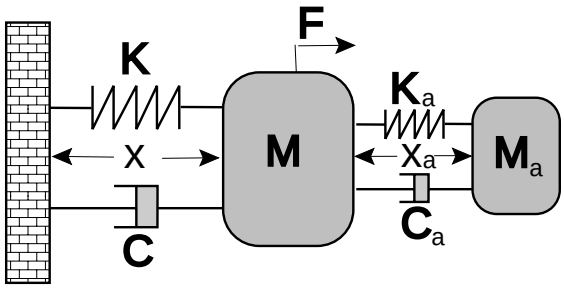

Figure 2.1: The mechanical vibration absorber.

Nonlinear stiffness of both the system and absorber will be considered of the form:

$$K(X) = KX + \Gamma X^3 \tag{2.1a}$$

$$K_a(X_a) = K_a X_a + \Gamma_a X_a^3 \tag{2.1b}$$

From Newton's law, the equations of motion for the mechanical vibration absorber are then:

$$M\ddot{X} + C\dot{X} - C_a\dot{X}_a + KX - K_aX_a = F - \Gamma X^3 + \Gamma_a X_a^3 \tag{2.2a}$$

$$M_a\ddot{X} + M_a\ddot{X}_a + C_a\dot{X}_a + K_aX_a = -\Gamma_a X_a^3 \tag{2.2b}$$

where the overdot denotes total differentiation with respect to time, T. The term $\ddot{X}$ is then solved for in Equation (2.2a) and substituted for in Equation (2.2b), thereby diagonalizing the mass matrix. The ratio M_a/M is denoted α^2 and the equations of motion are thus

$$M\ddot{X} + C\dot{X} - C_a\dot{X}_a + KX - K_aX_a = F - \Gamma X^3 + \Gamma_a X_a^3 \tag{2.3a}$$

$$\begin{aligned} M_a\ddot{X}_a - \alpha^2 C\dot{X} + (1+\alpha^2)C_a\dot{X}_a - \alpha^2 KX + (1+\alpha^2)K_aX_a \\ = -\alpha^2 F - (1+\alpha^2)\Gamma_a X_a^3 + \alpha^2\Gamma X^3 \end{aligned} \tag{2.3b}$$

Next, the time, T, is nondimensionalized using the system natural frequency, $\omega = \sqrt{K/M}$ and the differentiation is now with respect to nondimensional time, t. Both Equation (2.3a) and Equation (2.3b) are then divided by K and a similarity transformation,

$$\left\{ \begin{array}{c} x \\ x_a \end{array} \right\} = \left[\begin{array}{cc} 1 & 0 \\ 0 & \alpha \end{array} \right] \left\{ \begin{array}{c} X \\ X_a \end{array} \right\} \tag{2.4}$$

is performed. The non-dimensional equations of motion for the nonlinear mechanical vibration absorber are

$$\ddot{x} + 2\zeta\dot{x} - 2\alpha(1+\delta)\zeta_a\dot{x_a} + x - \alpha(1+\delta)^2 x_a = f - \gamma x^3 + \alpha\gamma_a(1+\delta)^2 x_a^3 \tag{2.5a}$$

$$\begin{aligned}\ddot{x_a} - 2\alpha\zeta\dot{x} + 2(1+\delta)(1+\alpha^2)\zeta_a\dot{x_a} - \alpha x + (1+\alpha^2)(1+\delta)^2 x_a \\ = -\alpha f - (1+\alpha^2)(1+\delta)^2\gamma_a x_a^3 + \alpha\gamma x^3\end{aligned} \tag{2.5b}$$

where the following nondimensional parameters are introduced:

$$\begin{array}{lll} \frac{C}{M} = 2\zeta\omega & \frac{K}{M} = \omega^2 & \frac{F}{K} = f \\ \frac{\Gamma}{M} = \omega^2\gamma & \frac{C_a}{M_a} = 2\zeta_a\omega_a & \frac{K_a}{M_a} = \omega_a^2 \\ \frac{M_a}{M} = \alpha^2 & \frac{\Gamma_a}{M_a} = \omega_a^2\alpha^2\gamma_a & \frac{K_a}{K} = \alpha^2(1+\delta)^2 \end{array} \tag{2.6}$$

Analysis for the case of small nonlinearity can be performed using perturbation techniques. For practical applications, the mass of the absorber is often constrained such that α is a small parameter. Next, introduce a small parameter ϵ as a bookkeeping parameter, and scale the coefficients as in Table 2.1. Using this scaling and including terms to order ϵ, the

Table 2.1: Scaling for the Mechanical Vibration Absorber

Variable	ζ	ζ_a	α	σ_a	γ	γ_a	f
Scaling	ϵ	ϵ	ϵ	ϵ	ϵ	ϵ	ϵ

non-dimensional equations of motion for the mechanical vibration absorber are found to be

$$\ddot{x} + 2\epsilon\zeta\dot{x} + x - \epsilon\alpha x_a = \epsilon f - \epsilon\gamma x^3 \tag{2.7a}$$

$$\ddot{x_a} + 2\epsilon\zeta_a\dot{x_a} - \epsilon\alpha x + (1 + 2\epsilon\delta)x_a = -\epsilon\gamma_a x_a^3 \tag{2.7b}$$

In Equations (2.7a)-(2.7b), x represents the displacement of the mass and x_a is proportional to the relative displacement (or strokelength) of the absorber. These are the variables that the design criteria are based upon, and thus the formulation is suited for design. If instead, the absolute displacement of the absorber or the linear modes are used (as in many references) the resulting solutions must be transformed before application, and

physical insight is hampered. Additionally, the form of the nonlinearity is simpler with this formulation. In the next two sections, the equations of motion for the LR-shunted piezoelectric vibration absorber and for Positive Position feedback control will be derived in an equivalent form.

2.2 LR-Shunted Piezoelectric Vibration Absorber

A modal model of a structure containing piezoelectric materials can be idealized as shown in Figure 2.2. The base system consists of a mass constrained by a structural spring, K_S, and a piezoelectric spring, K_P, arranged in parallel. The displacement of the structure, X, is to be minimized by a tuned resonant circuit with charge Q on the piezoelectric electrodes. The system thus has two degrees of freedom or 4 states.

The linear constitutive equations for piezoelectric materials, simplified for one-dimensional transverse actuation, are [47]:

$$\left\{ \begin{array}{c} E_3 \\ T_{11} \end{array} \right\} = \left[\begin{array}{cc} \frac{1}{\epsilon^S} & -h_{31} \\ -h_{31} & c^D \end{array} \right] \left\{ \begin{array}{c} D_3 \\ S_{11} \end{array} \right\} \tag{2.8}$$

Here, the standard IEEE notation is used (i.e. E is electric field, T is stress, D is electrical displacement, S is strain, ϵ^S is electrical permittivity, h is the piezoelectric coupling constant, and c^D is the elastic modulus). Assuming a standard patch-like application, these equations may be rewritten in terms of variables more convenient for this study. The equations for the piezoelectric spring are thus:

$$\left\{ \begin{array}{c} V \\ F \end{array} \right\} = \left[\begin{array}{cc} \frac{1}{C_P^S} & -H \\ -H & K_P^D \end{array} \right] \left\{ \begin{array}{c} Q \\ X \end{array} \right\} \tag{2.9}$$

where V is the voltage of the piezoelectric electrode, F is the force of the spring, Q is the charge flowing into the patch electrodes, X is the displacement of the spring, C_P^S is the capacitance of the patch under constant strain, K_P^D is the stiffness of the piezoelectric spring under constant charge, and H is the electro-mechanical coupling parameter. Note

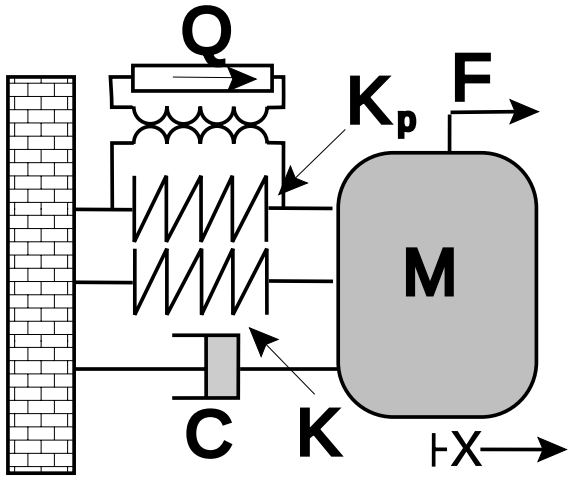

Figure 2.2: The piezoelectric vibration absorber.

that coefficients in these equations can be modified for more complicated geometries, but would assume a similar form.

Placing an inductive-resistive (LR) shunt across the electrodes of the piezoelectric spring, the equations of motion for the mass in Figure 2.2 are:

$$M\ddot{X} + C\dot{X} + K_P^D(X,Q) + K_S(X) - HQ = F(t) \tag{2.10a}$$

$$L\ddot{Q} + R\dot{Q} + \frac{1}{C_P^S}Q - HX = G(X,Q) \tag{2.10b}$$

Here, L is the shunt inductance; R, the shunt resistance; M, the structural mass; and $F(t)$ is an external disturbance. The function, $G(X,Q)$, of the displacement and charge represents the nonlinearity in the shunt, $K_P^D(X,Q)$ represents the nonlinear piezoelectric stiffness, and $K_S(X)$ is the nonlinear structural spring stiffness. The form of the nonlinearity is assumed as

$$G(X,Q) = \Gamma_a Q^3 \qquad K_P^D(X,Q) = K_P^D X \qquad K_S(X) = K_S X + \Gamma X^3 \tag{2.11}$$

These equations must be nondimensionalized to facilitate the scaling required by the per-

turbation analysis of the next chapter. The nondimensional equations of motion are:

$$\ddot{x} + 2\zeta\dot{x} + x - (1+\delta)\alpha_1 q = f(T) - \gamma x^3 \tag{2.12a}$$

$$\ddot{q} + r(1+\delta)^2\dot{q} + (1+\delta)^2 q - (1+\delta)\alpha_1 x = -\gamma_a q^3 \tag{2.12b}$$

Here, the nondimensional quantities used in Equations (2.12a,2.12b) are defined as follows:

$$\begin{aligned} \omega^D &= \sqrt{\tfrac{K_S+K_P^D}{M}} & \omega_e &= \tfrac{1}{\sqrt{LC_P^S}} \\ \alpha_1^2 = \tilde{K}_{31}^2 &= \tfrac{K^E}{K+K^E}\tfrac{k_{31}^2}{1-k_{31}^2} & \delta &= \tfrac{\omega_e}{\omega^D} - 1 \\ t &= T\omega^D & r &= RC_P^S\omega^D \\ q &= \sqrt{L}Q & x &= \sqrt{M}X \end{aligned} \tag{2.13}$$

Differentiation in Equations (2.12a,2.12b) is with respect to nondimensional time, t. Note that Equations (2.12a,2.12b,2.13) differ from those in the related literature [20, 22–24] since the constant charge (shorted) stiffness, K^D, of the piezoelectric spring is used in place of the usual constant voltage stiffness, K^E, for the nondimensional equations used in previous research because it simplifies the analysis. Also note, that the coupling term is the generalized electro-mechanical coupling coefficient which can be determined experimentally, as a modal quantity [22].

Next, introduce a small parameter ϵ as a bookkeeping parameter, and scale the coefficients as in Table 2.2. Using this scaling and including terms to order ϵ, the non-dimensional

Table 2.2: Scaling for the LR-Shunted Piezoelectric Vibration Absorber

Variable	ζ	r	α_1	δ	γ	γ_a	f
Scaling	ϵ	ϵ	ϵ	ϵ	ϵ	ϵ	ϵ

equations of motion for the Mechanical Vibration Absorber are found to be

$$\ddot{x} + 2\epsilon\zeta\dot{x} + x - \epsilon\alpha_1 q = \epsilon f(t) - \epsilon\gamma x^3 \tag{2.14a}$$

$$\ddot{q} + 2\epsilon r\dot{q} + (1+2\epsilon\delta)q - \epsilon\alpha_1 x = \gamma_a q^3 \tag{2.14b}$$

These equations are of the same form as those for the mechanical vibration absorber presented in Section 2.1. The coordinates x and q are proportional to the system displacement and shunt charge, respectively, thus maintaining physical significance. In the next section, the equations of motion for a single-degree-of-freedom structure under positive position feedback control will be derived of this same form.

2.3 Positive Position Feedback

A modal model of a structure containing an actuator can be idealized as shown in Figure 2.3. A single degree of freedom with mass, M, viscous damping, C, and stiffness, K, is driven by an external force, F. The displacement, X, of M is controlled by an actuation force, U. Considering a nonlinear stiffness, the equations of motion are

$$M\ddot{X} + C\dot{X} + K(X)X = F + U \tag{2.15}$$

The nonlinear stiffness is of the form

$$K(X) \quad = \quad KX + \Gamma X^3 \tag{2.16}$$

Introducing the usual non-dimensional parameters

$$\begin{array}{lll} \frac{C}{M} = 2\zeta\omega & \frac{K}{M} = \omega^2 & \\ \frac{f}{M} = \omega^2 f & \frac{U}{M} = \omega^2 u & \frac{\Gamma}{M} = \omega^2\gamma \end{array} \tag{2.17}$$

Equation (2.15) can be nondimensionalized. For positive position feedback, U is defined

$$U = Gx_c \tag{2.18a}$$

$$\ddot{x_c} + 2\zeta_c\omega_c\dot{x_c} + \omega_c^2 x_c + \gamma_c x_c^3 = Hx \tag{2.18b}$$

Substituting Equation (2.18a) and Equation (2.17) into Equation (2.15), defining $t = \omega T$, and dividing the resulting equations by ω^2:

$$\ddot{x} + 2\zeta\dot{x} + x - g(1+\delta)^2 x_c = f(t) - \gamma x^3 \tag{2.19a}$$

$$\ddot{x_c} + 2(1+\delta)\zeta_c\dot{x_c} + (1+\delta)^2 x_c - g(1+\delta)^2 x = -\gamma_c x_c^3 \tag{2.19b}$$

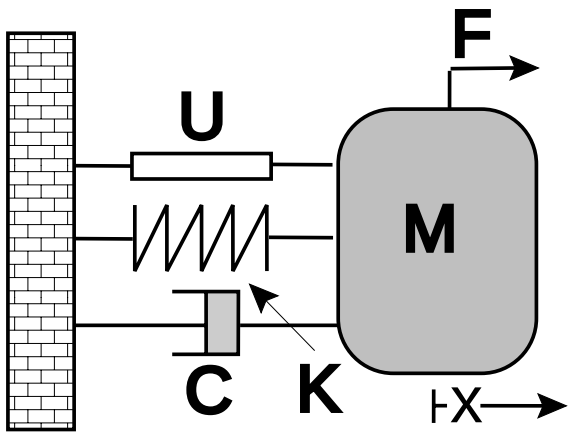

Figure 2.3: An Actuated Structure

The sensor and controller gains, H and G, have been set equal (as is conventional) and defined as $G = H = g\omega_c^2$. If nonsymmetric feedback is required, a transformation of the states, $\{x, x_c\}$ can be introduced, bringing the equations into this form. Interest in these equations is centered around primary resonance. Scaling of the equations for perturbation analysis is presented in Table 2.3 After scaling, the equations to order ϵ, where ϵ is a small

Table 2.3: Scaling for Positive Position Feedback

Variable	ζ	ζ_c	g	γ_c	γ	f
Scaling	ϵ	ϵ	ϵ	ϵ	ϵ	ϵ

bookkeeping parameter, are:

$$\ddot{x} + 2\epsilon\zeta\dot{x} + x - \epsilon g x_c = \epsilon f(t) - \epsilon\gamma x^3 \tag{2.20a}$$

$$\ddot{x_c} + 2\epsilon\zeta\dot{x_c} + (1 + 2\epsilon\delta)x_c - \epsilon g x = -\epsilon\gamma_c x_c^3 \tag{2.20b}$$

which are of the same form as those in the last two sections.

2.4 Unified Equation

Comparing Equation (2.7a) and Equation (2.7b) with Equation (2.12a) and Equation (2.12b) or Equation (2.20a) and Equation (2.20b) the nonlinear mechanical vibration absorber, piezoelectric vibration absorber, or positive position feedback control system can be modeled with a single set of equations:

$$\ddot{x_1} + 2\epsilon\zeta\dot{x_1} + x_1 - \epsilon\alpha_1 x_2 = \epsilon f(t) - \epsilon\alpha_3 x_1^3 \tag{2.21a}$$

$$\ddot{x_2} + 2\epsilon\zeta\dot{x_2} + (1 + 2\epsilon\delta_1)x_2 - \epsilon\alpha_1 x_1 = \epsilon\delta_3 x_2^3 \tag{2.21b}$$

The nondimensional parameters in the unified equations are defined in Table 2.4. Note that in each case, x_1 is proportional to the displacement of the system and x_2 is proportional to the "displacement" of the absorber. In the next chapter, the response of this equation will be determined using perturbation techniques.

Table 2.4: Unification of Nonlinear Vibration Absorbers.

System	MVA	PVA	PPF
x_1	X	$\sqrt{M}X$	X
x_2	X_a	$\sqrt{L}Q$	x_c
ζ_1	$\frac{C}{2\sqrt{KM}}$	$\frac{C}{2\sqrt{KM}}$	$\frac{C}{2\sqrt{KM}}$
ζ_2	$\frac{C_a}{2\sqrt{M_a K_a}}$	$\sqrt{\frac{R^2 C_P^S}{L}}$	ζ_c
α_1	$\sqrt{\frac{M_a}{M}}$	K_{ij}	$\frac{G}{\omega_c^2}$
α_3	$\frac{\Gamma}{K}$	$\frac{\Gamma}{MK}$	$\frac{\Gamma}{K}$
δ_1	$\sqrt{\frac{MK_a}{M_a K}} - 1$	$\sqrt{\frac{M}{KLC_P^S}} - 1$	$\sqrt{\frac{\omega_c^2 M}{K}} - 1$
δ_3	$\frac{M\Gamma_a}{M_a K_a}$	$\frac{M\Gamma_a}{KL^2}$	$\frac{M\Gamma_c}{K}$
f	$\frac{F}{K}$	$\frac{F}{\sqrt{KM}}$	$\frac{F}{\sqrt{KM}}$

Chapter 3

Performance of Vibration Absorbers for 1DOF Systems

Having derived the common model for the various vibration absorbers, their response must now be determined. For small nonlinearities, perturbation techniques are useful for determining the response. Herein, the method of multiple scales [48] is used to transform the system of two second order equations of motion into four first order modulation equations. Fixed points of the modulation equations represent periodic solutions of the system equations. Once the modulation equations are found, a series of systems is considered which are increasingly more difficult (i.e. they contain more nonlinear parameters). Since the modulation equations are in general a set of coupled nonlinear equations, numerical techniques, namely pseudo-arclength continuation methods are used to solve for the response. Since no available, robust, code existed, PSAL , a MATLAB® toolbox [49], was developed. An overview, with references, is found in Appendix A. The perturbation solutions are complemented by numerical time simulations to illustrate the effects of the various parameters. Many of the numerical results are also repeated by analog computer experiments which are detailed in Chapter 5.

The organization of the chapter is as follows. First, the modulation equations are

derived. Next, the influences of the various parameters are examined. First the linear parameters, then the nonlinear, are discussed. Finally, conclusions are drawn on the use of these results for design of nonlinear vibration absorbers.

3.1 Derivation of the Modulation Equations

The general system equations (2.21a)- (2.21b) describe the dynamics of the various vibration absorbers presented in the previous section. (It can be noted that positive position feedback with limited authority actuation as considered in the previous section can be regarded as an electronic vibration absorber.) Note the effects of nonlinearity, damping, excitation, and linear coupling have been brought together at $O(\epsilon)$. To determine the response, the method of multiple scales [48] was used. Thus we express nondimensional time, t, in its various scales

$$T_0 = t \qquad T_1 = \epsilon t \qquad T_2 = \epsilon^2 t \qquad \cdots \tag{3.1}$$

and thus by the chain rule find

$$D_t = D_0 + \epsilon D_1 + \cdots \tag{3.2a}$$

$$D_t^2 = D_0^2 + 2\epsilon D_0 D_1 + \epsilon^2 D_1^2 + \cdots \tag{3.2b}$$

where the operator D_x^n is the n^{th} derivative w.r.t. T_x. Expanding x_1 and x_2 in the small parameter ϵ,

$$x_1 = x_{10} + \epsilon x_{11} + O(\epsilon^2) \tag{3.3a}$$

$$x_2 = x_{20} + \epsilon x_{21} + O(\epsilon^2) \tag{3.3b}$$

and considering harmonic external forcing $f(t) = f\cos\Omega T_0$, the ordinary differential equations (2.21a-b) are replaced by partial (but solvable) differential equations of various orders in ϵ.

$O(1)$ Equations

$$D_0^2 x_{10} + x_{10} = 0 \tag{3.4a}$$

$$D_0^2 x_{20} + x_{20} = 0 \tag{3.4b}$$

$O(\epsilon)$ Equations

$$D_0^2 x_{11} + x_{11} = -2D_0 D_1 x_{10} - 2\zeta_1 D_0 x_{10} + \alpha_1 x_{20} - \alpha_3 x_{10}^3 + f\cos\Omega T_0 \tag{3.4c}$$

$$D_0^2 x_{21} + x_{21} = -2D_0 D_1 x_{20} - 2\zeta_1 D_0 x_{20} + \alpha x_{10} - \delta_3 x_{20}^3 \tag{3.4d}$$

Note that the sign of the nonlinear terms are such that hardening terms are positive. By solving the $O(1)$ equations, the following results:

$$x_{10} = A_1(T_1, ...)e^{iT_0} + cc \quad x_{20} = A_2(T_1, ...)e^{iT_0} + cc \tag{3.5}$$

where "cc" denotes the complex conjugate. By defining $\Omega = 1 + \epsilon\sigma$, the forced response near resonance can be investigated. Substituting these results into Equations (3.4c)-(3.4d), secular terms are identified leading to the following set of modulation equations:

$$2iA_1' = 2i\zeta_1 A_1 + \alpha_1 A_2 - 3\alpha_3 A_1^2 \bar{A}_1 + \frac{f}{2}e^{i\sigma T_1} \tag{3.6a}$$

$$2iA_2' = 2i\zeta_2 A_2 + \alpha_1 A_1 - 3\delta_3 A_2^2 \bar{A}_2 2\delta_1 A_2 \tag{3.6b}$$

The prime denotes differentiation w.r.t. T_1. These equations can then be solved by performing the "cartesian" substitution

$$A_x = (p_x - iq_x)e^{(i\sigma T_1)} \tag{3.7}$$

and separating the modulation equations into real and imaginary parts:

$$p_1' = -\sigma q_1 - \frac{\alpha_1}{2}q_2 - \zeta_1 p_1 + \frac{3}{8}\alpha_3(p_1^2 + q_1^2)q_1 \tag{3.8a}$$

$$q_1' = \sigma p_1 + \frac{\alpha_1}{2}p_2 - \zeta_1 q_1 - \frac{3}{8}\alpha_3(p_1^2 + q_1^2)p_1 + \frac{f}{2} \tag{3.8b}$$

$$p_2' = -(\sigma - \delta_1)q_2 - \frac{\alpha_1}{2}q_1 - \zeta_2 p_2 + \frac{3}{8}\delta_3(p_2^2 + q_2^2)q_2 \tag{3.8c}$$

$$q_2' = (\sigma - \delta_1)p_2 + \frac{\alpha_1}{2}p_1 - \zeta_2 q_2 - \frac{3}{8}\delta_3(p_2^2 + q_2^2)p_2 \tag{3.8d}$$

The fixed points of the resulting four- dimensional set of nonlinear equations can be computed using continuation methods.

3.2 The Linear Response

Before examining the nonlinear response, the linear response was first examined for two reasons. First, the linear solution could be checked against the perturbation solution (i.e. the solution of the modulation equations) thereby verifying the perturbation approach. Second, it allows a complete discussion of vibration absorbers to be presented in one reference. As noted in the literature review, the vibration absorber literature is spread over many sources with no definitive reference (even for the linear case).

3.2.1 Linear Tuning Parameters

Two design parameters exist for the classic vibration absorber: the linear coupling strength, α_1, and the tuning frequency, δ_1. For the undamped system, the modulation equations reduce to

$$\sigma p_1 + \frac{\alpha_1}{2} p_2 = \frac{f}{2} \tag{3.9a}$$

$$\frac{\alpha_1}{2} p_1 + (\sigma - \delta_1) p_2 = 0 \tag{3.9b}$$

since $q_1 = q_2 = 0$. Equations (3.9a)-(3.9b) can be solved for p_i, yielding:

$$p_1 = \frac{(\sigma - \delta_1) f}{2\sigma(\sigma - \delta_1) - \frac{\alpha_1^2}{2}} \tag{3.10a}$$

$$p_2 = \frac{-\alpha_1 f}{2\sigma(\sigma - \delta_1) - \frac{\alpha_1^2}{2}} \tag{3.10b}$$

Checking, if $\sigma = \delta_1$, $p_1 = 0$ and $p_2 = \frac{2f}{\alpha_1}$ which agrees with the linear results for vibration absorbers (found for example in [2]) to first order. In other words, if one uses the parameters defined in the last chapter and expands the complete linear solution in ϵ, the results are identical to $O(\epsilon)$.

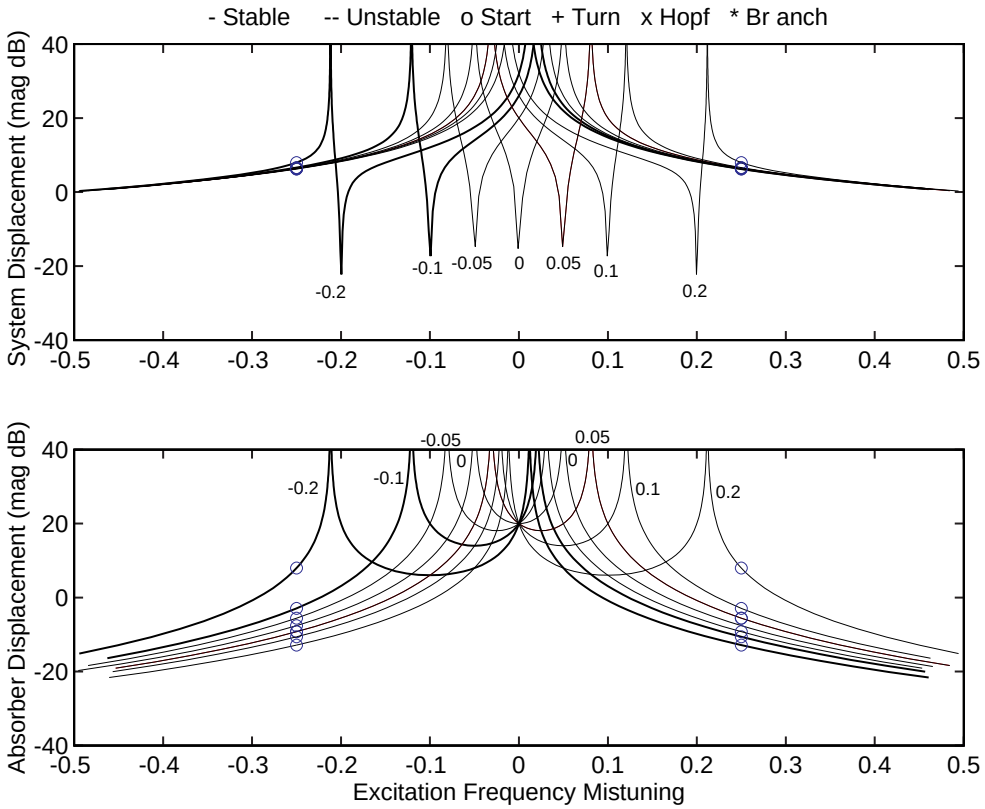

Figure 3.1: The LSLA response as δ_1 varies from -0.2 to 0.2 as indicated on the figure. System Parameters: $\zeta_1 = 0.001$, $\zeta_2 = 0$, $\alpha_1 = 0.1$, $f = 1.0$, $\alpha_3 = \delta_3 = 0$.

The linear system performance is thus perfect at $\sigma = \delta_1$ and rapidly declines as the excitation frequency moves away from the designed absorber frequency. This result is easily seen in Figure 3.1 which was computed using PSAL for very light damping of the main system. By varying δ_1, the absorber's effective range can be moved to the desired excitation frequency. The response of the system can be eliminated by the action of the absorber. However, since α_1 is a small parameter, large absorber response is required to do so.

Since α_1 is related to the absorber mass (or piezoelectric coupling or control gain) a tradeoff between the stroke of the absorber and the coupling, α_1, must be made. This is

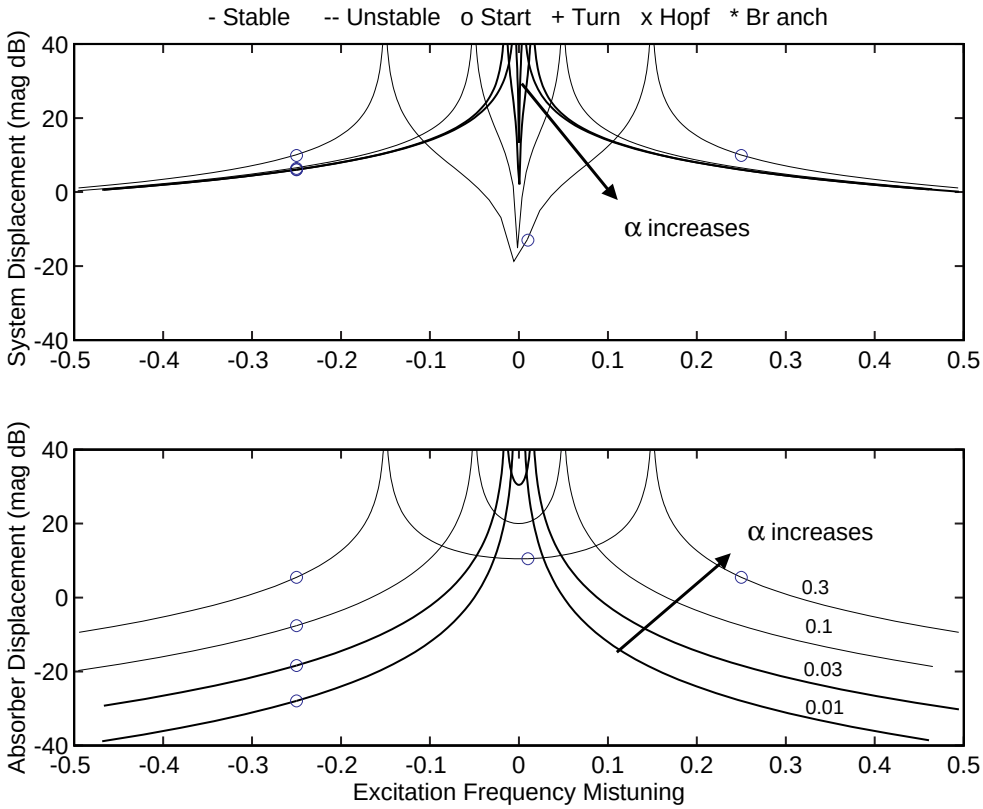

Figure 3.2: The LSLA response for various values of α_1 as indicated on the figure. System Parameters: $\zeta_1 = 0.001$, $\zeta_2 = 0$, $\delta_1 = 0$, $f = 1.0$, $\alpha_3 = \delta_3 = 0$.

clearly seen in Figure 3.2. Another benefit of increased α_1 is also apparent: the increase in suppression bandwidth.

The suppression bandwidth is usually defined as the frequency span over which the response of the system is less than the response of the system for a static load of equal magnitude. For linear transfer functions, this implies the response lies below zero dB. As seen in Figure 3.2 and Figure 3.1, the suppression bandwidth for a linear system increases with α_1, but is unaffected by δ_1. Mathematically, the suppression bandwidth is defined by $p_1 = \pm f$. Plugging this value into Equations (3.9a)-(3.9b), the in-phase (+) and out-of-phase (-) suppression bandwidth edges can be found. Substituting, a quadratic equation in

$\sigma^{\pm}$ can be solved by expansion in small parameters to yield:

$$\sigma^{+} = \delta - \frac{\alpha_1^2}{2} \tag{3.11a}$$

$$\sigma^{-} = \delta + \frac{\alpha_1^2}{2} \tag{3.11b}$$

The bandwidth is thus α_1^2, an ϵ^2 value. The larger α_1 is, the more robust the system is to tuning errors. In general, the largest feasible value of α_1 will yield the best results. This is not surprising, as more control power is usually associated with better performance. However, in practice, α_1 is constrained by other design considerations and hence a method for achieving larger bandwidths and lower absorber stroke-lengths is desirable. One method for doing so is the introduction of damping into the absorber.

3.2.2 The Influence of Damping

The damped vibration absorber is discussed at length in many texts [2, 50]. In the classic analysis, the system is treated as undamped with viscous damping in the absorber only. DenHartog [16, 50] provided the first analysis with damping. By varying the damping, the resonant response can be reduced at the expense of decreased narrowband vibration suppression, as seen in Figure 3.3. From this figure, the effect of absorber damping is to reduce the required stroke (especially at resonance) with reduced suppression bandwidth (frequency range) and depth (system response level). This classic tradeoff is well recognized in the literature [17]. As the damping is increased, the broadband response of the system approaches a minimum while the narrowband response increases. Thus, it is possible to divide vibration absorbers into two classes, the narrowband absorber which requires small vibration damping and the broadband absorber with larger damping. Given a fixed linear coupling α_1, narrowband problems are those in which the excitation lies between the two resonant peaks defined by the undamped system:

$$\sigma_{1,2} = \frac{1}{2}(\delta_1 + \sqrt{\alpha_1^2 + \delta_1^2}) + O(\epsilon)^2 \tag{3.12}$$

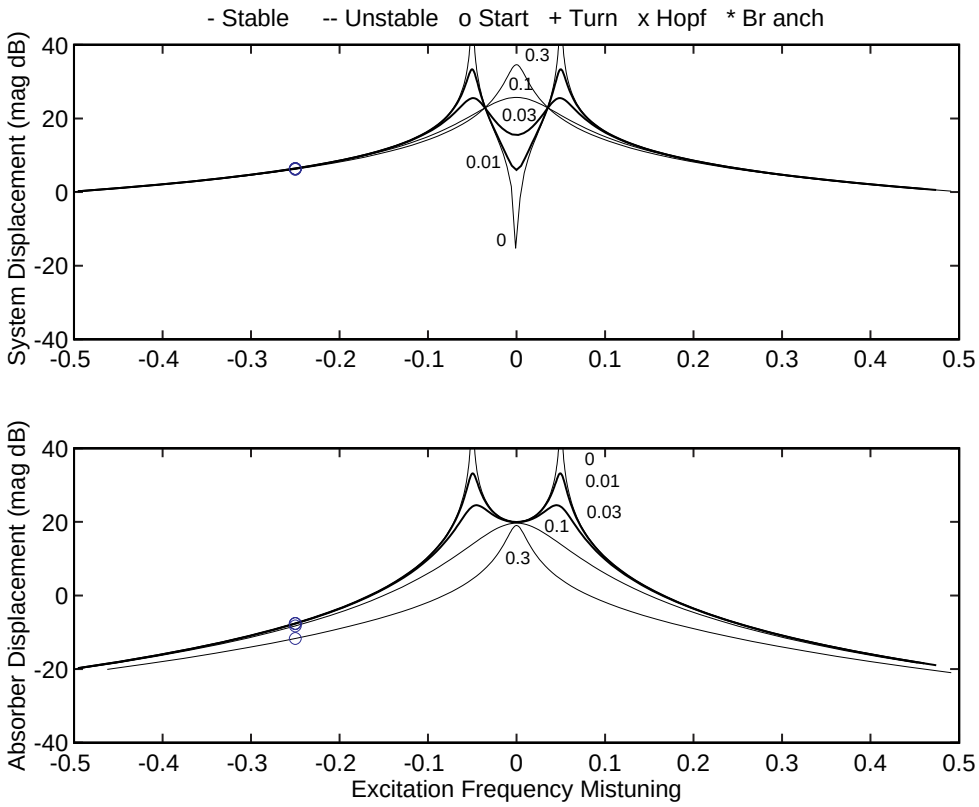

Figure 3.3: The LSLA response as absorber damping ζ_2 varies. $\zeta_2 = 0$, 0.001, 0.01, 0.03, 0.1, 0.3. System Parameters: $\zeta_1 = 0.001$, $\alpha_1 = 0.1$, $\delta_1 = 0$, $f = 1.0$, $\alpha_3 = \delta_3 = 0$.

The effect of damping on the vibration absorber is to reduce the required stroke-length at the cost of reduced suppression band. If the damping is too high, the suppression band is eliminated. Such a device is still useful for broadband applications, but, since the scope of this study is limited to narrowband disturbances, won't be discussed further.

A second source of damping is system damping which is less often treated in the literature. The response of the linear absorber as the damping of the system is varied is plotted in Figure 3.4. Compared with absorber damping, system damping has a much less pronounced effect on system response. Again, the resonant response is reduced, but without the large penalty in absorber performance. The depth of the notch is reduced, and the

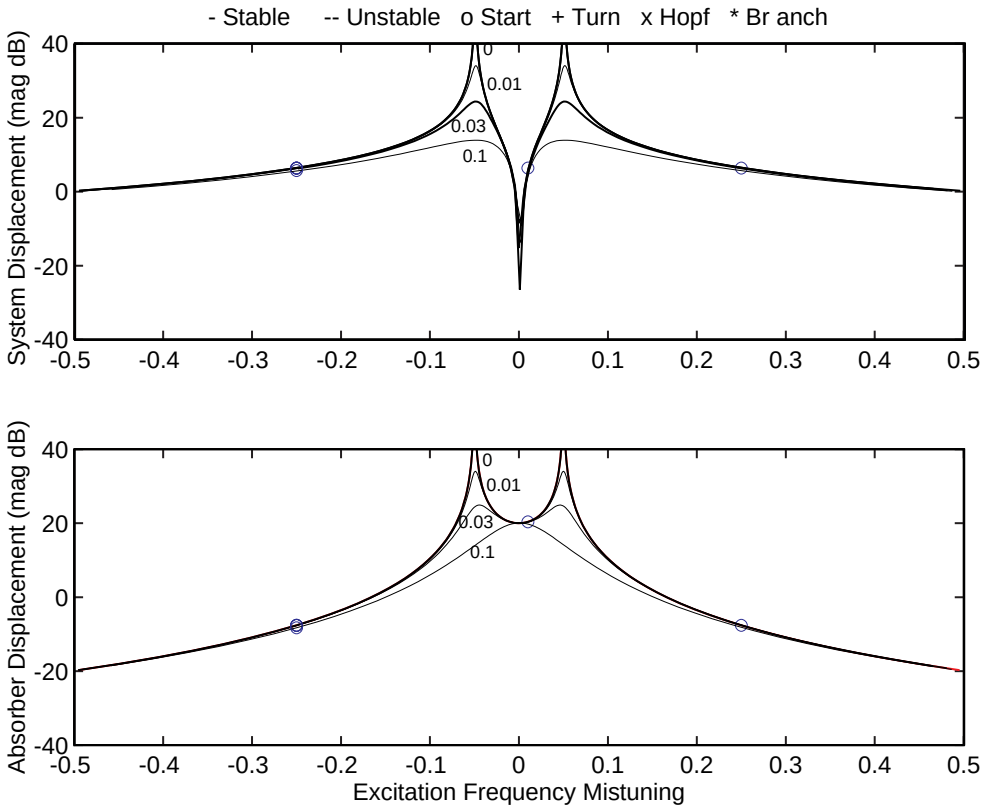

Figure 3.4: The LSLA response as system damping ζ_1 varies. $\zeta_1 = 0$, 0.001, 0.01, 0.03, 0.1, 0.3. System Parameters: $\zeta_2 = 0.001$, $\alpha_1 = 0.1$, $\delta_1 = 0$, $f = 1.0$, $\alpha_3 = \delta_3 = 0$.

bandwidth narrowed, but only slightly. System damping therefore has a beneficial effect of reducing resonant response with only slight tradeoff in narrowband suppression performance. Increasing the system damping can thus be beneficial without sacrificing absorber performance.

An absorber design methodology is still required which can expand the bandwidth without sacrificing absorber performance. Such a device was presented in 1952 by Roberson: the nonlinear vibration absorber.

3.3 Linear Structure, Nonlinear Absorber

The nonlinear absorber is formed by replacing the linear spring (or the electrical shunt circuit) with a nonlinear element. Cubic nonlinearities are considered herein to both limit the scope and because they are most often discussed in the literature. Quadratic plus cubic nonlinearities were considered in the initial study into the nonlinear piezoelectric vibration absorber [46]. The effect of the quadratic nonlinearity, which will be shown in the next section, was to soften the cubic nonlinearity in a manner similar to that reported in [4, 48]. The effect of a nonlinear absorber on a linear system will be illustrated with the example of [46].

3.3.1 Example: Nonlinear Piezoelectric Vibration Absorber

In this example, the response of a mass supported by a linear spring to harmonic input is considered. A piezoelectric spring is attached in parallel so a piezoelectric vibration absorber is formed by attaching an electrical shunt to its electrodes. Both quadratic and cubic nonlinearities in the electrical shunt are considered. These would correspond to nonlinear capacitance of the piezoceramic, or could be added to the shunt with electrical components, hoping to improve performance. Since our previous derivation considered only cubic nonlinearities, the derivation of the modulation equations for this example is presented first. Then numerical simulations of the performance are presented.

For a harmonic input of frequency Ω, the equations of motion are:

$$\ddot{q} + \delta^2 q = \delta\alpha_1 x - r\delta\dot{q} + \alpha_2 q^2 + \alpha_3 q^3 \tag{3.13a}$$

$$\ddot{x} + x = \delta\alpha_1 q + f\cos(\Omega T) \tag{3.13b}$$

A "perfect" tuning of the linear system ($\delta = 1$) is assumed throughout. According to the method of multiple scales, x, q and T are expanded in power series with ϵ, a small parameter, and take the form:

$$T_0 = t \qquad T_1 = \epsilon t \qquad T_2 = \epsilon^2 t \qquad \cdots \tag{3.14a}$$

$$x = x_0 + \epsilon x_1 + \epsilon^2 x_2 + ... \tag{3.14b}$$

$$q = q_0 + \epsilon q_1 + \epsilon^2 q_2 + ... \tag{3.14c}$$

The coupled system of ordinary differential equations thus becomes a system of partial differential equations in the different time scales $(T_0, T_1, \dots)$. Absorber performance is analyzed near primary resonance, so $\Omega = 1 + \epsilon^2\sigma$. At this point, the nonlinearities must be scaled. The piezoelectric coupling between the mechanical deformation and the electrical charge is typically small in piezoelectric vibration absorbers, on the order of 0.1. The effects of damping, excitation, nonlinear stiffness, and coupling effects must all occur at the same order. Quadratic nonlinearities influence the equations as a feedback term and must therefore be of lower order than cubic to achieve this balance. Hence the quadradic term is scaled to be first order in ϵ while the damping, excitation, cubic stiffness, and coupling terms are second order in ϵ. Substituting Equation (3.14b) into Equation (3.13b) and including the proper scaling:

$$\begin{aligned}
&(D_0 + \epsilon D_1 + ...)^2(q_0 + \epsilon q_1 + ...) + \delta^2(q_0 + \epsilon q_1 + ...) = \\
&\quad \epsilon^2\delta\alpha_1(x_0 + \epsilon x_1 + ...) - \epsilon^2 r\delta(D_0 + \epsilon D_1 + ...)(q_0 + \epsilon q_1 + ...) + \\
&\quad \epsilon\alpha_2(q_0 + \epsilon q_1 + ...)^2 + \epsilon^2\alpha_3(q_0 + \epsilon q_1 + ...)^3
\end{aligned} \tag{3.15a}$$

$$\begin{aligned}
&(D_0 + \epsilon D_1 + ...)^2(x_0 + \epsilon x_1 + ...) + (x_0 + \epsilon x_1 + ...) = \\
&\quad \epsilon^2\delta\alpha_1(q_0 + \epsilon q_1 + ...) + \epsilon^2 f\cos(\Omega T)
\end{aligned} \tag{3.15b}$$

Expanding, and gathering like powers of ϵ, yields the following set of equations:
Order 0

$$D_0^2 q_0 + q_0 = 0 \tag{3.16a}$$

$$D_0^2 x_0 + x_0 = 0 \tag{3.16b}$$

Order 1

$$D_0^2 q_1 + q_1 = -\alpha_2 q_0^2 - 2D_0 D_1 q_0 \tag{3.16c}$$

$$D_0^2 x_1 + x_1 = -2D_0 D_1 x_0 \tag{3.16d}$$

Order 2

$$D_0^2 q_2 + q_2 = -2D_0D_1q_1 - 2D_0D_2q_0 - D_1^2q_0 - rD_0q_0 - 2\alpha_2 q_0 q_1 - \alpha_3 q_0^3 + \alpha_1 x_0 \quad (3.16e)$$

$$D_0^2 x_2 + x_2 = -2D_0D_1x_1 - 2D_0D_2x_0 - D_1^2x_0 - D_1^2x_0 + \alpha_1 q_0 + f\cos(T_0 + \sigma T_2) \quad (3.16f)$$

Note that $D_i x$ is the derivative of x with respect to T_i. Solving these equations yields a solution of the form

$$q = q_0 = A_1(T_1, T_2)e^{iT_0} \qquad x = x_0 = A_2(T_1, T_2)e^{iT_0} \quad (3.17)$$

where the coefficients must satisfy the following differential equation (first order in T_2) to eliminate secular terms:

$$2iA_1' - \alpha_1 A_2 - \left(3\alpha_3 - \frac{10}{3}\alpha_2^2\right) A_1^2\overline{A}_1 + irA_1 = 0 \quad (3.18a)$$

$$2iA_2' - \alpha_1 A_1 - \frac{1}{2}fe^{i\sigma T_2} = 0 \quad (3.18b)$$

Note $i = \sqrt{-1}$ and the over bar indicates the complex conjugate. Solutions are more readily obtained if we use the polar form and thus define

$$\begin{aligned} A_1 &= a_1 e^{i\beta_1}, \quad \gamma_1 = \sigma T_2 - \beta_1 \\ A_2 &= a_2 e^{i\beta_2}, \quad \gamma_2 = \sigma T_2 - \beta_2 \\ \alpha_{NL} &= 3\alpha_3 - \tfrac{10}{3}\alpha_2^2 \end{aligned} \quad (3.19)$$

where a_1 and a_2 are the amplitudes of the nondimensional shunt charge and mass vibration, respectively. The result is four autonomous differential equations in four unknowns:

$$a_1' = -\frac{1}{2}ra_1 + \frac{1}{2}a_2\sin(\gamma_1 - \gamma_2) \quad (3.20a)$$

$$a_1\gamma_1' = \sigma a_1 - \frac{1}{8}\alpha_{NL}a_1^3 - \frac{1}{2}a_2\cos(\gamma_1 - \gamma_2) \quad (3.20b)$$

$$a_2' = \frac{1}{2}f\sin(\gamma_2) - \frac{1}{2}a_2\sin(\gamma_1 - \gamma_2) \quad (3.20c)$$

$$a_2\gamma_2' = \sigma a_2 - \frac{1}{2}f\cos(\gamma_2) - \frac{1}{2}a_2\cos(\gamma_1 - \gamma_2) \quad (3.20d)$$

These form the modulation equations in polar form. The cartesian form presented in the previous section is more suitable for numerical analysis since it does not contain singularities if a_i passes through zero. Steady state solutions are obtained by setting the left hand

side of these equations to zero and solving the remaining algebraic equations for the unknowns. The amplitude of the mass vibration, a_2, may then be found in terms of a_1 using Equations (3.20a)-(3.20b):

$$a_2^2 = \frac{1}{\alpha_1^2}\left[\left(r^2 + 4\sigma^2\right)a_1^2 - \alpha_{NL}\sigma a_1^4 + \alpha_{NL}^2 a_1^6\right] \tag{3.21}$$

The frequency response equations can then be obtained by squaring and adding Equations (3.20c)-(3.20d), resulting in a third order equation in a_1^2. The resulting equation,

$$\frac{1}{4}\sigma^2\alpha_{NL}^2 a_1^6 + \sigma\alpha_{NL}\left(\alpha_1^2 - 4\sigma^2\right)a_1^4 + \left(4r^2\sigma^2 + \left(\alpha_1^2 - 4\sigma^2\right)\right)a_1^2 - \alpha_1^2 f^2 = 0 \tag{3.22}$$

can thus be solved for a_1, and the solution used in Equation (3.21) to find a_2, the amplitude of the primary mass vibration.

The frequency response Equation (3.22) can be solved using numerical techniques. The results duplicate those obtained in the next section, so instead the numerical integration of the system equations is presented. The system of equations was integrated numerically for a range of excitation levels and frequencies. Several sets of parameters were used. Some of these results are presented in Figures 3.5-3.9. The broadening of the suppression bandwidth and the presence of strong resonances are both visible in Figures 3.5 and 3.6. Both the linear, cubic and cubic-quadratic responses are plotted. The gray scale indicates the rms magnitude of the response. The rms response was calculated using 1000 seconds of data starting at 4000 seconds when the system had reached steady state. The presence of larger damping (Figure 3.6) still does not prevent the presence of strong resonances, even for small nonlinearities. Only light damping is within the scope of this work, but this result bears further study in subsequent investigations. Looking at time traces in Figures 3.7-3.9,the source of the resonances can be seen. As the excitation level is increased from 0.1 in Figure 3.7 to 0.3 in Figure 3.8, a bifurcation occurs and the response becomes quasiperiodic. As the excitation further increases to 0.7 (Figure 3.9) the response magnitude appears to be chaotic and increases drastically. The averaged pointwise dimension [51] was found to be approximately 2.5 (Figure 3.10), verifying the chaotic nature of this response. Fifteen

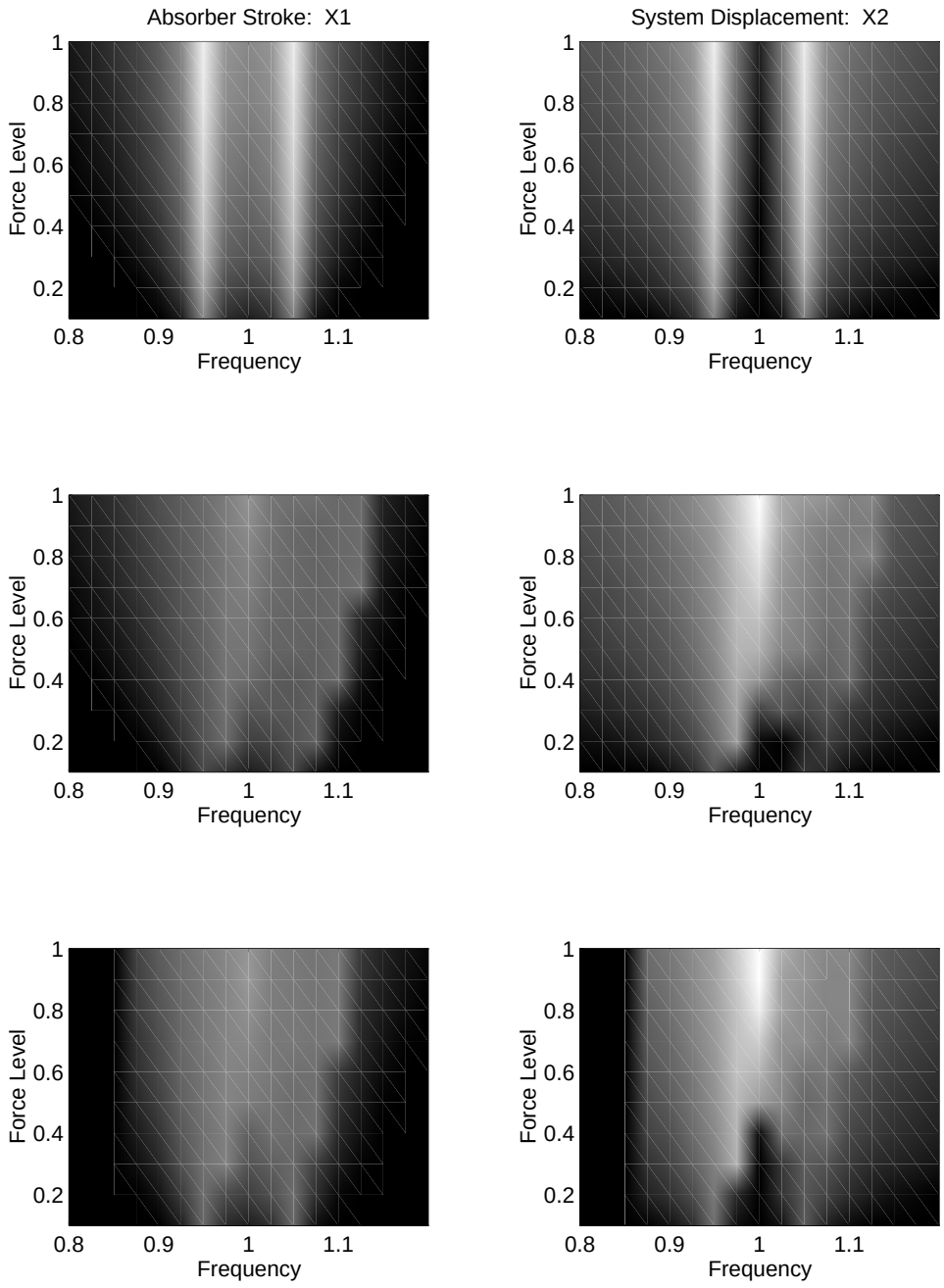

Figure 3.5: Displacement for linear, cubic and quadratic+cubic absorbers with low damping. These are plots of force vs frequency with the third parameter, rms displacement, visualized by shading. Response magnitudes vary from -10 dB (black) to 40 dB (white). Responses were calculated using ode45 in MATLAB® .

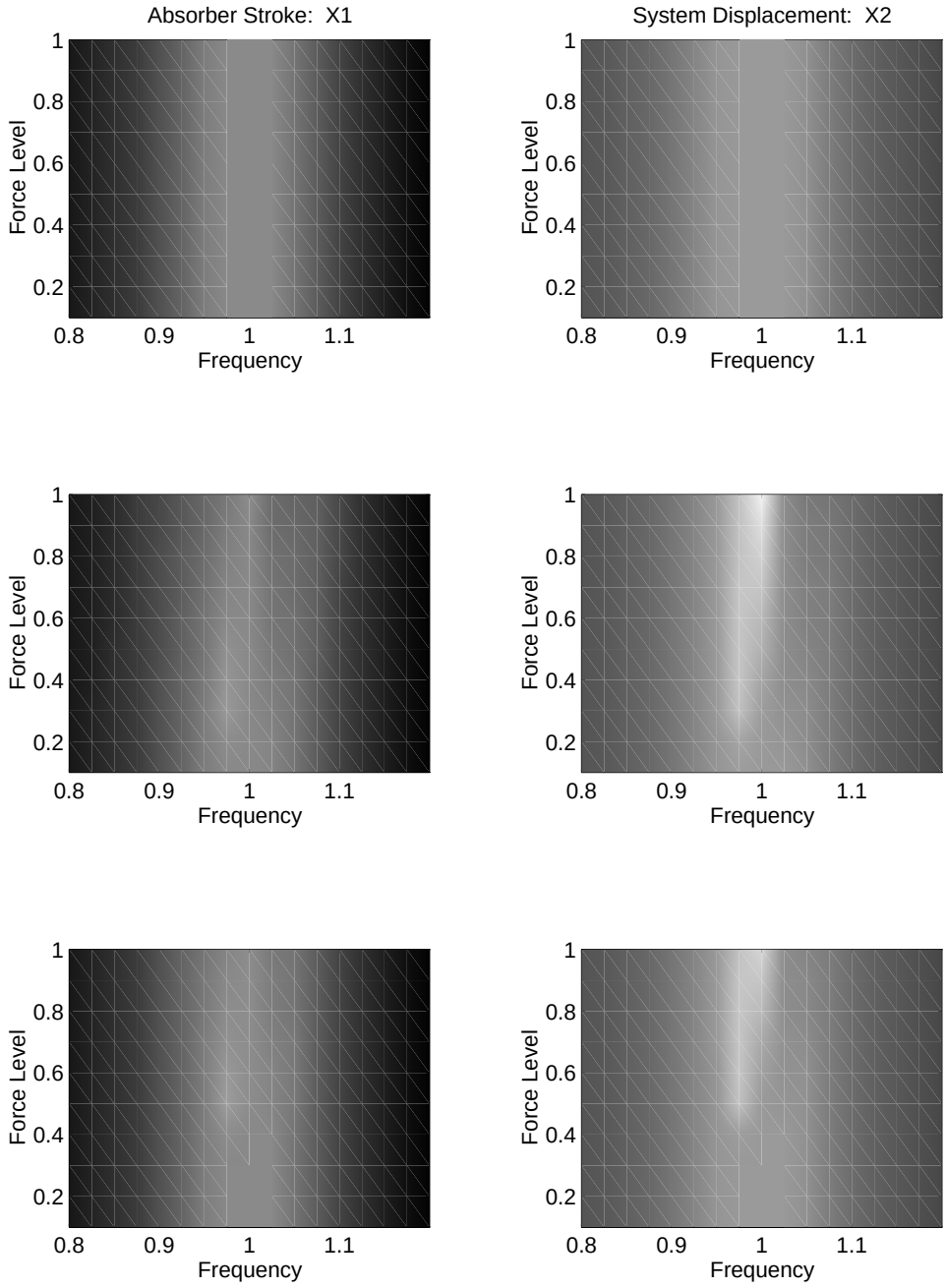

Figure 3.6: Displacement for linear, cubic and quadratic+cubic absorbers with higher damping. These are plots of force vs frequency with the third parameter,rms displacement, visualized by shading. Response magnitudes vary from -10 dB (black) to 40 dB (white). Responses were calculated using ode45 in MATLAB® .

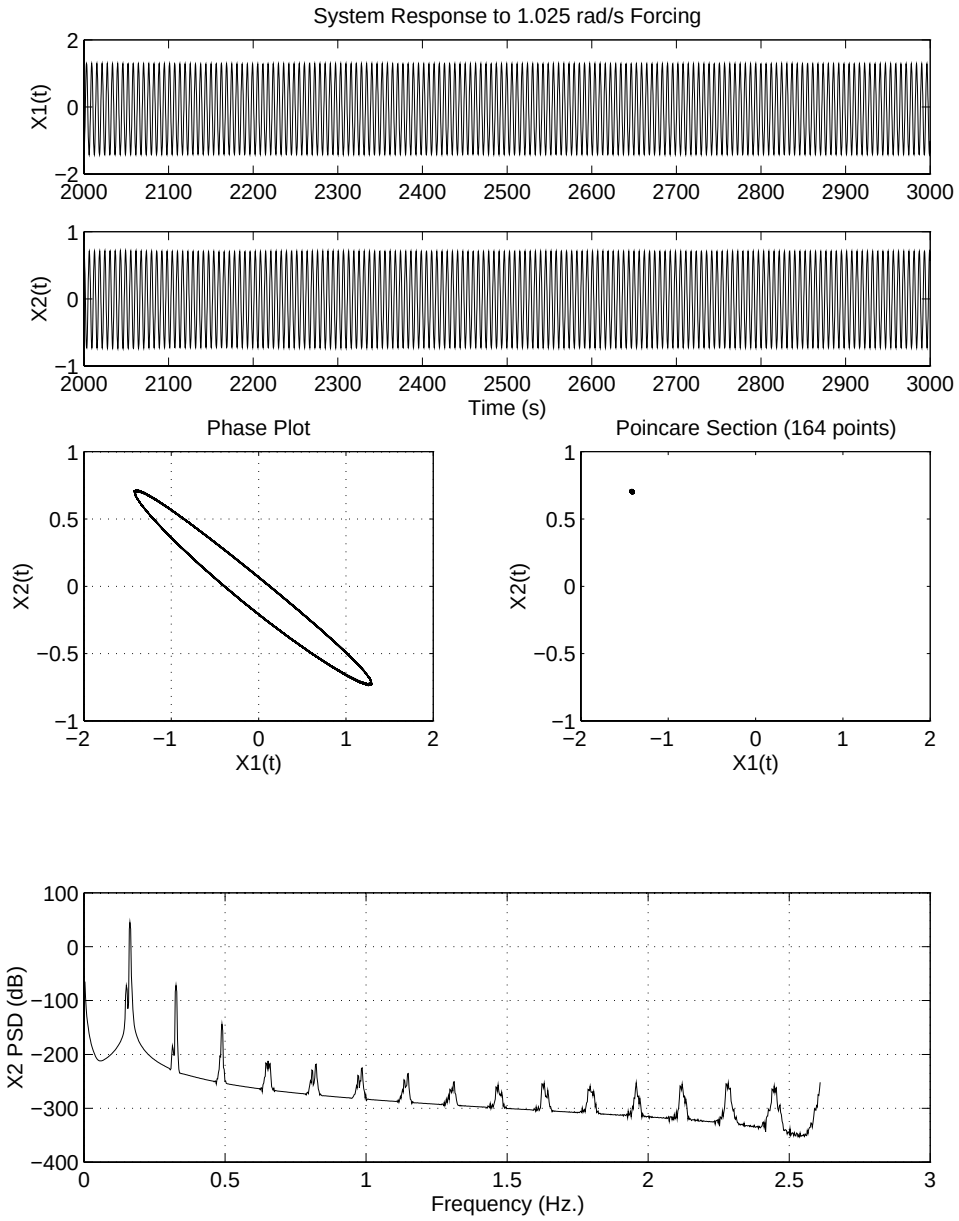

Figure 3.7: Numerical simulation of the piezoelectric vibration absorber with $r = 0.01$, $\alpha_1 = 0.1$, $\alpha_2 = 0.1$,$\alpha_3 = 0.01$, $\Omega = 1.025$, and $f = 0.1$. Note the response is periodic and the absorber performance is comparable to the linear case. Note, however, the presence of higher harmonics in the frequency response function.

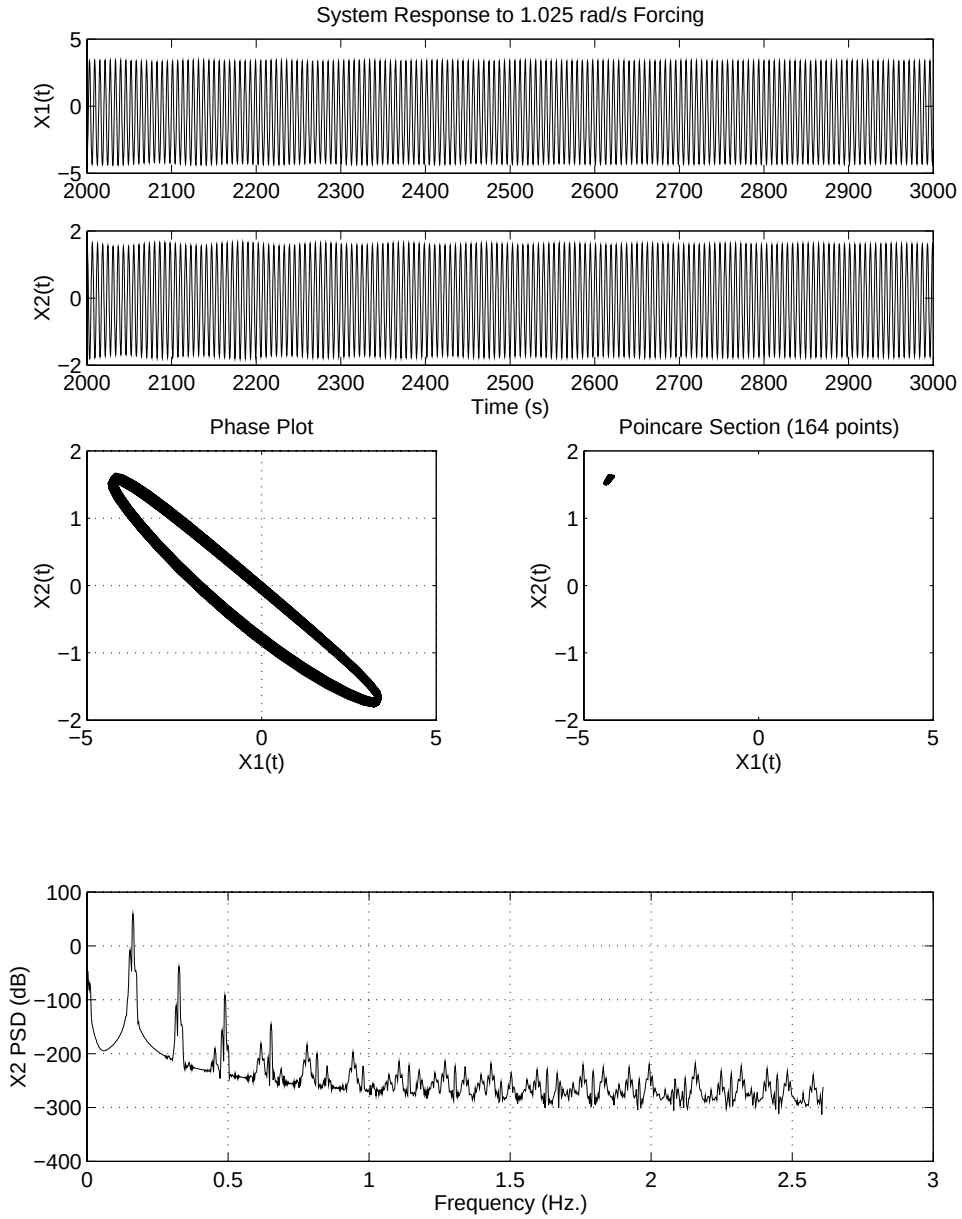

Figure 3.8: Numerical simulation of the piezoelectric vibration absorber with $r = 0.01$, $\alpha_1 = 0.1$, $\alpha_2 = 0.1$, $\alpha_3 = 0.01$,$\Omega = 1.025$, and $f = 0.3$. Note the response is quasiperiodic and the absorber performance is maintained.

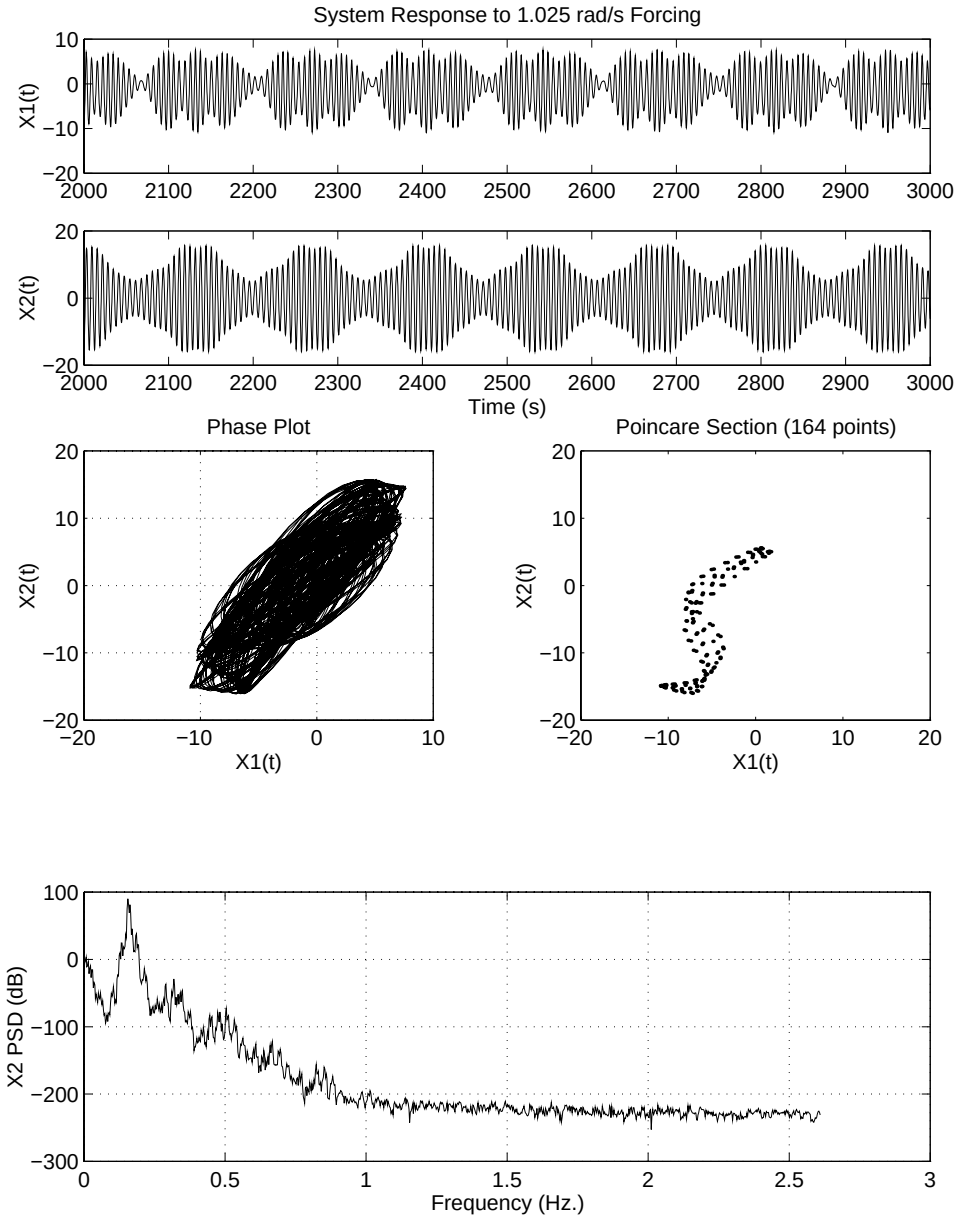

Figure 3.9: Numerical simulation of the piezoelectric vibration absorber with $r = 0.01$, $\alpha_1 = 0.1$, $\alpha_2 = 0.1$, $\alpha_3 = 0.01$,$\Omega = 1.025$, and $f = 0.7$. Note the response is chaotic and the absorber performance is poor.

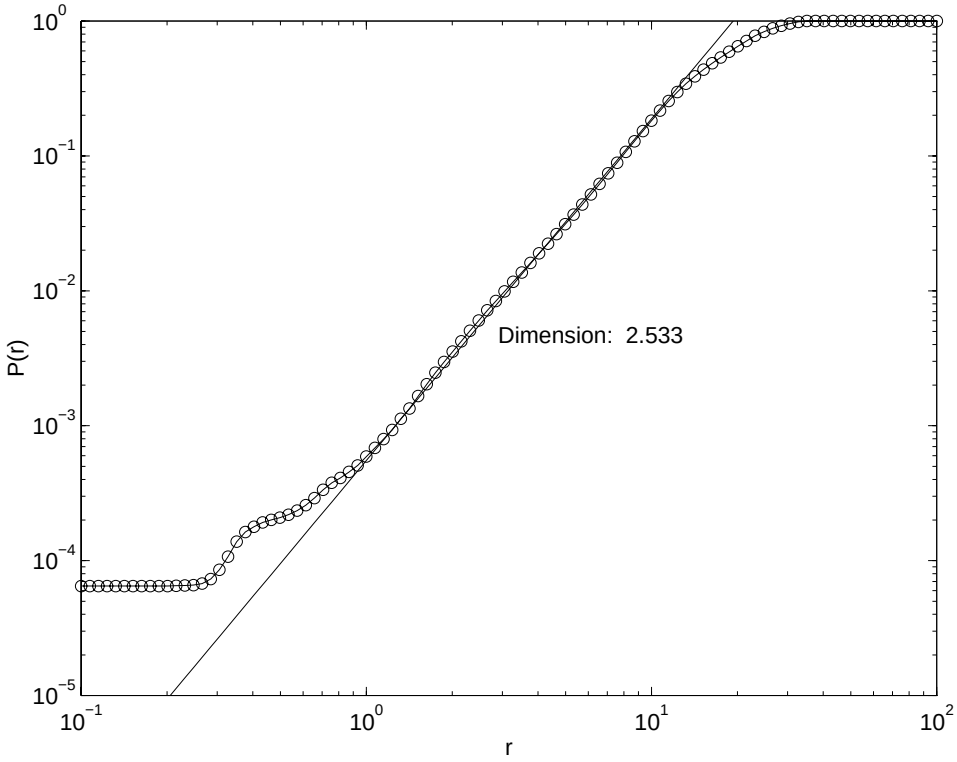

Figure 3.10: Dimension of the piezoelectric vibration absorber response with $r = 0.01$, $\alpha_1 = 0.1$, $\alpha_2 = 0.1$, $\alpha_3 = 0.01$,$\Omega = 1.025$, and $f = 0.7$. Note the response is chaotic with dimension 2.533.

thousand seconds of data were sampled at thirty-two times the driving frequency. The first five thousand seconds were discarded (leaving 55,202 samples). One thousand points were used in the averaging as reference points. *These quasiperiodic and chaotic regions must therefore be avoided in designing shunts for piezoelectric vibration absorbers which contain nonlinearities, modeled or not.*

The effect of small nonlinearities on the response of piezoelectric vibration absorbers indicates that while increased bandwidth is obtained by introducing nonlinear shunts, the price is the presence of resonant response, even in the case of the damped piezoelectric vibration absorber. The presence of periodic, quasiperiodic, and chaotic solutions is established. Further numerical analysis of the effect of nonlinearity is required to better understand this behavior. These results also indicate that if nonlinearity is present in a linear shunt design and unaccounted for, the resulting absorber performance could degrade without the designer's knowledge.

3.3.2 Analysis

Motivated by the bandwidth increase demonstrated by the Nonlinear Piezoelectric Vibration Absorber study presented in Section 3.3.1, detailed analysis of the linear structure with a nonlinear absorber was undertaken. Using the cartesian form of the modulation equations, the LSNA (Linear System, Nonlinear Absorber) modulation equations are obtained from Equations (3.8a)-(3.8d):

$$p_1' = -\sigma q_1 - \frac{\alpha_1}{2} q_2 - \zeta_1 p_1 \tag{3.23a}$$

$$q_1' = \sigma p_1 + \frac{\alpha_1}{2} p_2 - \zeta_1 q_1 + \frac{f}{2} \tag{3.23b}$$

$$p_2' = -(\sigma - \delta_1) q_2 - \frac{\alpha_1}{2} q_1 - \zeta_2 p_2 + \frac{3}{8}\delta_3 (p_2^2 + q_2^2) q_2 \tag{3.23c}$$

$$q_2' = (\sigma - \delta_1) p_2 + \frac{\alpha_1}{2} p_1 - \zeta_2 q_2 - \frac{3}{8}\delta_3 (p_2^2 + q_2^2) p_2 \tag{3.23d}$$

The performance of the absorber can be seen in Figure 3.11. Multiple frequency response curves are plotted for varying forcing levels as indicated in the caption. When $f = 0.01$, the

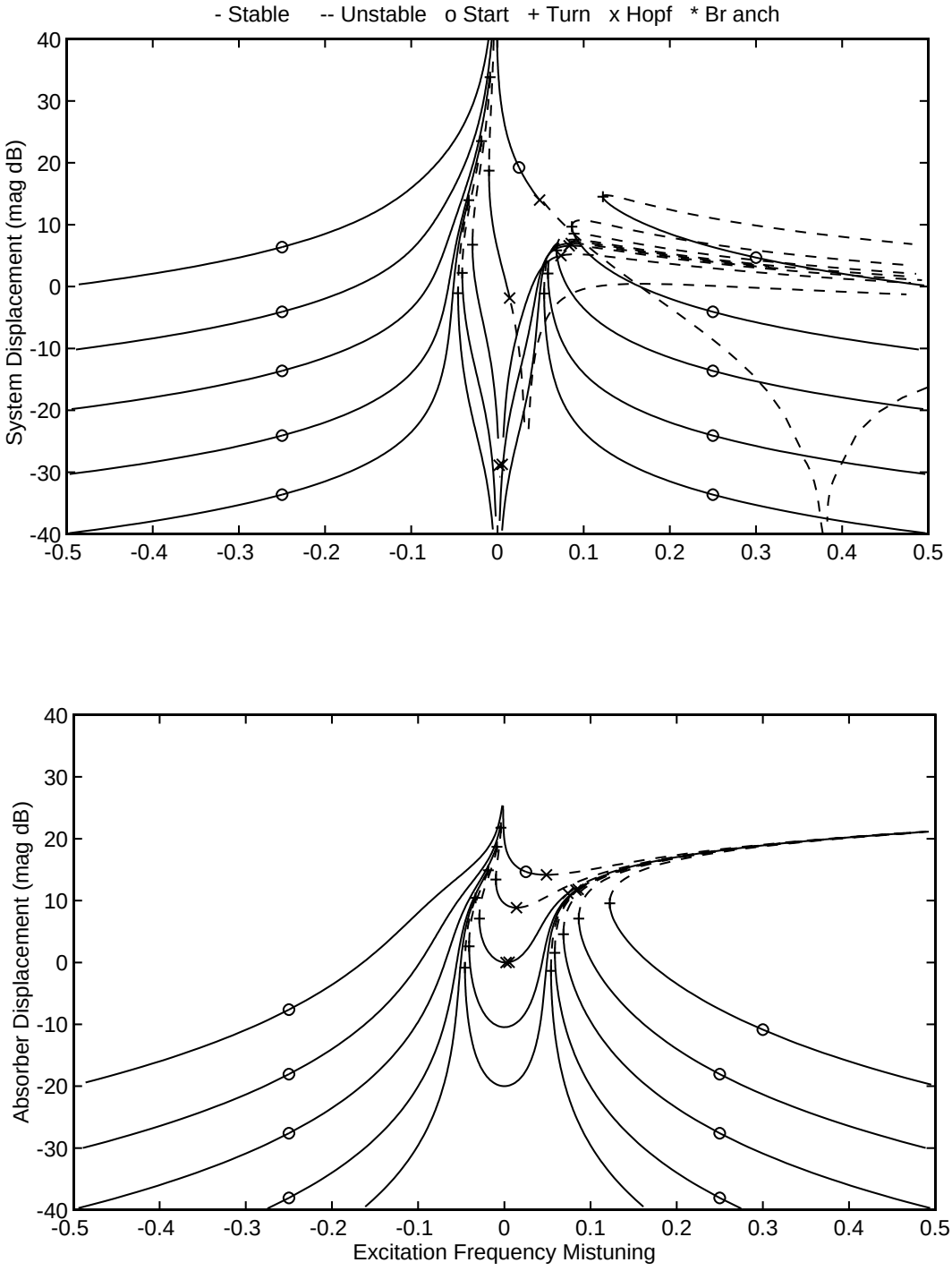

Figure 3.11: The LSNA response as f varies for $\delta_3 = 0.01$ and $\delta_1 = 0$. $f = 0.01$, 0.03, 0.1, 0.3,1.0. System Parameters: $\zeta_1 = 0.001$, $\zeta_2 = 0$, $\alpha_1 = 0.1$, $\alpha_3 = 0$

response is almost linear except for some bend in the left-hand peak. The right resonance bends significantly and note the Hopf bifurcation which takes place at $\sigma = 0.085$. Within the suppression bandwidth, the response of the system is acceptable.

If the force increases to 0.03, the response essentially remains the same with larger bending of the resonant peaks. However, when the force increases to 0.1, a second set of Hopf bifurcations occur at $\sigma = 0.0019$ and $\sigma = 0.0056$ which is right within the suppression region. As shown in the last section, the performance of the vibration absorber deteriorates when the response becomes quasiperiodic. Increasing the force to 0.3 returns to a single Hopf bifurcation (within our plotting window) at $\sigma = 0.0142$ and the suppression region has moved with a zero location of $\sigma = 0.03$, but the entire suppression region is quasiperiodic. This agrees with the solution of the previous section. Thus for positive values of δ_3, as the force increases, Hopf bifurcations appear which lead to poor absorber performance. Additionally, the suppression band moves to the right and expands. This increased suppression bandwidth is of little use especially when unstable. The coexistence of stable (but poor performance) fixed point solutions with the quasiperiodic solutions further complicates absorber performance.

These results expand on those reported in [34] which treated the absorber as a combination resonance and was thus unable to model both the suppression bandwidth and the resonant behaviour modeled here. Since the resonant peaks bend into the suppression bandwidth, the model must account for resonant and suppressed response. This ability is a strength of the current analysis. The treatment of the absorber problem as an internal resonance is more accurate for a small coupling of the absorber to the system. As seen in Figure 3.11, there co-exists both suppressed and resonant response to excitation near the absorber tuning frequency. This implies that the response of the system is dependent on initial conditions. Moreover, a disturbance to the system could cause it to jump from suppressed to resonant behavior implying the absorber lacks robustness required for good design.

Linear tuning of the nonlinear vibration absorber is examined next. In Figures 3.12-3.13

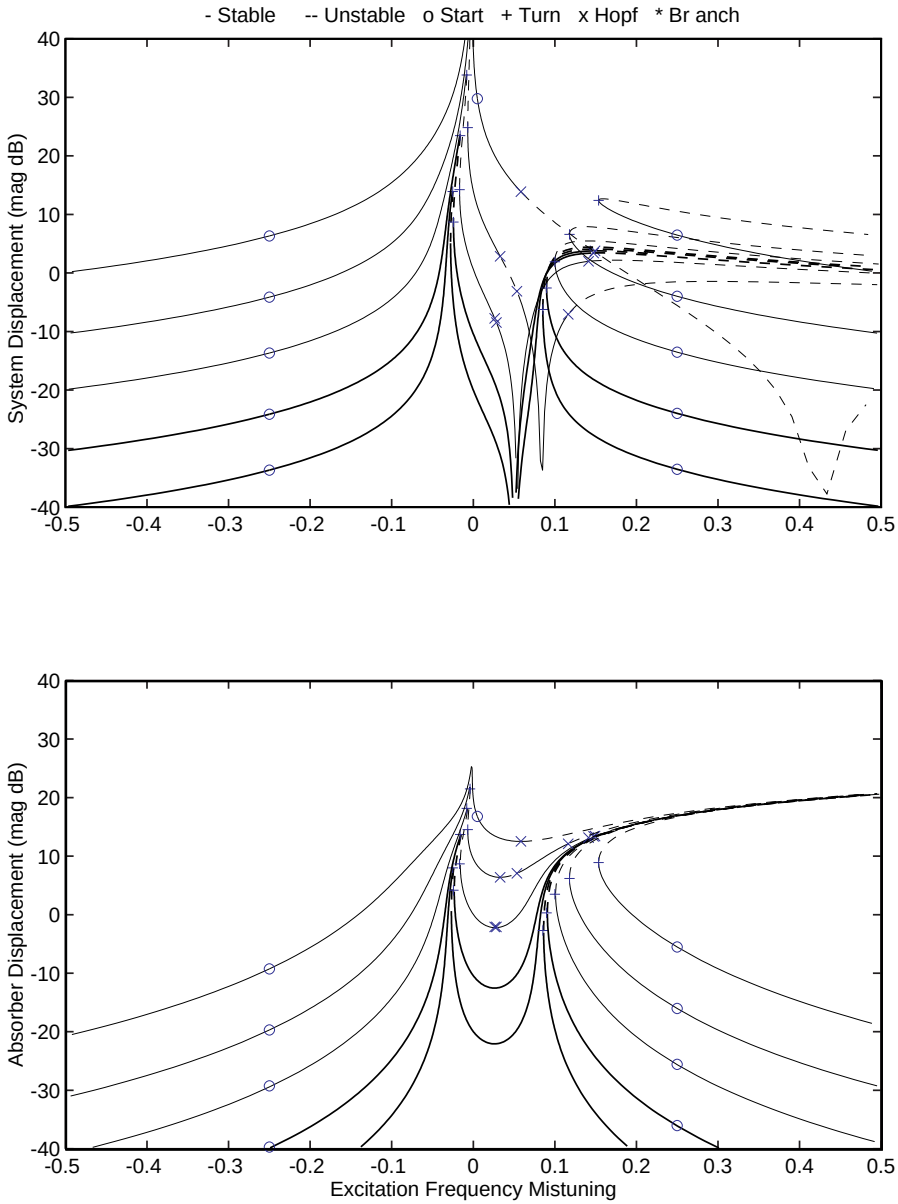

Figure 3.12: The LSNA response as f varies for $\delta_3 = 0.01$ and $\delta_1 = 0.05$. $f = 0.01$, 0.03, 0.1, 0.3,1.0. System Parameters: $\zeta_1 = 0.001$, $\zeta_2 = 0$, $\alpha_1 = 0.1$, $\alpha_3 = 0$

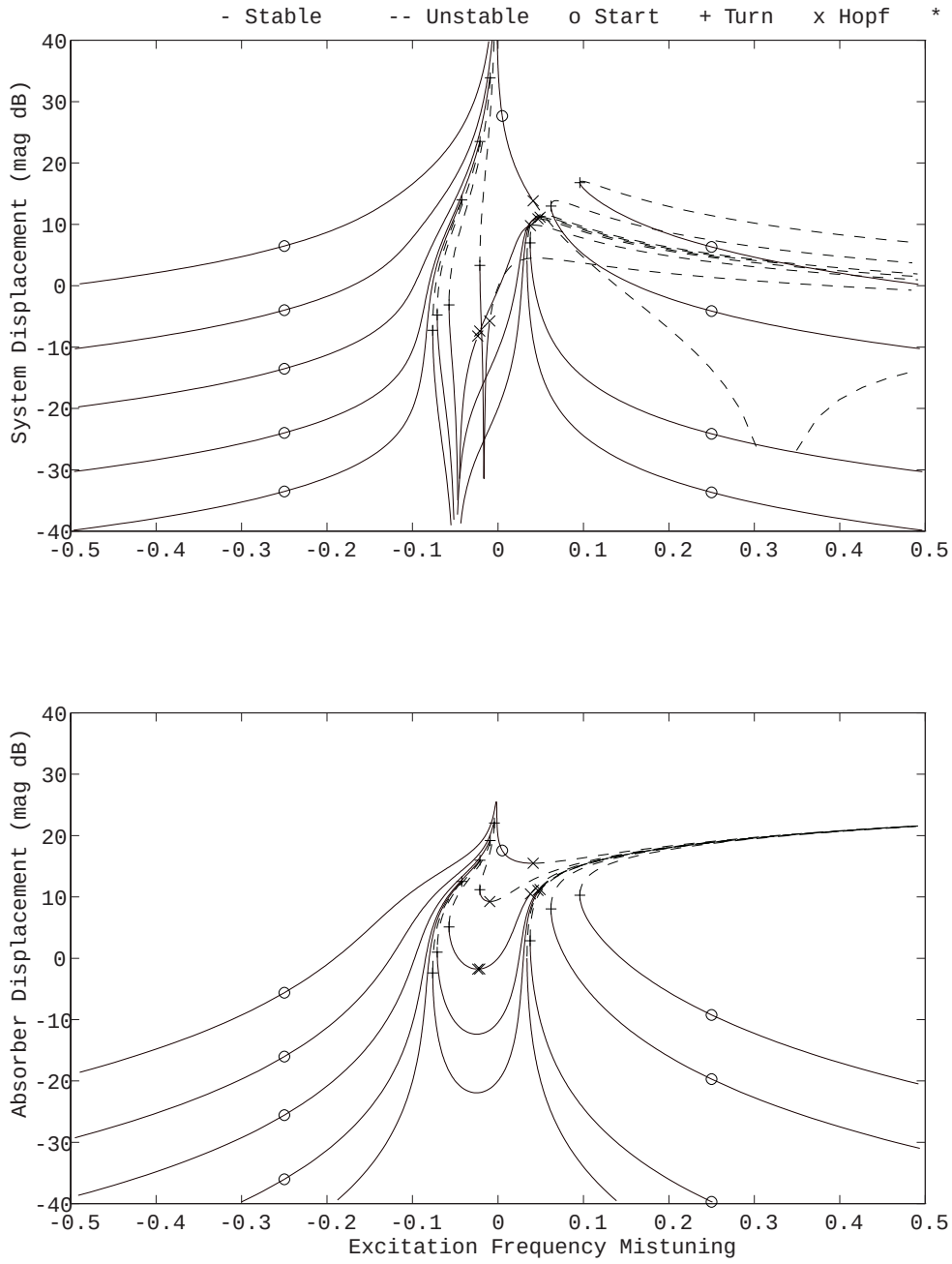

Figure 3.13: The LSNA response as f varies for $\delta_3 = 0.01$ and $\delta_1 = -0.05$. $f = 0.001$, 0.01, 0.03, 0.1, 0.3, 1.0. System Parameters: $\zeta_1 = 0.001$, $\zeta_2 = 0$, $\alpha_1 = 0.1$, $\alpha_3 = 0$

the linear tuning δ_1 is varied with otherwise identical system parameters as Figure 3.11. For $\delta_1 > 0$, the response improves. The suppression region is shifted upwards in frequency, eliminating the robustness issue. Furthermore, the stability of the system improves as although the Hopf bifurcation occurs for $f = 0.1$, it is outside the suppression bandwidth. For $f = 0.3$, the unstable region occurs on the edges of the suppression bandwidth, but when the force is increased to $f = 1.0$, performance again suffers. Negative absorber tuning, $\delta_1 < 0$, has similar results for stability, but the robustness is still a concern since multiple stable fixed points are present.

Changing the sign of the nonlinearity produces a mirrored response as plotted in Figure 3.14 for otherwise identical parameters to Figure 3.11. The system thus produces mirrored, but identical, results for $\{\sigma,\delta_1,\delta_3\}$ and $\{-\sigma,-\delta_1,-\delta_3\}$. For $\sigma > (<)0$, $\delta_3 > (<)0$ produces an increased vibration suppression bandwidth. Tuning the linear absorber frequency, δ_1 behaves in a manner similar to the linear system although the effective absorber frequency shifts with increased forcing level, an important consideration for nonlinear absorber design.

For system parameters identical except for damping level to Figure 3.11, numerical integration of the system equations was performed. The damping was increased slightly to improve computation time (lighter damping results in longer time to come to steady state). The equations of motion were integrated for 3500 seconds and the response is plotted for the next 500 seconds. The results are shown for multiple forcing levels in Figure 3.15. Clearly, the presence of Hopf bifurcations, and the corresponding quasiperiodic response cause a deterioration in absorber performance as the force was increased from 0.1 to 0.3. Note that the response of the system is less for the nonlinear absorber for $f = 0.1$, but greater for $f = 0.3, 1.0$. These results are similar to those of the previous section. To maintain performance of the absorber, the design force must be limited. The cost of force limitations must be offset by the larger suppression bandwidth evident in Figures 3.11-3.14 for the nonlinear absorber to be a viable design alternative.

Calculation of the suppression bandwidth for the undamped LSNA system is performed

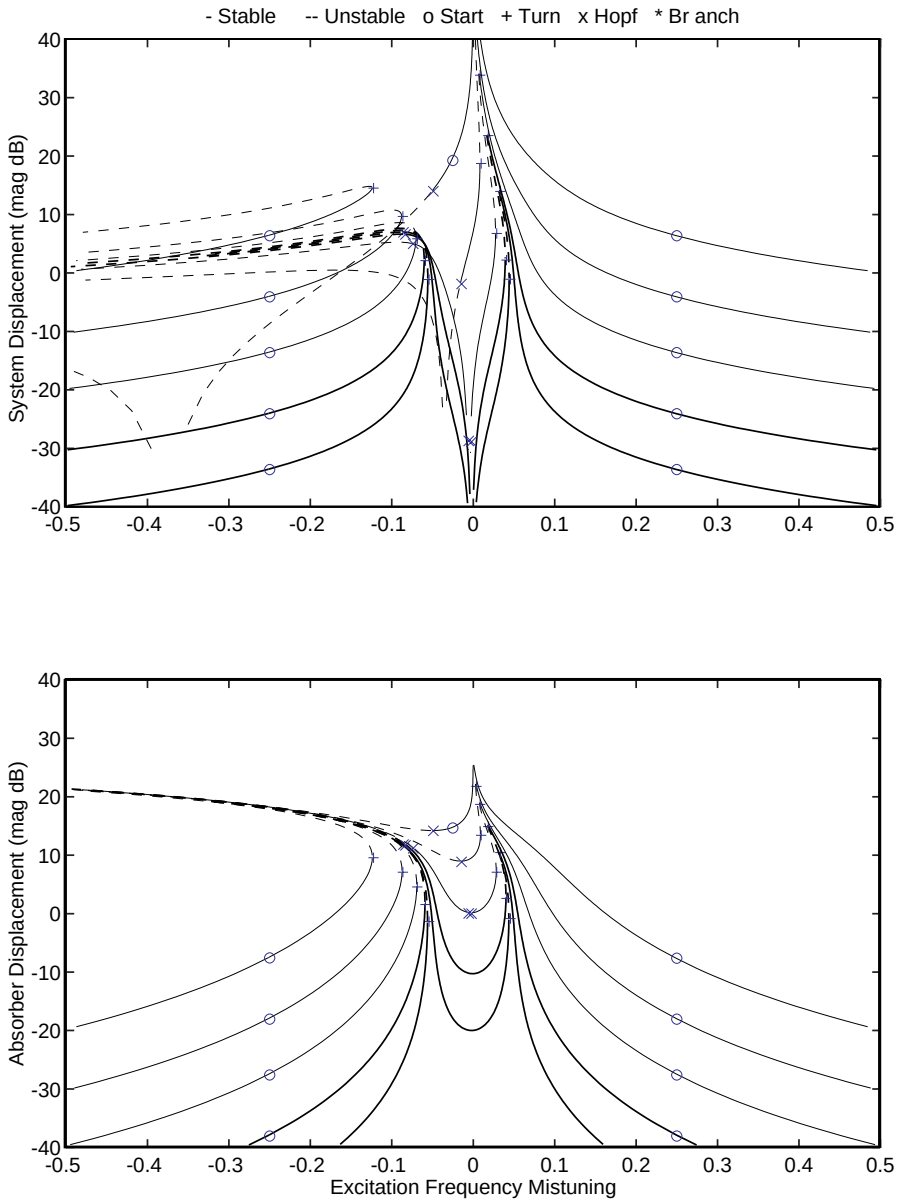

Figure 3.14: The LSNA response as f varies for $\delta_3 = -0.01$ and $\delta_1 = 0$. $f = 0.001$, 0.01, 0.03, 0.1, 0.3,1.0. System Parameters: $\zeta_1 = 0.001$, $\zeta_2 = 0$, $\alpha_1 = 0.1$, $\alpha_3 = 0$

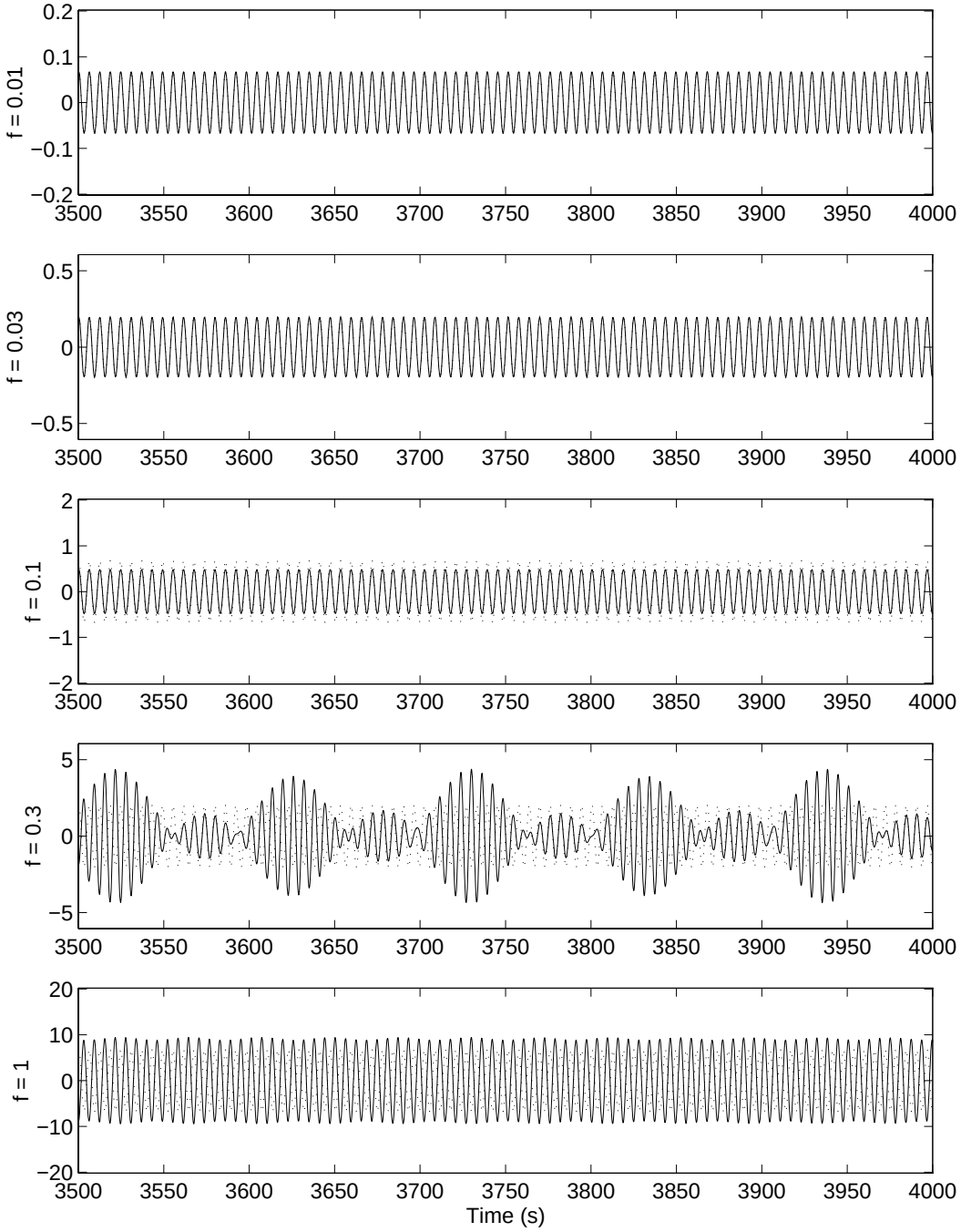

Figure 3.15: The LSNA time response as f varies for $\delta_3 = 0.01$ and $\delta_1 = 0$. $f = 0.01$, 0.03, 0.1, 0.3,1.0. Linear response (LSLA) is shown dotted on the figure also. System Parameters: $\zeta_1 = 0.001$, $\zeta_2 = 0$, $\alpha_1 = 0.1$,$\alpha_3 = 0$

by setting $p_1^2 + q_1^2 = f^2$ and solving the modulation equations for σ as was done for the linear case in Section 3.2. Two equations in σ result:

$$\alpha_1^4 - (3/4)(1+2\sigma)\alpha_1^2(\sigma - \delta_1) + 2(1+2\sigma)^3\delta_3 f^2 = 0 \tag{3.24a}$$

$$\alpha_1^4 + (3/4)(1-2\sigma)\alpha_1^2(\sigma - \delta_1) - 2(1-2\sigma)^3\delta_3 f^2 = 0 \tag{3.24b}$$

for the in-phase and out-of-phase solutions, respectively. Using a perturbation approach, these polynomial equations can be solved for $\sigma^{\pm}$:

$$\sigma^+ = \delta_1 + \frac{\delta_3 f^2}{\alpha_1^2} + \frac{\alpha_1^2}{2} + \frac{3\delta_1\delta_3 f^2}{2\alpha_1^2} + \frac{3\delta_3^2 f^4}{2\alpha_1^4} + O(\epsilon)^3 \tag{3.25a}$$

$$\sigma^- = \delta_1 + \frac{\delta_3 f^2}{\alpha_1^2} - \frac{\alpha_1^2}{2} - \frac{3\delta_1\delta_3 f^2}{2\alpha_1^2} - \frac{3\delta_3^2 f^4}{2\alpha_1^4} + O(\epsilon)^3 \tag{3.25b}$$

Similarly, the location of zero system response can be found as:

$$\sigma^0 = \delta_1 + \frac{3\delta_3 f^2}{8\alpha_1^2} \tag{3.26}$$

Thus like the linear case the nonlinear absorber bandwidth is centered around σ^0 with magnitude

$$\alpha_1^2 + \frac{3\delta_1\delta_3 f^2}{\alpha_1^2} + \frac{9\delta_3^2 f^4}{8\alpha_1^4} \tag{3.27}$$

which is in agreement with the numerical results presented in Figures 3.11-3.14. Several authors have contended that only softening springs lead to an increased absorber bandwidth. From Equation (3.27), the analysis shows this to be the case for $\delta_1 < 0$ only. Performance is symmetric for the case of $\delta_1 = 0$. For $\delta_1 > 0$, a hardening absorber has superior performance when first order nonlinear effects and small coupling ratio α_1 are assumed. If the forcing magnitude is larger, increases in bandwidth can be seen for either case. A plot of the bandwidth for various absorber tunings δ_1 can be seen in Figure 3.16. The nondimensional nonlinearity

$$\bar{\delta_3} = \frac{3\delta_3 f^2}{8\alpha_1^2} \tag{3.28}$$

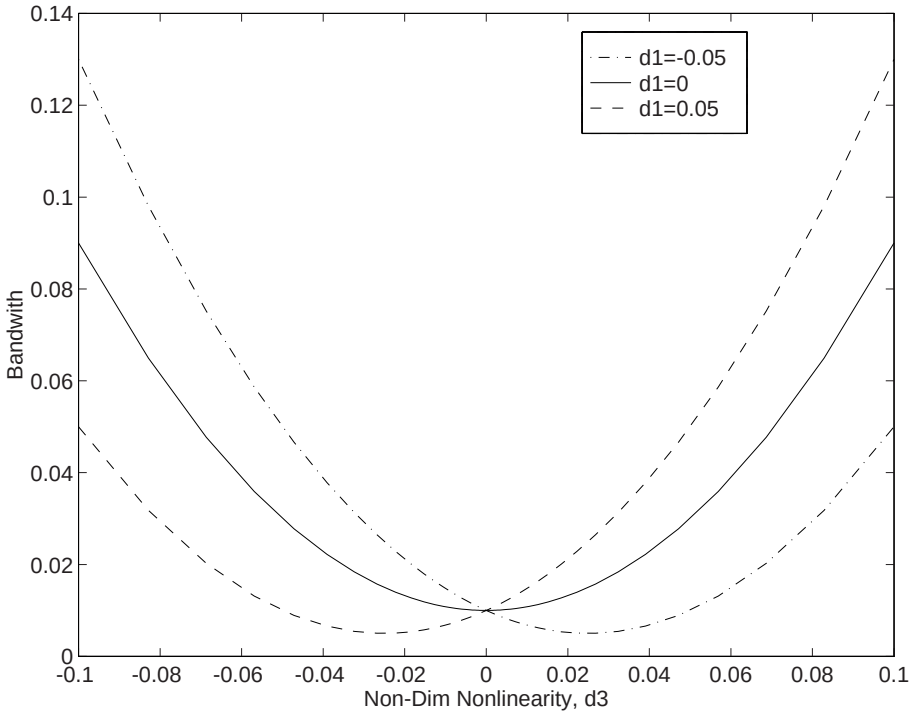

Figure 3.16: The LSNA bandwidth vs $\bar{\delta_3}$ for δ_1 as indicated on the figure. System Parameters: $\zeta_1 = 0$,$\zeta_2 = 0$,$\alpha_1 = 0.1$, $\alpha_3 = \alpha_2 = \delta_2 = 0$

is used in this plot. This nondimensional group arises often in the analysis and for a single nonlinearity the forcing magnitude f can be considered unity and the effect of force on the system is to change the effective nonlinearity. However, for multiple nonlinear parameters this cannot be done since changes in f would result in simultaneous changes in multiple parameters, possibly obscuring important relations.

The selection of absorber design parameters can be made using these results. To design an absorber which has a given bandwidth at a frequency σ_0 and force f, one first solves Equation (3.26) for δ_1,

$$\delta_1 = \sigma_0 - \frac{3\delta_3 f^2}{8\alpha_1^2} \tag{3.29}$$

and substitutes the result into Equation (3.27) to yield the bandwidth, $\Delta\sigma$:

$$\Delta\sigma = \alpha_1^2(1 + \frac{3\sigma_0\delta_3 f^2}{\alpha_1^4}) \tag{3.30}$$

The implications of this result are many. First, for $\sigma_0 = 0$, no improvement in the absorber bandwidth can be achieved while maintaining the (undamped) zero response at $\sigma = 0$. Second, although the zero frequency can theoretically be placed anywhere, care must be taken if it is placed near the linear resonances of the system. In this case, the system could be in resonance for low forcing levels only to achieve good performance as the forcing increased. Such a design would not yield acceptable performance in most instances. Finally, limitations on the achievable bandwidth will arise due to the presence of Hopf bifurcations and their corresponding quasiperiodic response.

The presence of nonlinearity thus has both benefits and costs. As seen in Equation (3.27), the suppression bandwidth of the system can be increased. This comes at the expense of moving the location of zero system response (perfect absorption) as the forcing level increases and the possible presence of Hopf bifurcations leading to quasiperiodic behavior and breakdown of absorption.

3.4 Nonlinear Structure, Linear Absorber

A second case to consider is that of a linear absorber on a nonlinear structure. The assumption of a linear absorber is more likely to be accurate for either the electronic vibration absorber or the piezoelectric vibration absorber where electronic components comprise the absorber. Thus even for large displacement of the structure, the response of the absorber

can be considered linear. The modulation equations in this case reduce to

$$p_1' = -\sigma q_1 - \frac{\alpha_1}{2} q_2 - \zeta_1 p_1 + \frac{3}{8}\alpha_3 (p_1^2 + q_1^2) q_1 \tag{3.31a}$$

$$q_1' = \sigma p_1 + \frac{\alpha_1}{2} p_2 - \zeta_1 q_1 - \frac{3}{8}\alpha_3 (p_1^2 + q_1^2) p_1 + \frac{f}{2} \tag{3.31b}$$

$$p_2' = -(\sigma - \delta_1) q_2 - \frac{\alpha_1}{2} q_1 - \zeta_2 p_2 \tag{3.31c}$$

$$q_2' = -(\sigma - \delta_1) p_2 - \frac{\alpha_1}{2} p_1 - \zeta_2 q_2 \tag{3.31d}$$

As in the last section, these equations are solved using continuation methods. In Figure 3.17, the response is shown for a variety of forcing levels. Contrary to the nonlinearity in the absorber, nonlinear system stiffness affects only the resonant behavior, not the suppression bandwidth. Calculating the system bandwidth as in the previous section yields the identical result to a linear system:

$$\sigma^+ = \delta_1 + \frac{\alpha_1^2}{2} + O(\epsilon)^3 \tag{3.32a}$$

$$\sigma^- = \delta_1 - \frac{\alpha_1^2}{2} + O(\epsilon)^3 \tag{3.32b}$$

$$\sigma^0 = \delta_1 \tag{3.32c}$$

Robustness is again a concern since multiple solutions exist for some frequencies within the absorber suppression region. The performance of the absorber for various forcing levels is shown in Figure 3.18. The time response for $f = \{0.01, 0.03, 0.1, 0.3, 1.0\}$ shows system nonlinearity does not affect the performance of the absorber. Both the nonlinear and linear response are shown, but overlayed so only one trace is visible. However, this may not be the case from all initial conditions or if a disturbance was to shock the system, causing it to respond with resonant rather than suppressed behavior.

Thus, the effect of a nonlinear structure on the performance of a linear absorber is detrimental, but not as severe as for the nonlinear absorber. The bandwidth of the absorber is unaffected and, although Hopf bifurcations are present, they occur in resonant regions outside of the operating range of the absorber. However, the influence of nonlinear systems

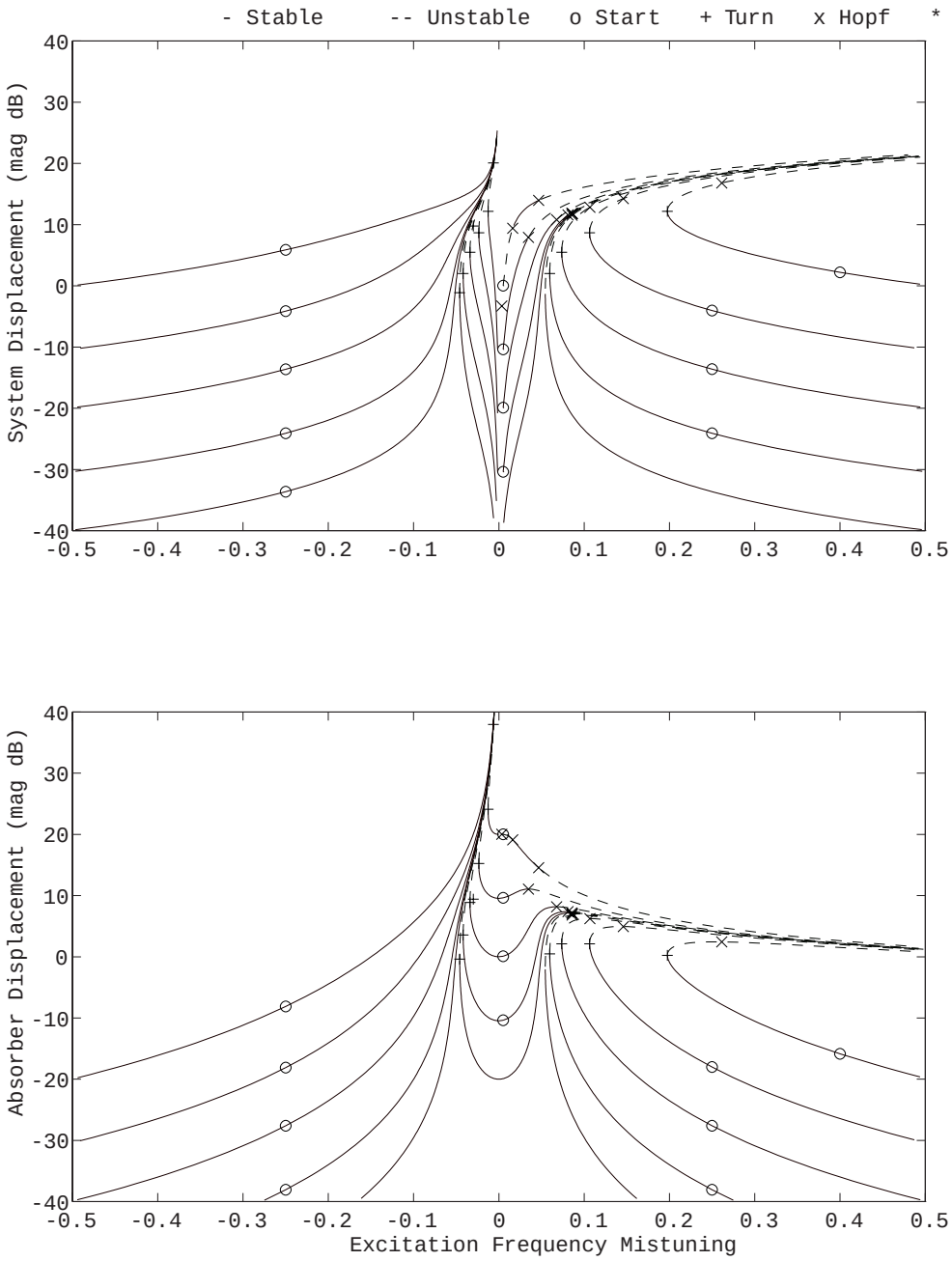

Figure 3.17: The NSLA response as f varies for $\alpha_3 = 0.01$ and $\delta_1 = 0$. $f = 0.01$, 0.03, 0.1, 0.3, 1.0. System Parameters: $\zeta_1 = 0.001$, $\zeta_2 = 0$, $\alpha_1 = 0.1$, $\delta_1 = \delta_3 = 0$

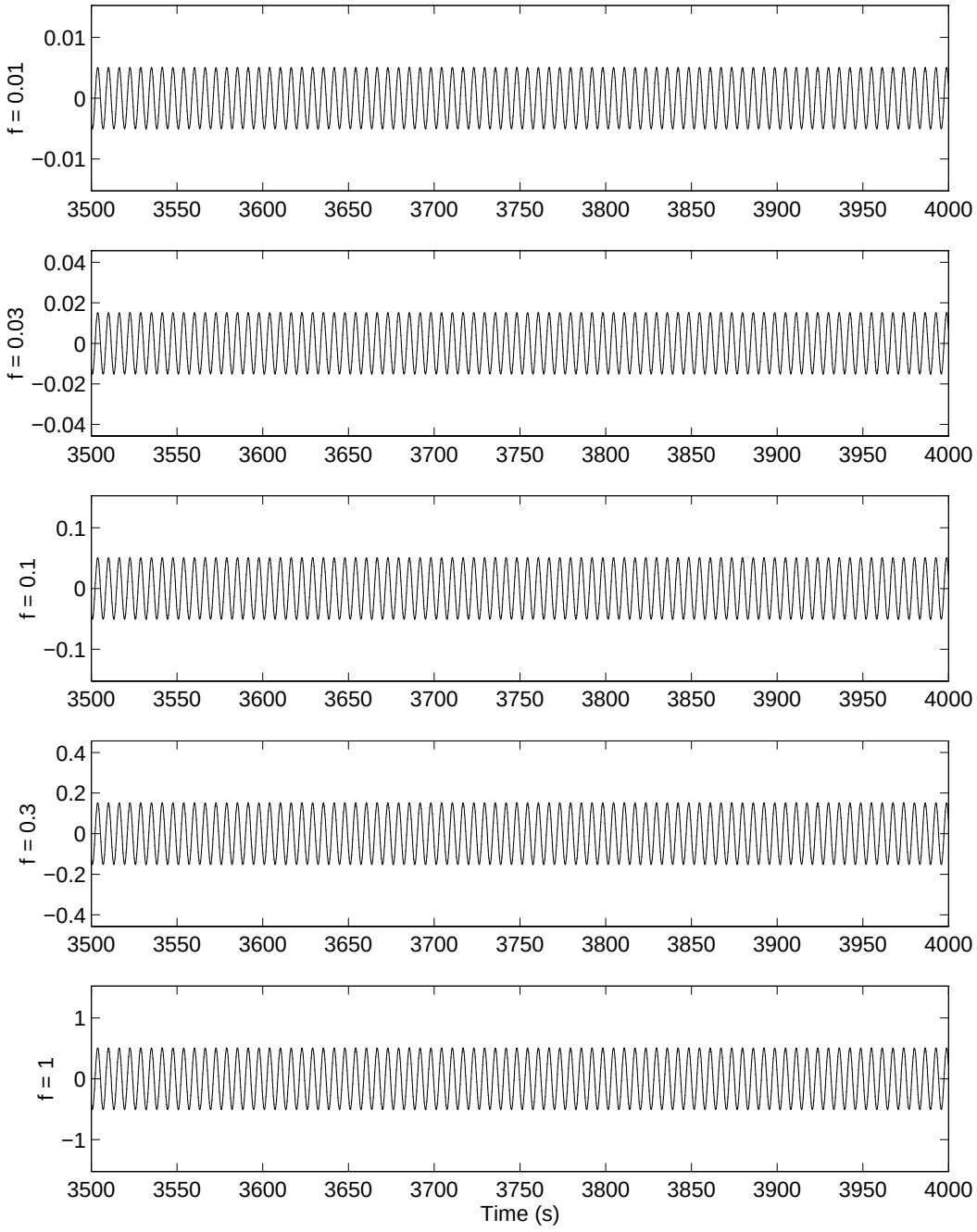

Figure 3.18: The LSNA response as f varies for $\alpha_3 = 0.01$ and $\sigma = 0.0025$. System Parameters: $\zeta_1 = 0.001$,$\zeta_2 = 0$,$\alpha_1 = 0.1$, ,$\delta_1 = \delta_3 = 0$

on performance is important if the absorber is nonlinear, which will be demonstrated in the next section.

3.5 Nonlinear Structure, Nonlinear Absorber

The final case considered in this chapter is a nonlinear system with a nonlinear absorber. By controlling the absorber nonlinearity, enhancements in performance will be shown. The modulation equations for this case are:

$$p_1' = -\sigma q_1 - \frac{\alpha_1}{2} q_2 - \zeta_1 p_1 + \frac{3}{8}\alpha_3 (p_1^2 + q_1^2) q_1 \tag{3.33a}$$

$$q_1' = \sigma p_1 + \frac{\alpha_1}{2} p_2 - \zeta_1 q_1 - \frac{3}{8}\alpha_3 (p_1^2 + q_1^2) p_1 + \frac{f}{2} \tag{3.33b}$$

$$p_2' = -(\sigma - \delta_1) q_2 - \frac{\alpha_1}{2} q_1 - \zeta_2 p_2 + \frac{3}{8}\delta_3 (p_2^2 + q_2^2) q_2 \tag{3.33c}$$

$$q_2' = (\sigma - \delta_1) p_2 + \frac{\alpha_1}{2} p_1 - \zeta_2 q_2 - \frac{3}{8}\delta_3 (p_2^2 + q_2^2) p_2 \tag{3.33d}$$

Fixed points for these equations were numerically examined using continuation methods and direct integration as in the previous cases. Results for various forcing levels are plotted in Figures 3.19-3.22. Note that only three forcing levels were plotted to allow a clearer view of the response. The results for $\delta_3 \alpha_3 > 0$ indicate that the robustness issue is more severe than for the previous cases. The resonance curves bend more severely even for low forcing levels. The symmetry in results for changing signs is again evident. However when $\delta_3 \alpha_3 < 0$, the response is improved since the resonant curves bend away from the suppression region. The bandwidth of the suppression region is identical to the LSNA result Equation (3.27). The system nonlinearity affects only the resonant peaks, not the absorber suppression region. Heuristically, if absorption is occurring, the system response is suppressed, minimizing the nonlinear system effects, but the absorber response is large. At resonance, both system and absorber response are large. *System nonlinearities are thus important in resonant response, but not in suppressed response while the absorber nonlinearities are significant in both cases.*

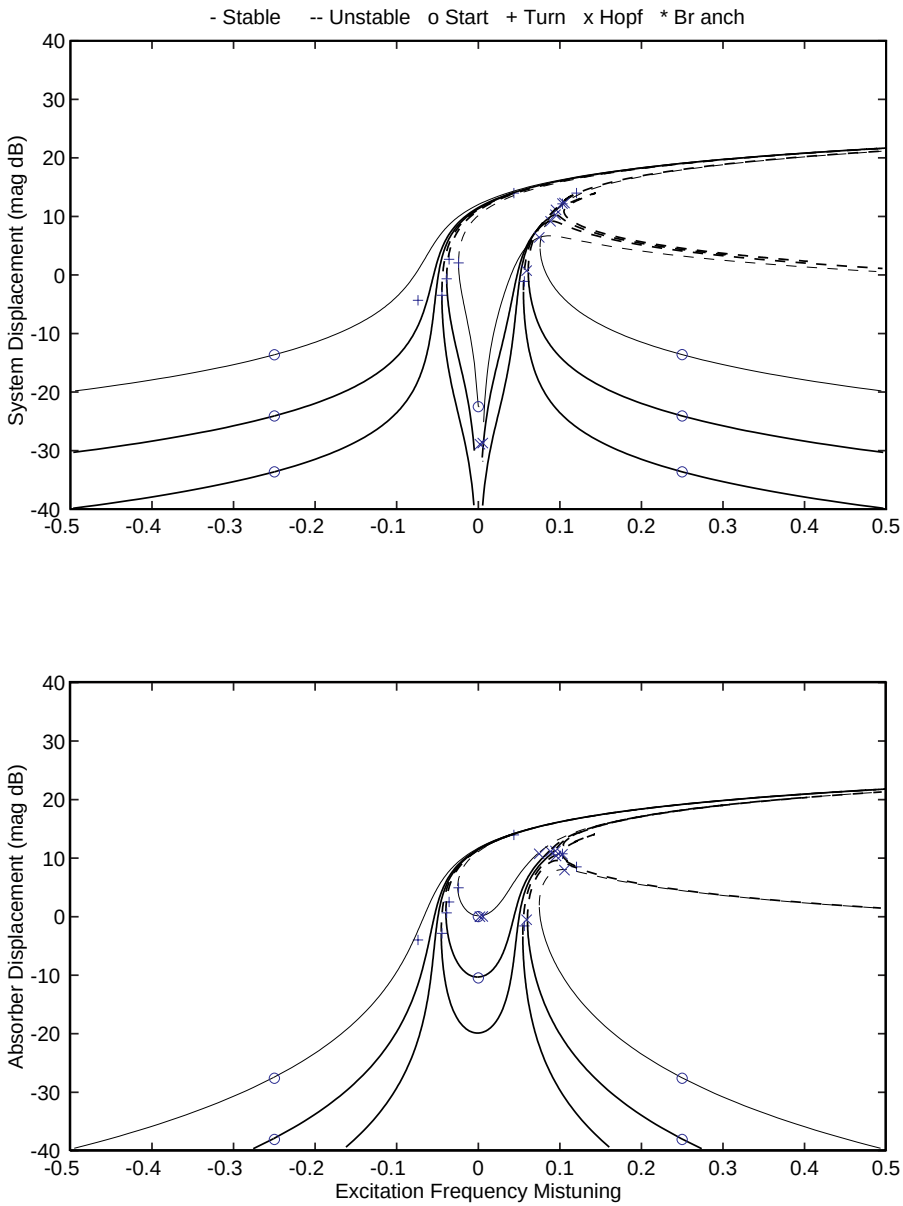

Figure 3.19: The NSNA response as f varies for $\alpha_3 = 0.01$ and $\delta_3 = 0.01$. $f = 0.01$, 0.03, 0.1. System Parameters: $\zeta_1 = 0.001$, $\zeta_2 = 0$, $\alpha_1 = 0.1$, $\delta_1 = 0$

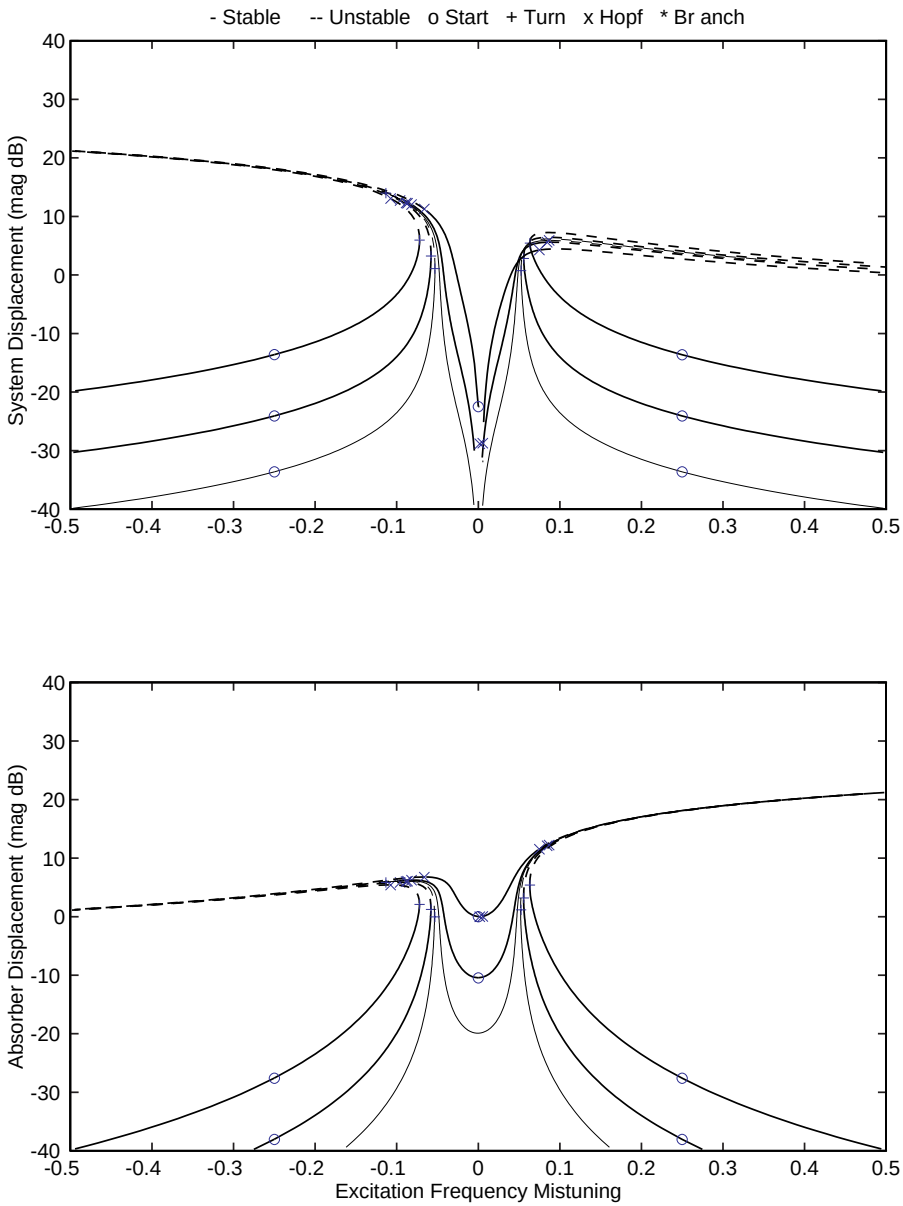

Figure 3.20: The NSNA response as f varies for $\alpha_3 = 0.01$ and $\delta_3 = -0.01$. $f = 0.01$, 0.03, 0.1. System Parameters: $\zeta_1 = 0.001$, $\zeta_2 = 0$, $\alpha_1 = 0.1$, $\delta_1 = 0$

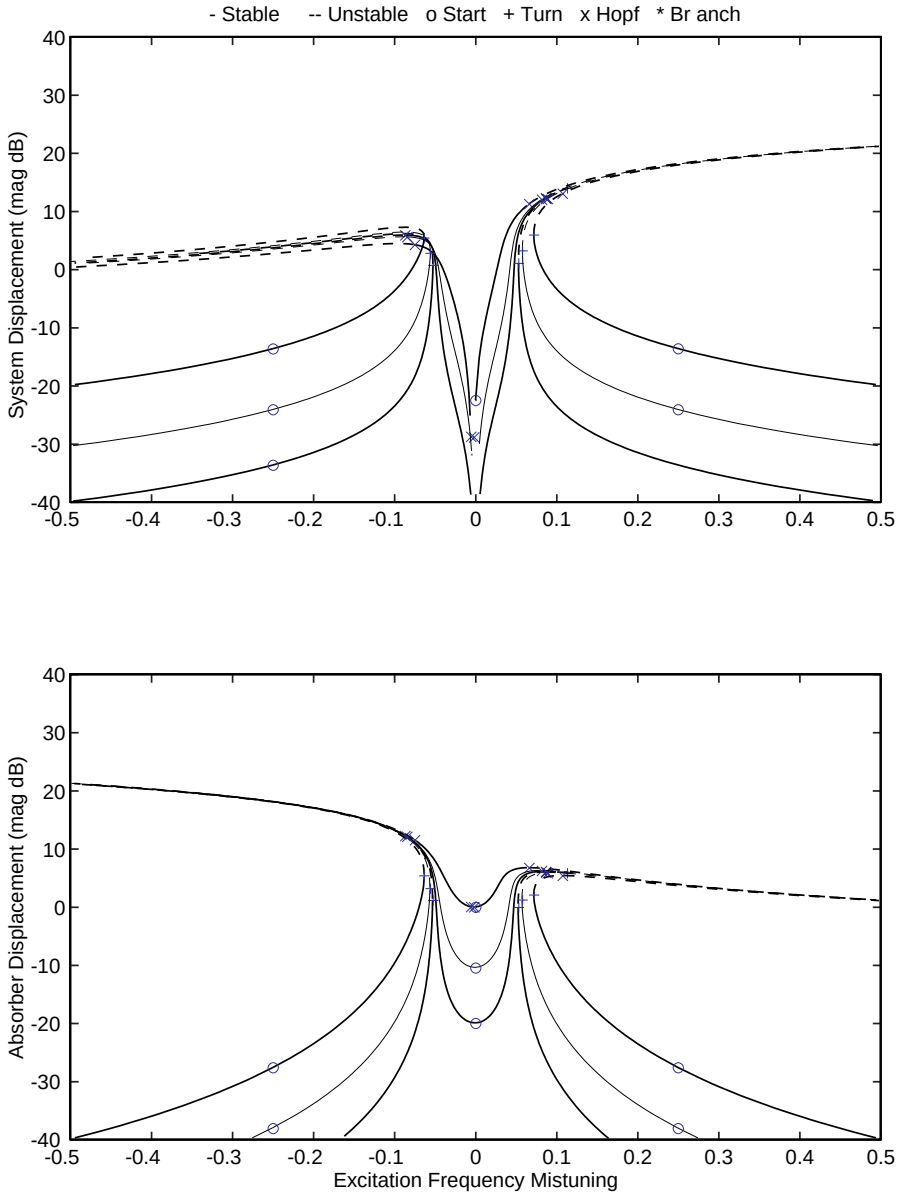

Figure 3.21: The NSNA response as f varies for $\alpha_3 = -0.01$ and $\delta_3 = 0.01$. $f = 0.01$, 0.03, 0.1. System Parameters: $\zeta_1 = 0.001$, $\zeta_2 = 0$, $\alpha_1 = 0.1$, $\delta_1 = 0$

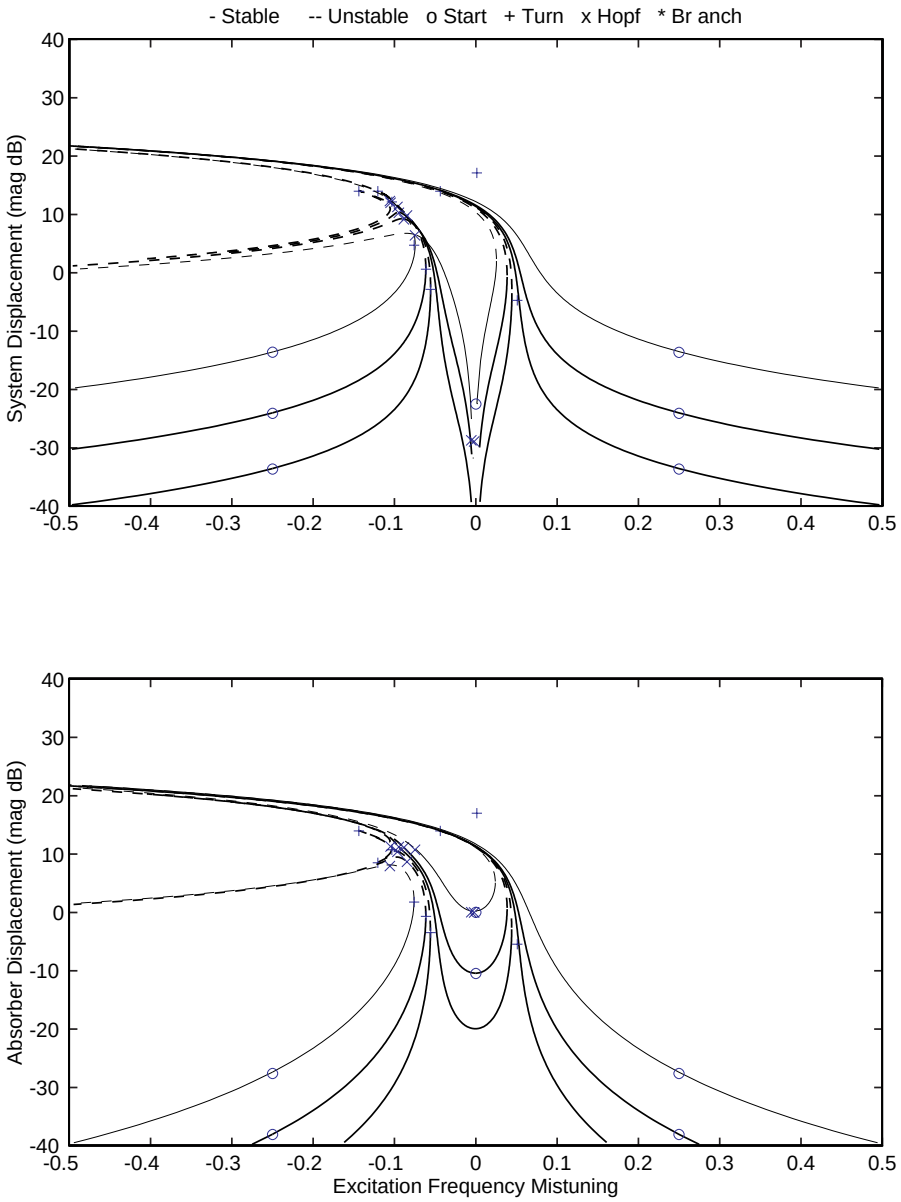

Figure 3.22: The NSNA response as f varies for $\alpha_3 = -0.01$ and $\delta_3 = -0.01$. $f = 0.01$, 0.03, 0.1. System Parameters: $\zeta_1 = 0.001$, $\zeta_2 = 0$, $\alpha_1 = 0.1$, $\delta_1 = 0$

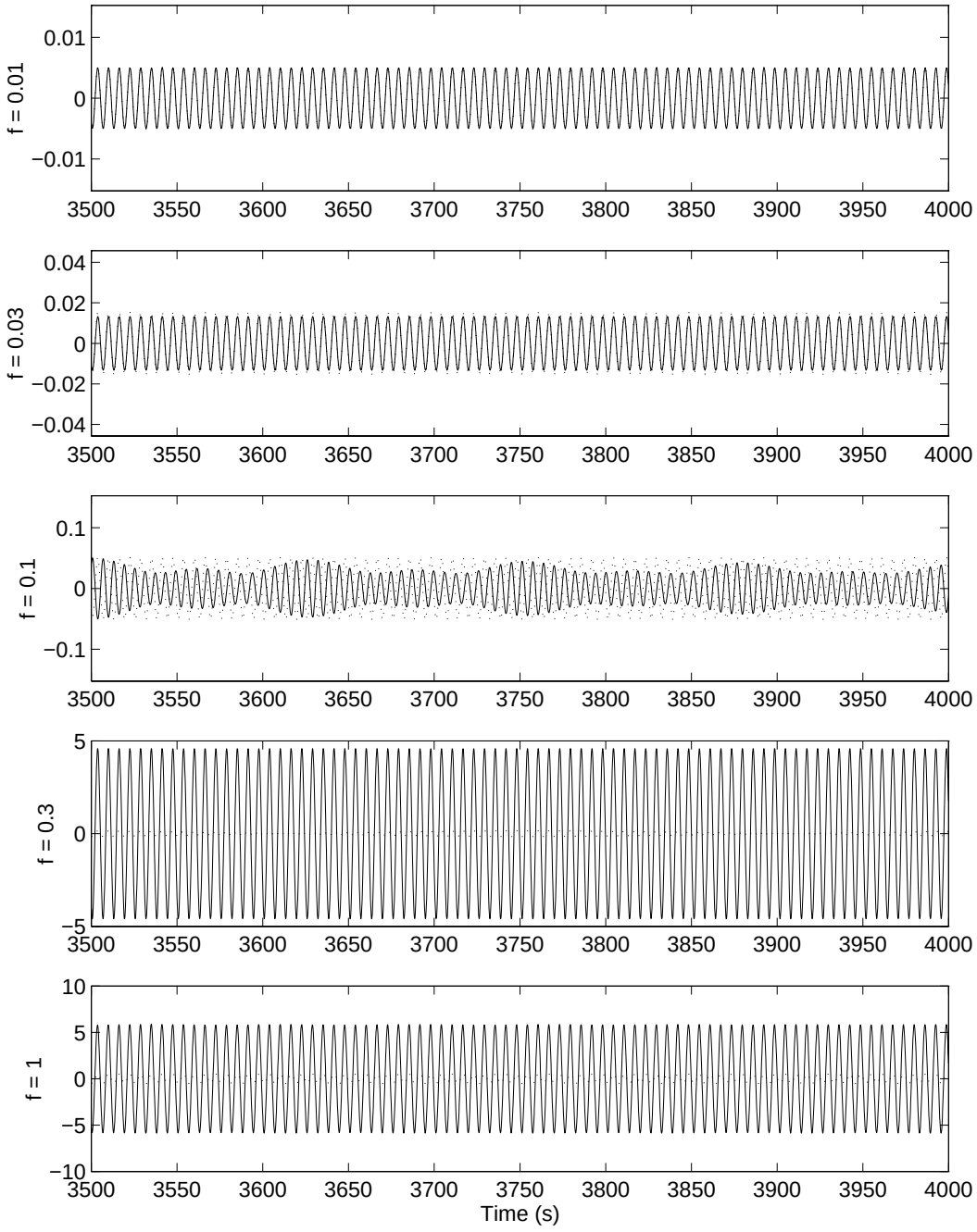

Figure 3.23: The NSNA response as f varies and $\sigma = 0.0025$ for $\alpha_3 = 0.01$ and $\delta_3 = 0.01$. System Parameters: $\zeta_1 = 0.001$, $\zeta_2 = 0$, $\alpha_1 = 0.1$, $\delta_1 = 0$

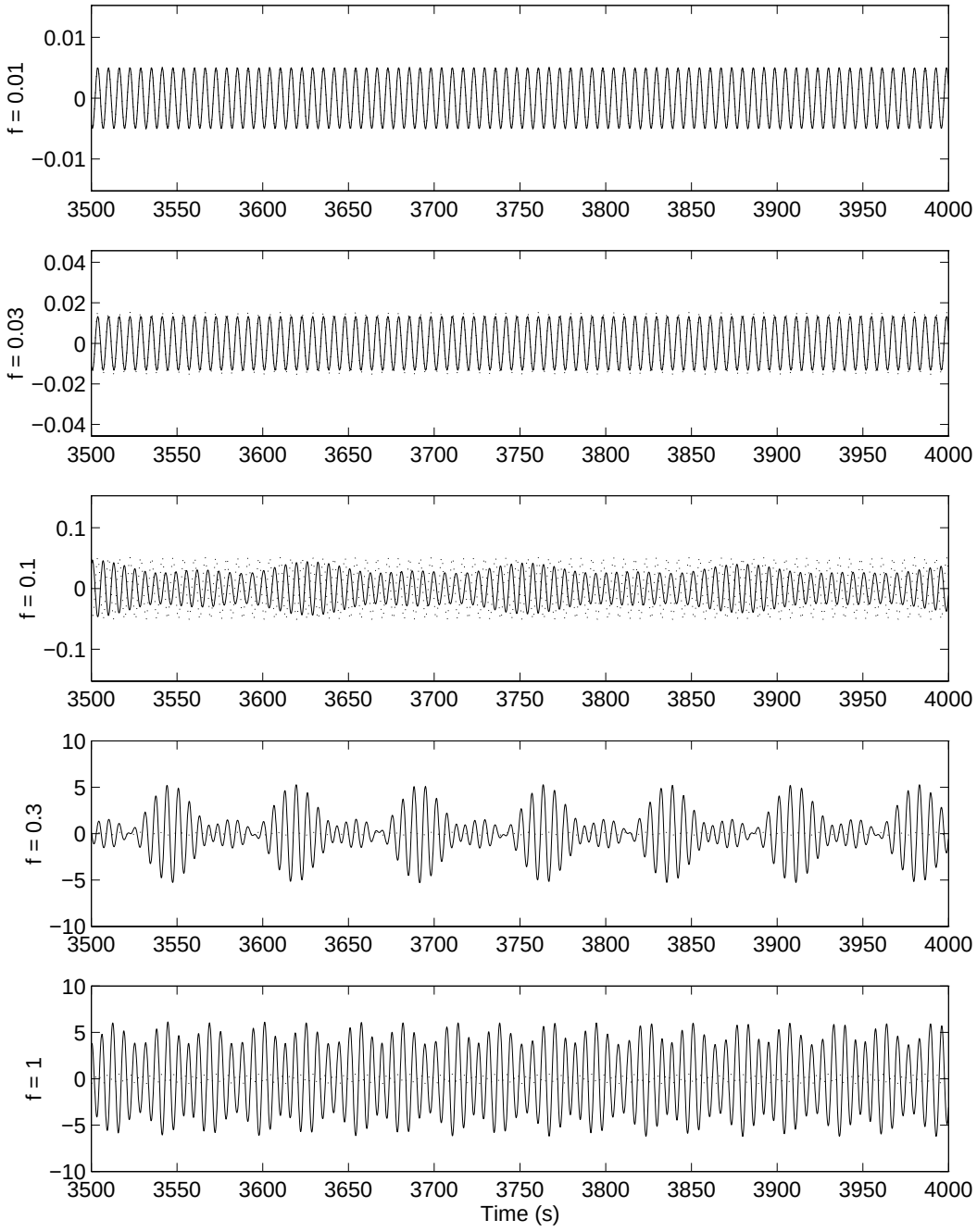

Figure 3.24: The NSNA response as f varies and $\sigma = 0.0025$ for $\alpha_3 = 0.01$ and $\delta_3 = -0.01$. System Parameters: $\zeta_1 = 0.001$, $\zeta_2 = 0$, $\alpha_1 = 0.1$, ,$\delta_1 = 0$

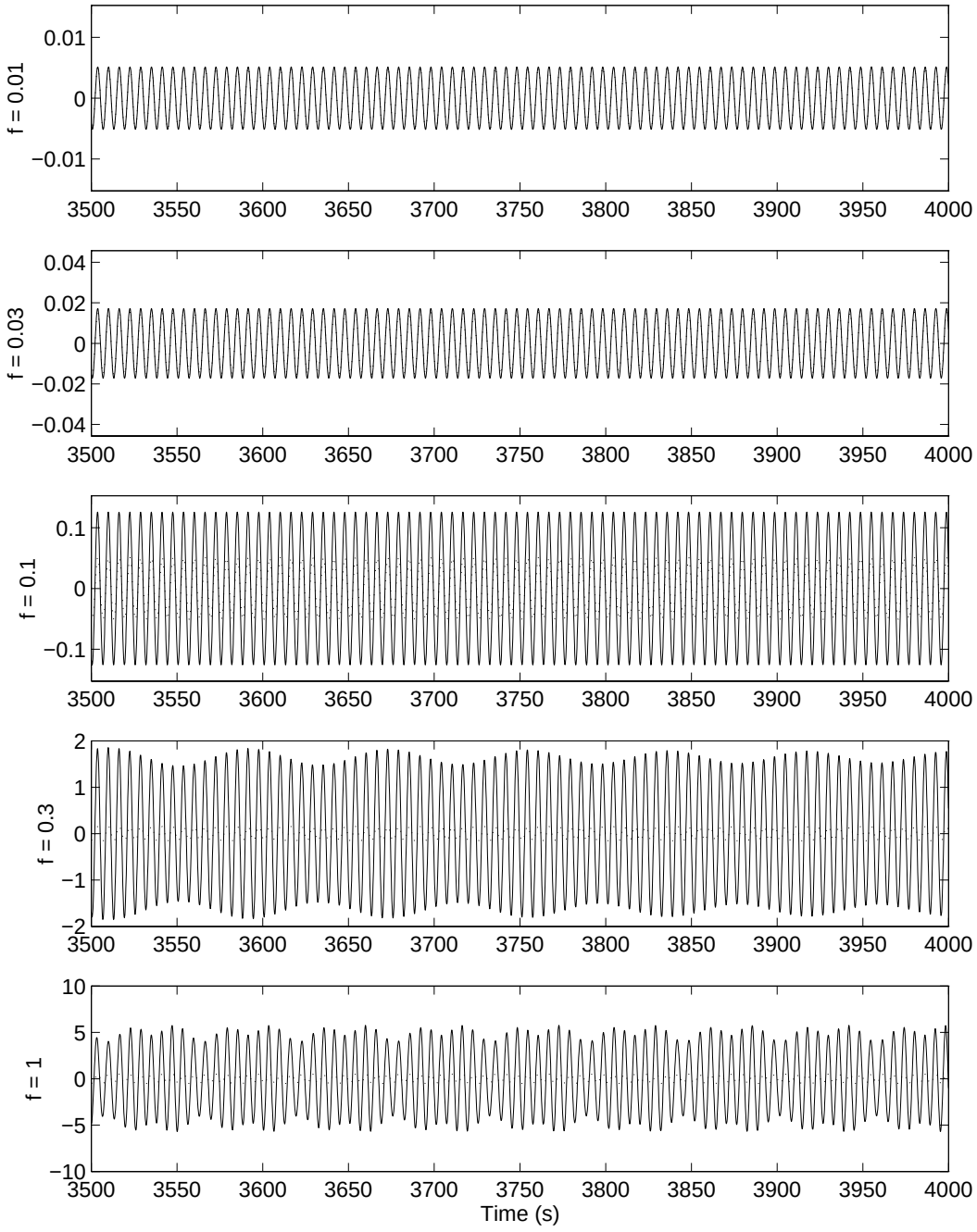

Figure 3.25: The NSNA response as f varies and $\sigma = 0.0025$ for $\alpha_3 = -0.01$ and $\delta_3 = 0.01$. System Parameters: $\zeta_1 = 0.001$, $\zeta_2 = 0$, $\alpha_1 = 0.1$, ,$\delta_1 = 0$

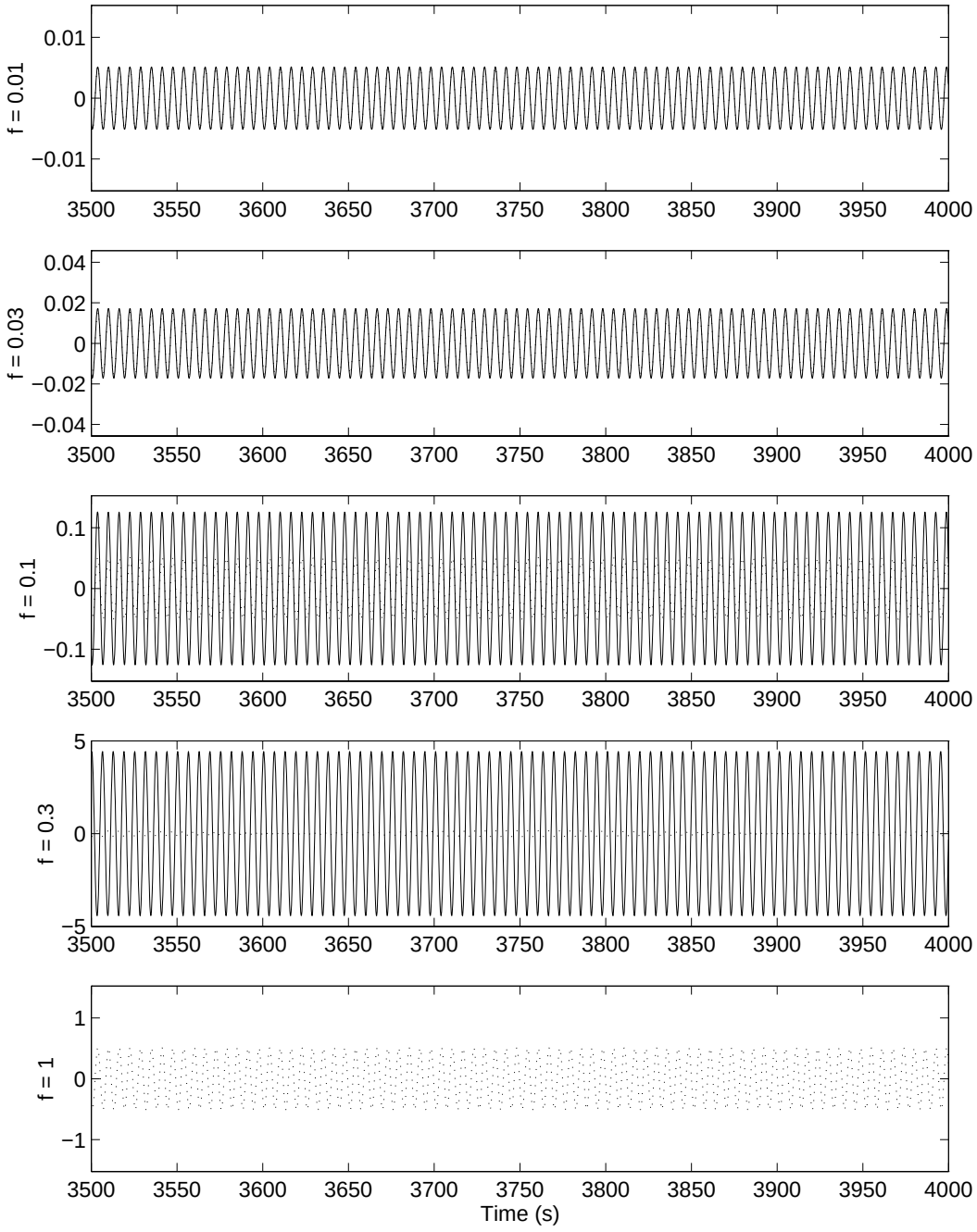

Figure 3.26: The NSNA response as f varies and $\sigma = 0.0025$ for $\alpha_3 = -0.01$ and $\delta_3 = -0.01$. System Parameters: $\zeta_1 = 0.001$, $\zeta_2 = 0$, $\alpha_1 = 0.1$, ,$\delta_1 = 0$

Time responses were again calculated and showed similar behavior to the LSNA results. Note that in Figure 3.26 the nonlinear response for $f = 1.0$ is not plotted. This case diverged at $t = 68$ sec., becoming unbounded. Realistically, other nonlinear terms would bound this behavior. Clearly these instabilities must be avoided for successful absorber design.

It is possible to achieve significant increases in absorber bandwidth with acceptable stability and robustness. For the softening nonlinear system with $\alpha_3 = -0.01$, $\zeta_1 = 0.0$, and linear coupling fixed as α_1=0, a nonlinear absorber was designed using the results of this chapter for a frequency of 1.05 rad/sec. For an undamped linear absorber, the suppression bandwidth would be 0.01 rad/sec. A nonlinear absorber was designed with $\delta_1 = 0.025$ and $\delta_3 = 0.017$. The absorber damping was set as $\zeta_2 = 0.002$ in both cases. The frequency response plots for $f = 0.2$ for both the linear and nonlinear absorber are shown in Figure 3.27. A close-up of the suppression region is plotted in Figure 3.28. From the plots, the suppression bandwidth (defined at -14dB) has more than doubled from 0.009 to 0.018 around 1.05 rad/sec by the introduction of nonlinearity in the absorber. Note that the unstable response of the nonlinear absorber is not within the bandwidth and both systems are single-valued within the suppression bandwidth.

3.6 Summary

Using the method of multiple scales, the unified vibration absorber equation can be transformed from the second order equations of motion into the first order modulation equations. These equations were then used to perform parameter studies using pseudo-arclength continuation with PSAL, a MATLAB® toolbox. The effects of the conventional nonlinear absorber design parameters on absorber performance have been considered.

Three key absorber performance qualities were identified: suppression bandwidth, stability (lack of quasiperiodic response) and robustness (lack of multiple solutions in the absorber bandwidth). If stability is lacking within the absorber bandwidth, the system will undergo large amplitude quasiperiodic motions. If multiple solutions are present, absorber

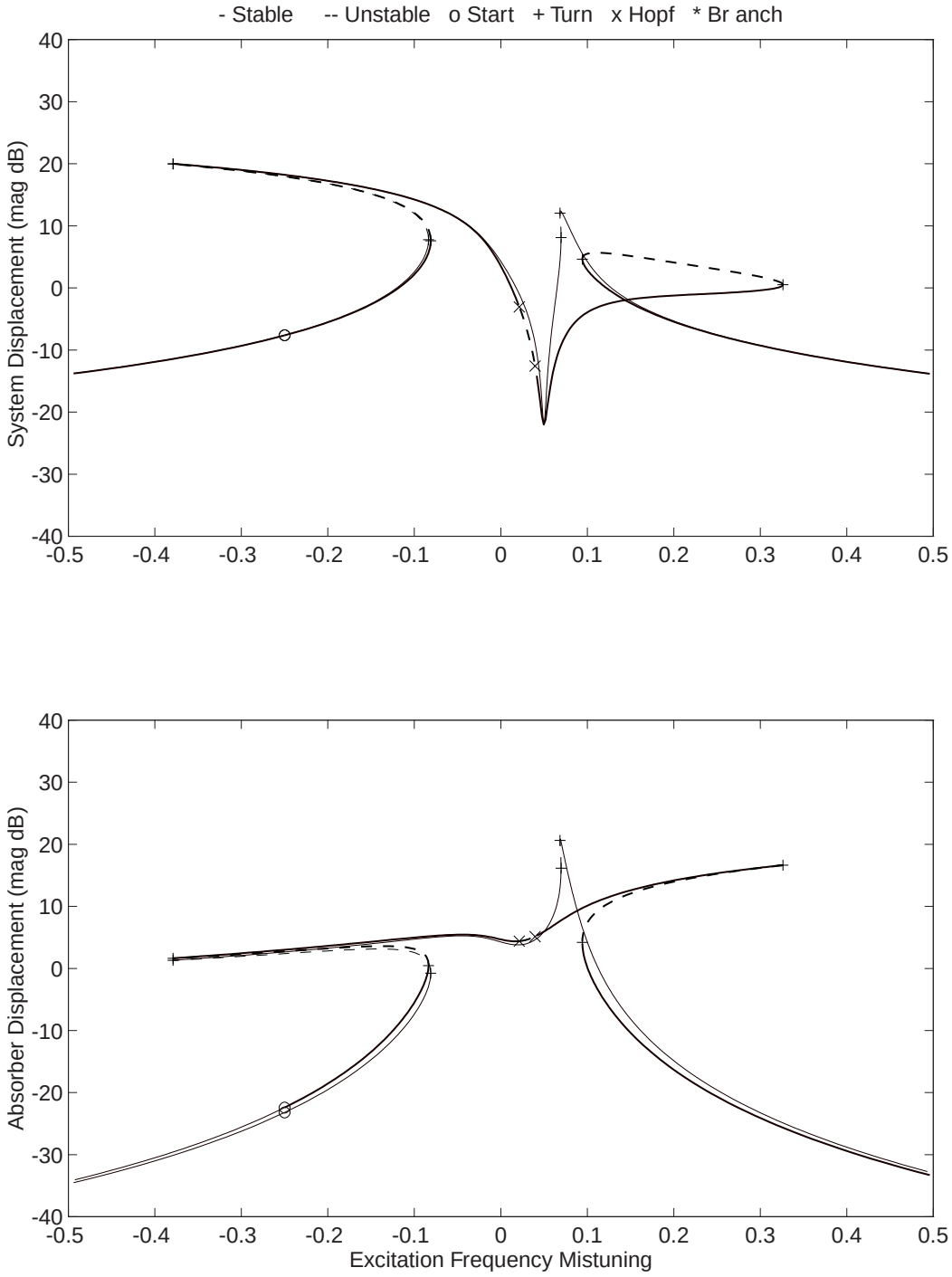

Figure 3.27: The NSNA response for $\delta_3 = -0.01$ and $\delta_1 = 0.025$ (thick lines) and the NSLA response for $\delta_3 = 0$ and $\delta_1 = 0.05$ (thin lines) System Parameters: $\zeta_1 = 0.01$, $\zeta_2 = 0.002$, $\alpha_1 = 0.1$, $\alpha_3 = -0.01$, $f = 0.2$

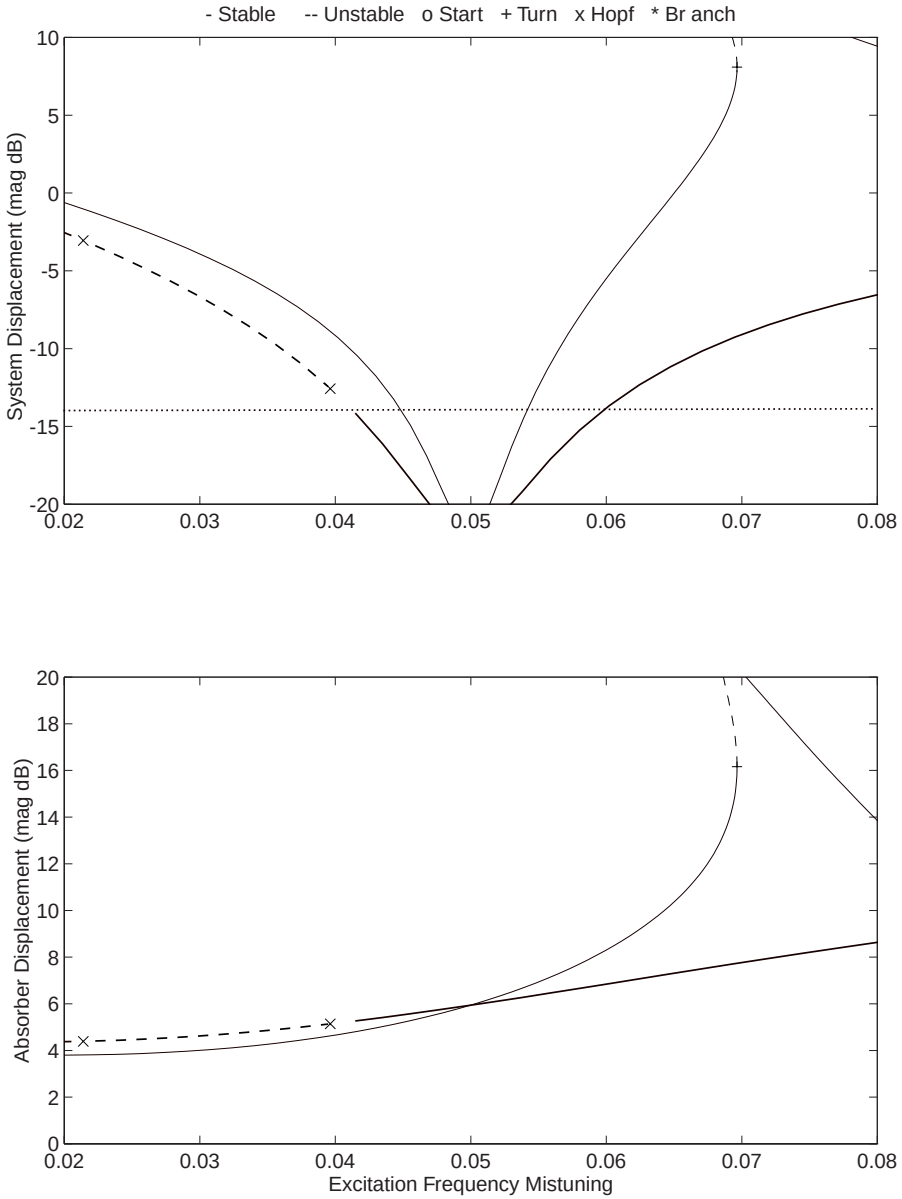

Figure 3.28: Closeup of the NSNA response for $\delta_3 = -0.01$ and $\delta_1 = 0.025$ (thick lines) and the NSLA response for $\delta_3 = 0$ and $\delta_1 = 0.05$ (thin lines) System Parameters: $\zeta_1 = 0.01$, $\zeta_2 = 0.002$, $\alpha_1 = 0.1$, $\alpha_3 = -0.01$, $f = 0.2$

performance becomes dependent on initial conditions. An impulse to the system could transfer performance from suppressed to resonant response. Good absorber performance depends on achieving acceptable absorber bandwidth with stability and robustness. The stability and robustness issues have received only passing discussion in the literature. The effect of absorber design parameters was considered using four systems: the LSLA, LSNA, NSLA, and NSNA.

First, the linear parameters (α_1,δ_1,ζ_1, and ζ_2) were examined. Increasing the linear coupling α_1 was determined to control the suppression bandwidth. As large a value of α_1 as possible should be used. Linear absorber frequency tuning is accomplished via δ_1 which controls the frequency of the linear absorber suppression bandwidth. Damping of the system ζ_1 has little effect on the suppression region, but reduces the resonant response significantly. Increased absorber damping, on the other hand, reduces and even eliminates the suppression bandwidth while simultaneously reducing resonant response of the system and the absorber stroke. It thus can be used to trade suppression bandwidth for strokelength and reduced resonant response.

The second system, the LSNA, examined the effect of the nonlinear absorber stiffness δ_3. Shifting of the suppression frequency was observed as the forcing level of the system varied. The suppression bandwidth increases with increased forcing provided $\delta_1\delta_3 \geq 0$. Otherwise, an initial decrease followed by an increase in the suppression bandwidth was noted. The increased performance does, however, come at a cost: the existence of quasiperiodic and chaotic motion within the absorber suppression region, affecting the stability of the design. Additionally, for $\delta_1\delta_3 < 0$ multivalued solutions were observed within the suppression region. Thus although the suppression bandwidth increases, the stability and robustness of the absorber enter as concerns.

The third system, the NSLA, demonstrated that nonlinear system stiffness was of concern for linear absorber performance. Although quasiperiodic response was observed, it was at resonance, outside of the suppression bandwidth. Robustness was however an issue. Multiple solutions were possible within the absorption region even for very low forcing

amplitudes. However, as demonstrated on the final system, the NSNA, use of a nonlinear absorber on a nonlinear system can address the robustness issue. For the NSNA system the issue of stability is similar to that of the LSNA.

Performance of the vibration absorber must account not only for suppression bandwidth, but also the stability and robustness of the design. Limited discussion of these effects was found in the literature. *Since the NSLA can have robustness issues, the designer must utilize a nonlinear absorber to achieve the more favorable behavior of the NSNA system as noted above.* Achieving an acceptable absorber design will result in a tradeoff between acceptable absorber bandwidth, tuning frequency and maximum disturbance levels. The performance of the nonlinear vibration absorber is complex. By systematically investigating the various effects, insight into the design have been gained. However, few real-world systems are single-degree-of-freedom and thus the performance of absorbers for N-degree-of-freedom systems was next considered.

Chapter 4

Performance of Vibration Absorbers for NDOF Systems

Having established performance criteria and a design approach for single-degree-of-freedom systems, N-degree-of-freedom systems were next considered. Motivated by the work of Slater [12, 14], an approach using nonlinear normal modes (NNM) was developed as follows:

i. Find the system equations of motion.

ii. Use Nonlinear Normal Modes to transform the equations of motion to modal coordinates.

iii. Design the vibration absorber in modal coordinates for the two- dimensional modal manifold being excited. (Note that it is assumed that the mode of interest is not in internal resonance.)

iv. Evaluate the response by transforming the modal coordinates back to physical coordinates using nonlinear normal mode theory.

To illustrate the design process, the example of Shaw and Pierre [10] is used. The system, Figure 4.1, consists of two equal masses connected with one nonlinear and two linear springs.

This example essentially outlines the procedure for absorber design for multi-degree-of-freedom discrete (or discretized continuous) systems. The concepts of nonlinear normal modes will be reviewed, then applied to vibration absorber design and an example presented.

4.1 Nonlinear Normal Modes

As discussed in Chapter 1, two definitions of Nonlinear Normal Modes are present in the literature: one due to Rosenberg [5–7] and another due to Shaw and Pierre [10, 11]. For this work the definition due to Shaw and Pierre and later extended by Slater [12, 14] is assumed. With this definition, a nonlinear normal mode is an invariant manifold tangent to the linear modal plane as the nonlinearity in the system decreases to zero. In the absence of internal resonance, each mode of the n-degree-of-freedom system

$$M_{ij}\ddot{x_j} = f_i(x_j, \dot{x_j}) \qquad\qquad i, j = 1, ..., n \tag{4.1}$$

is a two-dimensional manifold parametrized as:

$$x_i = X_i(u, v) \qquad and \qquad y_i = \dot{x}_i = Y_i(u, v) \tag{4.2}$$

The choice of u and v is arbitrary. Shaw and Pierre use the first physical coordinate, (x_1,y_1) whereas Nayfeh [8] first transforms the system using the linear eigenvectors and uses (q_k,p_k) where $p_k = \dot{q_k}$ to find the nonlinear normal mode tangent to the k^{th} linear mode. It should be noted that the form of the nonlinear stiffness on the manifold is dependent on the choice of reference coordinates. The dynamics described remain the same and transformation between definitions is possible. For the problem at hand, the modal coordinate approach proved simplest. Using standard tensor notation, the system equations

$$M_{ij}\ddot{x_j} + K_{ij}x_j + \epsilon N_i(x_j) = 0 \tag{4.3}$$

undergo a linear modal transformation,

$$x_i = \Phi_{ij}q_j \tag{4.4}$$

where the eigenvectors, Φ_{ij}, are normalized such that

$$M_ij\Phi_{ir}\Phi sj = \delta_{sr} \qquad and \qquad K_{ij}\Phi_{ir}\Phi_{sj} = \delta_{sr}\omega^2_{(r)} \tag{4.5}$$

The () on the index indicates summation is not performed on that term. The modal equations of motion are then

$$\ddot{q_j} + \omega^2_{(j)}q_j + \epsilon G_j(q) = 0 \tag{4.6}$$

where

$$G_j(q) = g_{jrst}q_rq_sq_t \tag{4.7}$$

is assumed for the form of the nonlinearities considered for this study. Using the method of multiple scales, we can solve for the nonlinear normal modes as in [8]. Expanding q_j as power series in ϵ

$$q_j = q_{j0} + \epsilon q_{j1} + ... \tag{4.8}$$

and defining time as

$$T_0 = t, T_1 = \epsilon t, ... \tag{4.9}$$

the equations may be ordered in ϵ to yield

$$D^2_0q_{j0} + \omega^2_{(j)}q_{j0} = 0 \tag{4.10a}$$

$$D^2_0q_{j1} + \omega^2_{(j)}q_{j1} = -2D_0D_1q_{j0} - g_{jrst}q_{r0}q_{s0}q_{t0} \tag{4.10b}$$

To construct the nonlinear normal mode which tends to the k$^{\text{th}}$ mode as $\epsilon -> 0$, let

$$q_{j0} = \begin{cases} A_ke^{i\omega_kT_0} + cc & j = k, \\ 0 & j \neq k. \end{cases} \tag{4.11}$$

in Equation (4.10b):

$$D^2_0q_{j1} + \omega^2_{(j)}q_{j1} = \begin{cases} -2D_0D_1q_{k0} - g_{kkkk}q^3_{k0} & j = k \\ -g_{jkkk}q^3_{k0} & j \neq k \end{cases} \tag{4.12}$$

Substituting Equation (4.11) into Equation (4.12) and eliminating secular terms, the response on the k$^{\text{th}}$ nonlinear normal mode is

$$q_j = \begin{cases} A_k e^{i\omega_k T_0} + \frac{g_{kkkk}}{8\omega_k^2} A_k^3 e^{3i\omega_k T_0} + cc + O(\epsilon)^2 & j = k \\ \frac{3g_{jkkk}}{\omega_k^2 - \omega_j^2} A_k^2 \bar{A}_k e^{i\omega_k T_0} + \frac{g_{kkkk}}{9\omega_k^2 - \omega_j^2} A_k^3 e^{3i\omega_k T_0} + cc + O(\epsilon)^2 & j \neq k \end{cases} \tag{4.13}$$

where

$$D_1 A_k = \frac{3i}{2\omega_k} g_{kkkk} A_k^2 \bar{A}_k \tag{4.14}$$

can be solved using standard perturbation techniques. To place this result in a more common form, express (see[8])

$$q_j = \begin{cases} u_k & j = k \\ \Gamma_1 jk q_k^3 + \Gamma_2 jk q_k \dot{q_k}^2 & j \neq k \end{cases} \tag{4.15}$$

with

$$\Gamma_1 jk = \frac{7\omega_k^2 - \omega_j^2}{(9\omega_k^2 - \omega_j^2)(\omega_k^2 - \omega_j^2)} g_{jkkk} \tag{4.16}$$

$$\Gamma_2 jk = \frac{6}{(9\omega_k^2 - \omega_j^2)(\omega_k^2 - \omega_j^2)} g_{jkkk} \tag{4.17}$$

This solution procedure is valid unless the k$^{\text{th}}$ mode is in internal resonance. For the undamped case presented here, the manifold is parametrized by the single variable q_k. This will not be true for nonconservative systems. However, for lightly damped and forced systems, the response of the system to harmonic forcing near the modal frequency will tend to the undamped nonlinear mode defined above [9, 14]. Using this result, the forced response of the vibration absorber attached to a forced and lightly damped structure can be analyzed.

4.2 NDOF absorber design

To model a vibration absorber coupled to an N-degree-of-freedom system, the same approach as in Chapter 2 can be followed. The equations of motion in physical coordinates

are

$$M_{ij}\ddot{x_j} + K_{ij}x_j + \epsilon N_i(x_j) - \epsilon A_i x_a = 0 \tag{4.18a}$$

$$m\ddot{x_a} + kx_a + \epsilon N_a x_a^3 - \epsilon B_i x_i = 0 \tag{4.18b}$$

Introducing the similarity transformation similar to the previous section,

$$x_i = \Phi_{ij} q_j \tag{4.19a}$$

$$x_a = \frac{1}{\sqrt{m}} q_a \tag{4.19b}$$

the equations can be rewritten in modal coordinates:

$$\ddot{q_j} + \omega_{(j)}^2 q_j + \epsilon g_{jrst} q_r q_s q_t - \epsilon \alpha_j q_a = 0 \tag{4.20a}$$

$$\ddot{q_a} + \omega_a^2 q_a + \epsilon g_a q_a^3 - \epsilon \beta_j q_j = 0 \tag{4.20b}$$

As in Chapter 3 the absorber is tuned to be near a resonance of the system. Thus $\omega_a = (1+\delta_1)\omega_k$ and a 1:1 internal resonance is formed between the absorber and the k^{th} mode. Note that $\beta_k = \alpha_k$. Applying the method of multiple scales, the equations can be transformed into a series of partial differential equations. The $O(\epsilon^0)$ equations are:

$$D_0^2 q_{j0} + \omega_{(j)}^2 q_{j0} = 0 \tag{4.21a}$$

$$D_0^2 q_{a0} + \omega_{(k)}^2 q_{a0} = 0 \tag{4.21b}$$

The solution for the k^{th} mode is

$$q_{j0} = \begin{cases} A_k e^{i\omega_k T_0} + cc & j = k \\ 0 & j \neq k \end{cases} \tag{4.22a}$$

$$q_{a0} = A_a e^{i\omega_k T_0} + cc \tag{4.22b}$$

The $O(\epsilon)$ equations are:

$$D_0^2 q_{j1} + \omega_{(j)}^2 q_{j1} = -2D_0 D_1 q_{j0} - g_{jrst} q_{r0} q_{s0} q_{t0} + \alpha_j q_{a0} \tag{4.23a}$$

$$D_0^2 q_{a1} + \omega_{(k)}^2 q_{a0} = -2D_0 D_1 q_{a0} - g_a q_{a0}^3 + \alpha_j q_{j0} \tag{4.23b}$$

Substituting Equations (4.22a)-(4.22b) into Equations (4.23a)-(4.23b),

$$D_0^2 q_{j1} + \omega_{(j)}^2 q_{j1} = \begin{cases} -2D_0 D_1 q_{k0} - g_{kkkk} q_{k0}^3 + \alpha_k q_{a0} & j = k \\ -g_{jkkk} q_{k0}^3 + \alpha_j q_{a0} & j \neq k \end{cases} \tag{4.24a}$$

$$D_0^2 q_{a1} + \omega_{(k)}^2 q_{a0} = -2D_0 D_1 q_{a0} - g_a q_{a0}^3 + \alpha_k q_{k0} \tag{4.24b}$$

Therefore, for a vibration absorber coupled to an NDOF system, the nonlinear modal response for an absorber coupled to the k$^{\text{th}}$ linear mode is

$$q_j = \begin{cases} A_k e^{i\omega_k T_0} + \frac{g_{kkkk}}{8\omega_k^2} A_k^3 e^{3i\omega_k T_0} + cc & j = k \\ \frac{3g_{jkkk} A_k^2 \bar{A}_k - \alpha_j A_a}{\omega_k^2 - \omega_j^2} e^{i\omega_k T_0} + \frac{g_{jkkk}}{9\omega_k^2 - \omega_j^2} A_k^3 e^{3i\omega_k T_0} + cc & j \neq k \end{cases} \tag{4.25a}$$

$$q_a = A_a e^{i\omega_k T_0} + \frac{g_a}{8\omega_k^2} A_a^3 e^{3i\omega_k T_0} + cc \tag{4.25b}$$

where

$$D_1 A_k = \frac{3ig_{kkkk}}{2\omega_k} A_k^2 \bar{A}_k - \frac{i\alpha_k}{2\omega_k} A_a \tag{4.26a}$$

$$D_1 A_a = \frac{3ig_a}{2\omega_k} A_a^2 \bar{A}_a - \frac{i\alpha_k}{2\omega_k} A_k \tag{4.26b}$$

These equations are identical to the solution for a single-degree-of-freedom system with a vibration absorber presented in Chapter 3 in the absence of external forcing and damping. The solution of the "absorbed" mode from Chapter 3 can be used to find (A_k,A_a) which were denoted (A_1,A_2).

Since the forced and lightly damped response will tend towards the nonlinear normal mode, nonlinear normal mode theory can be modified to include forcing and proportional damping. First Equations (4.20a)-(4.20b) are modified to include forcing and damping:

$$\ddot{q}_j + 2\zeta_{(j)}\ddot{q}_j + \omega_{(j)}^2 q_j + \epsilon g_{jrst} q_r q_s q_t - \epsilon\alpha_j q_a = \gamma_j q_f \tag{4.27a}$$

$$\ddot{q}_a + 2\zeta_a \dot{q}_a + \omega_a^2 q_a + \epsilon g_a q_a^3 - \epsilon\beta_j q_j = 0 \tag{4.27b}$$

$$\ddot{q}_f + \omega_f^2 q_f = 0 \tag{4.27c}$$

Note that in Equation (4.27c) the forcing has been written as a harmonic variable coupled to each mode (linearly) by γ_j, but not coupled to the force. Again allow $\omega_a = (1+\delta_1)\omega_k$ and set $\omega_f = (1+\sigma)\omega_k$ to to construct the response of the k$^{\text{th}}$ mode. Again $\beta_k = \alpha_k$. Applying the method of multiple scales, the equations can be transformed into a series of partial differential equations. The $O(\epsilon^0)$ equations are:

$$D_0^2 q_{j0} + \omega_{(j)}^2 q_{j0} = 0 \tag{4.28a}$$

$$D_0^2 q_{a0} + \omega_{(k)}^2 q_{a0} = 0 \tag{4.28b}$$

$$D_0^2 q_{f0} + \omega_{(k)}^2 q_{f0} = 0 \tag{4.28c}$$

The solution for the k$^{\text{th}}$ mode is

$$q_{j0} = \begin{cases} u = A_k e^{i\omega_k T_0} + cc & j = k \\ 0 & j \neq k \end{cases} \tag{4.29a}$$

$$q_{a0} = u_a = A_a e^{i\omega_k T_0} + cc \tag{4.29b}$$

$$q_{f0} = f_0 = \frac{f}{2} e^{i\omega_k T_0} + cc \tag{4.29c}$$

The $O(\epsilon)$ equations are:

$$D_0^2 q_{j1} + \omega_{(j)}^2 q_{j1} = -2D_0 D_1 q_{j0} - 2\zeta_{(j)}\omega_{(j)} D_0 q_{j0} - g_{jrst} q_{r0} q_{s0} q_{t0} + \alpha_j q_{a0} + \gamma_j q_{f0} \tag{4.30a}$$

$$D_0^2 q_{a1} + \omega_{(k)}^2 q_{a0} = -2D_0 D_1 q_{a0} - 2\zeta_a \omega_{(k)} D_0 q_{a0} - g_a q_{a0}^3 + \alpha_j q_{j0} \tag{4.30b}$$

$$D_0^2 q_{f1} + \omega_{(k)}^2 q_{f1} = -2D_0 D_1 q_{f0} \tag{4.30c}$$

Substituting Equations (4.29a)-(4.29b) into Equations (4.30a)-(4.30c),

$$D_0^2 q_{j1} + \omega_{(j)}^2 q_{j1} = \begin{cases} -2D_0 D_1 u_0 - 2\zeta_k D_0 u_0 - g_{kkkk} u_0^3 + \alpha_k u_a + \gamma_k f_0 & j = k \\ -g_{jkkk} u^3 + \alpha_j u_a 0 & j \neq k \end{cases} \tag{4.31a}$$

$$D_0^2 q_{a1} + \omega_{(k)}^2 q_{a1} = -2D_0 D_1 u_a - 2\zeta_a D_0 u_a - g_a u_a^3 + \alpha_k u_0 \tag{4.31b}$$

$$D_0^2 q_{f1} + \omega_{(k)}^2 q_{f1} = -2D_0 D_1 f_0 - 2\sigma f_0 \tag{4.31c}$$

the nonlinear normal mode which reduces to the k$^{\text{th}}$ linear mode can be found. Noting

$$2u^3 = [u_0^3 - \frac{u_0 \dot{u}_0^2}{\omega_k^2}] + [u_0^3 + \frac{u_0 \dot{u}_0^2}{\omega_k^2}] \tag{4.32}$$

where the first bracketed term is harmonic with frequency $3\omega_k$ while the second term is harmonic with frequency ω_k, the nonlinear normal mode can be expressed:

$$q_j = \begin{cases} u_0 + \frac{g_{kkkk}}{16\omega_k^2}(u_0^3 - \frac{u_0 \dot{u}_0^2}{\omega_k^2}) & j = k \\ \frac{\alpha_j}{(\omega_j^2 - \omega_k^2)} u_a - \frac{g_{jkkk}}{2(\omega_j^2 - 9\omega_k^2)}(u_0^3 - \frac{u_0 \dot{u}_0^2}{\omega_k^2}) - \frac{3g_{jkkk}}{2(\omega_j^2 - \omega_k^2)}(u_0^3 + \frac{u_0 \dot{u}_0^2}{\omega_k^2}) + \frac{\gamma_j}{\omega_j^2 - \omega_k^2} q_f & j \neq k \end{cases} \tag{4.33a}$$

$$q_a = u_a + \frac{g_a}{16\omega_k^2}(u_a^3 - \frac{u_a \dot{u}_a^2}{\omega_k^2}) \tag{4.33b}$$

$$q_f = \frac{f}{2} e^{i\omega_k(T_0 + \sigma T_1) + \phi_0} + cc \tag{4.33c}$$

The dynamics on the manifold are:

$$\ddot{u}_0 + 2\zeta_k \omega_k \dot{u}_0 + \omega_k^2 u_0 + g_{kkkk} u_0^3 - \alpha_k u_a = \frac{f}{2} e^{i\omega_k(T_0 + \sigma T_1) + \phi_0} + cc \tag{4.34a}$$

$$\ddot{u}_a + 2\zeta_a \omega_k \dot{u}_a + (1 + 2\delta)\omega_k^2 u_a + g_a u_a^3 - \alpha_k u_0 = 0 \tag{4.34b}$$

These are identical to the equations of a vibration absorber on a single-degree-of-freedom system derived in Chapter 2.

Having solved for the k$^{\text{th}}$ mode solution, the l$^{\text{th}}$ mode solution is now derived to determine the effect of the vibration absorber on the other modes of the structure. The solution to Equations (4.27a)-(4.27c) for the l$^{\text{th}}$ mode is

$$q_{j0} = \begin{cases} u_l = A_l e^{i\omega_l T_0} + cc & j = l \neq k \\ 0 & j \neq l \end{cases} \tag{4.35a}$$

$$q_{a0} = 0 \tag{4.35b}$$

$$q_{f0} = 0 \tag{4.35c}$$

The $O(\epsilon)$ equations of motion thus are

$$D_0^2 q_{j1} + \omega_{(}j)^2 q_{j1} = \begin{cases} -2D_0 D_1 u_l - 2\zeta_l \omega_l D_0 u_l - g_{lll} u_l^3 & j = l \neq k \\ -g_{jlll} u_l^3 & j \neq l \end{cases} \tag{4.36a}$$

$$D_0^2 q_{a1} + \omega_{(}k)^2 q_{a1} = \alpha_l u_l D_0^2 q_{f1} + \omega_{(}k)^2 q_{f1} \qquad = 0 \tag{4.36b}$$

The dynamics of the l^{th} nonlinear mode are thus unaffected by the presence of the vibration absorber tuned to the k^{th} mode (in the absence of a k-l internal resonance). They represent the free response of a nonlinear single-degree-of-freedom system

$$\ddot{u}_l + 2\zeta_l \omega_l \dot{u}_l + \omega_l^2 u_l + g_{lll} u_l^3 = 0 \tag{4.37}$$

For steady state solutions these solutions will decay to zero for positive damping. *The design of a nonlinear vibration absorber for a nonlinear N-degree-of-freedom system therefore reduces to that of the single-degree-of-freedom design presented in Chapter 3.* To verify this result, a nonlinear two-degree-of-freedom system used in [10] was examined.

4.3 Example: 2DOF Shaw & Pierre System

The two-mass, three-spring system shown in Figure 4.1 was used in [10] and later by subsequent authors [9, 12, 14, 52] to illustrate the concept of nonlinear normal modes. Herein it is used to illustrate the design procedure developed in the previous section. The equations of motion of the 2DOF system with a vibration absorber attached to mass 1 and external forcing applied to mass 2 are:

$$M\ddot{X}_1 + C\dot{X}_1 - C_a\dot{X}_a + 2KX_1 - KX_2 + NX_1^3 - K_aX_a - N_aX_a^3 = 0 \tag{4.38a}$$

$$M\ddot{x}_2 + C\dot{x}_2 + 2KX_2 - KX_1 = F \tag{4.38b}$$

$$M_a(\ddot{X}_a + \ddot{X}_1) + C_a\dot{X}_a + K_aX_a + N_aX_a^3 = 0 \tag{4.38c}$$

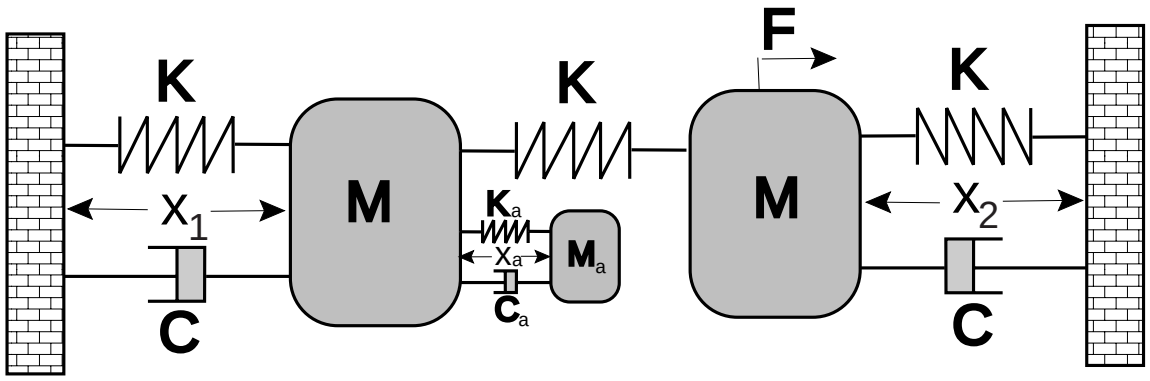

Figure 4.1: 2DOF Nonlinear System

Following the methodology outlined in Chapter 2, these equations can be nondimensionalized and written

$$\ddot{x_1} + 2\epsilon c\dot{x_1} + 2x_1 - x_2 + \epsilon n x_1^3 - \epsilon\alpha x_a - \epsilon n_a x_a^3 = 0 \tag{4.39a}$$

$$\ddot{x_2} + 2\epsilon c\dot{x_2} + 2x_2 - x_1 = f \tag{4.39b}$$

$$\ddot{x_a} + 2\epsilon c_a\dot{x_a} + (1 + 2\epsilon\delta_1)x_a + \epsilon n_a x_a^3 + 2\epsilon\alpha x_1 - \epsilon\alpha x_2 = 0 \tag{4.39c}$$

where the following parameters were defined:

$$\begin{array}{cccc} t = \omega T & c = \frac{C}{2\sqrt{KM}} & \omega = \sqrt{\frac{K}{M}} & n = \frac{N}{K} \\ \alpha = \sqrt{\frac{M_a}{M}} & f = \frac{F}{K} & c_a = \frac{C_a}{2\sqrt{K_a M_a}} & \omega_a = \sqrt{\frac{K_a}{M_a}} \\ n_a = \frac{N_a}{\alpha^2 K} & (1+\delta) = \frac{\omega_a}{\omega} & x_i = X_i & x_a = \alpha X_a \end{array} \tag{4.40}$$

These equations are of the form assumed in the previous section. Applying the modal transform

$$\left\{ \begin{array}{c} x_1 \\ x_2 \\ x_a \end{array} \right\} = \left[\begin{array}{ccc} \frac{1}{\sqrt{2}} & \frac{1}{\sqrt{2}} & 0 \\ \frac{1}{\sqrt{2}} & -\frac{1}{\sqrt{2}} & 0 \\ 0 & 0 & 1 \end{array} \right] \left\{ \begin{array}{c} q_1 \\ q_2 \\ q_a \end{array} \right\} \tag{4.41}$$

the equations are transformed into (linear) modal coordinates:

$$\ddot{q}_1 + 2\zeta_1\dot{q}_1 + q_1 - \epsilon\frac{\alpha}{\sqrt{2}}q_a + \epsilon\frac{n}{4}(q_1+q_2)^3 = \frac{f}{\sqrt{2}} \tag{4.42a}$$

$$\ddot{q}_2 + 2\sqrt{3}\zeta_2\dot{q}_2 + 3q_2 - \epsilon\frac{\alpha}{\sqrt{2}}q_a + \epsilon\frac{n}{4}(q_1+q_2)^3 = -\frac{f}{\sqrt{2}} \tag{4.42b}$$

$$\ddot{q}_a + 2\zeta_a\dot{q}_a + (1+2\delta)q_a - \epsilon\frac{\alpha}{\sqrt{2}}q_1 - \epsilon\frac{3\alpha}{\sqrt{2}}q_2 + \epsilon n_a q_a^3 = 0 \tag{4.42c}$$

Applying the results of the previous section, the nonlinear normal mode of interest is:

$$q_1 = u - \frac{n}{64}(u^3 - u\dot{u}^2) \tag{4.43a}$$

$$q_2 = \frac{\alpha}{2\sqrt{2}}u_a - \frac{n}{48}(u^3 - u\dot{u}^2) - \frac{3n}{16}(u^3 + u\dot{u}^2) - \frac{f}{2} \tag{4.43b}$$

$$q_a = u_a + \frac{n_a}{16}(u_a^3 - u_a\dot{u}^2) \tag{4.43c}$$

with the dynamics on the manifold:

$$\ddot{u} + \zeta_1\dot{u} + u + \epsilon\frac{n}{4}u^3 - \epsilon\frac{\alpha}{\sqrt{2}}u_a = \frac{f}{\sqrt{2}} \tag{4.44a}$$

$$\ddot{u}_a + \zeta_a\dot{u}_a + u_a + \epsilon n_a u_a^3 - \epsilon\frac{\alpha}{\sqrt{2}}u = 0 \tag{4.44b}$$

Here u and u_a represent the manifold coordinates. The solution to these equations was examined in the previous chapter. To evaluate the performance of the nonlinear normal mode approach, time integration was used. Assuming $n = -0.04$, $n_a = 0.01$, $\zeta_1 = 0.01$, $\alpha_1 = 0.1\sqrt(2)$, Equations (4.44a)-(4.44b) were integrated numerically using MATLAB® , and compared with direct integration of the equations of motion in physical coordinates and the $O(\epsilon)$ correct modal coordinates. Various harmonic forcing amplitudes were considered for a frequency of 1.0 rad/s. Results are plotted in Figures 4.2-4.13 for both the calculated physical coordinates, X_i, and the linear modal coordinates, q_i. All integrations were performed from rest, and both the initial response and the steady state response are plotted as indicated on the figure captions.

Examining Figures 4.2-4.5, several observations can be made. First, the qualitative responses of the figures are similar. All responses appear harmonic. Second, the transient

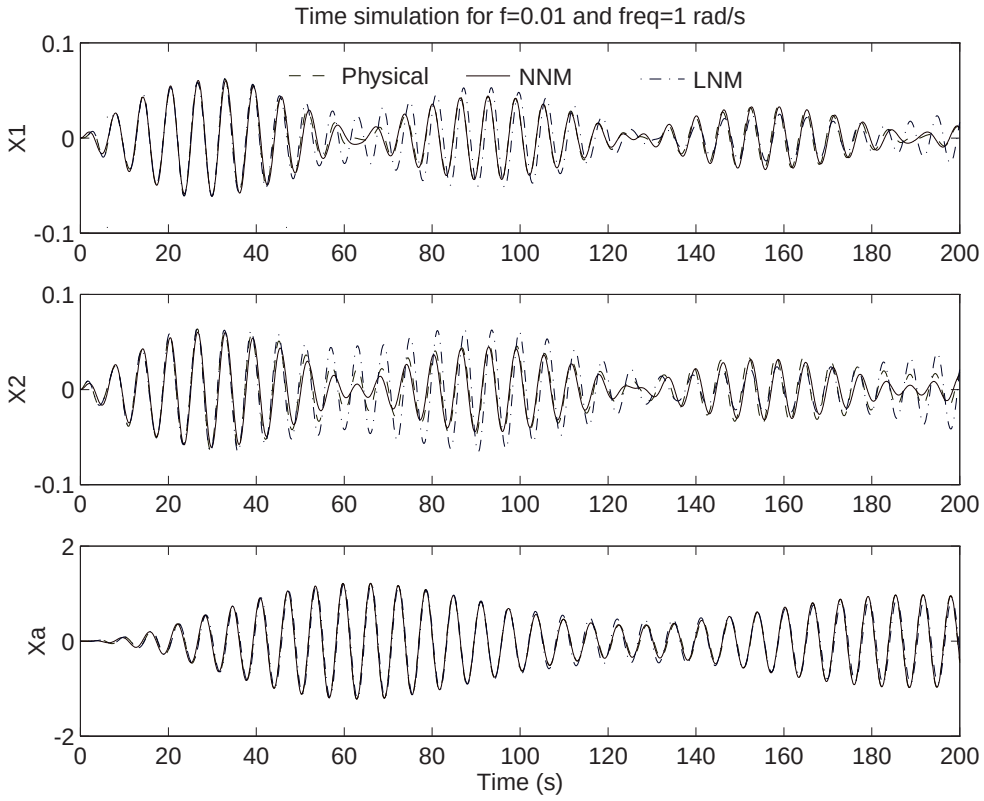

Figure 4.2: Transient response of the 2DOF system in physical coordinates for $f = 0.01$ and $\sigma = 0$.

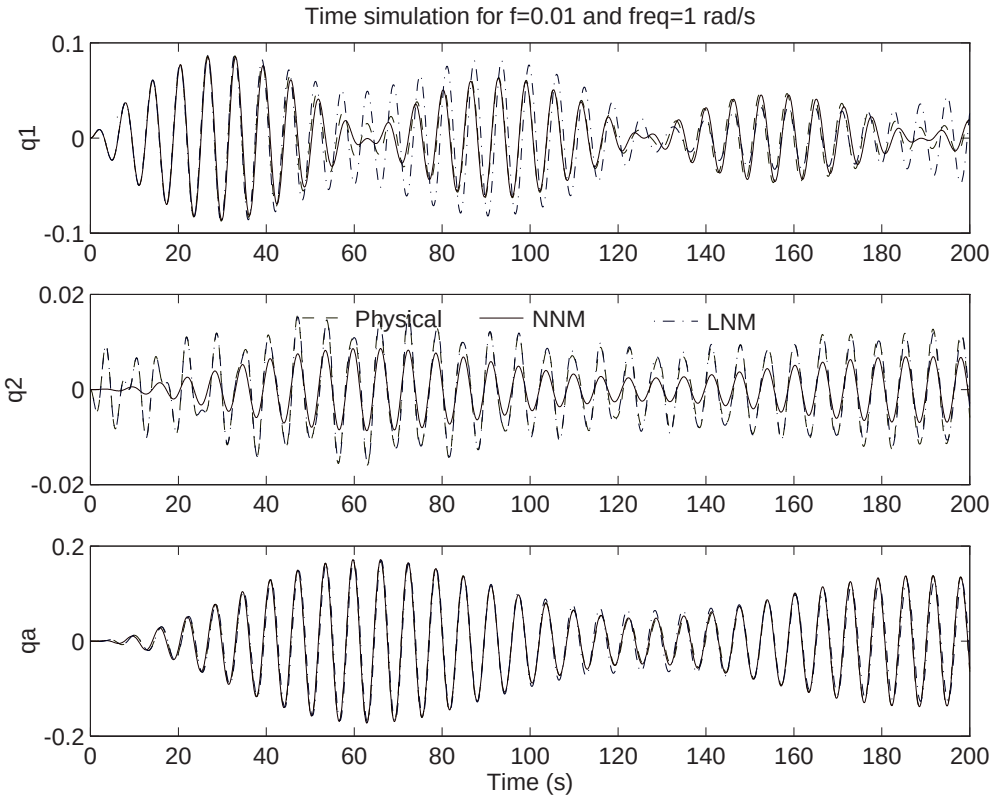

Figure 4.3: Transient response of the 2DOF system in modal coordinates for $f = 0.01$ and $\sigma = 0$.

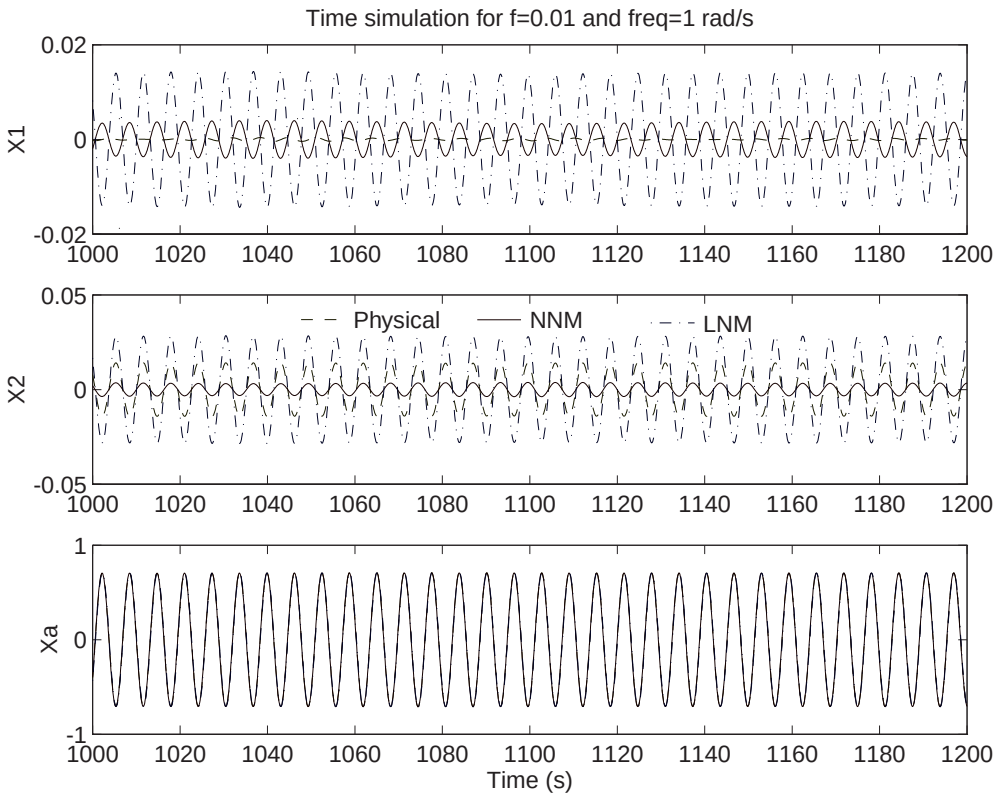

Figure 4.4: Steady-state response of the 2DOF system in physical coordinates for $f = 0.01$ and $\sigma = 0$.

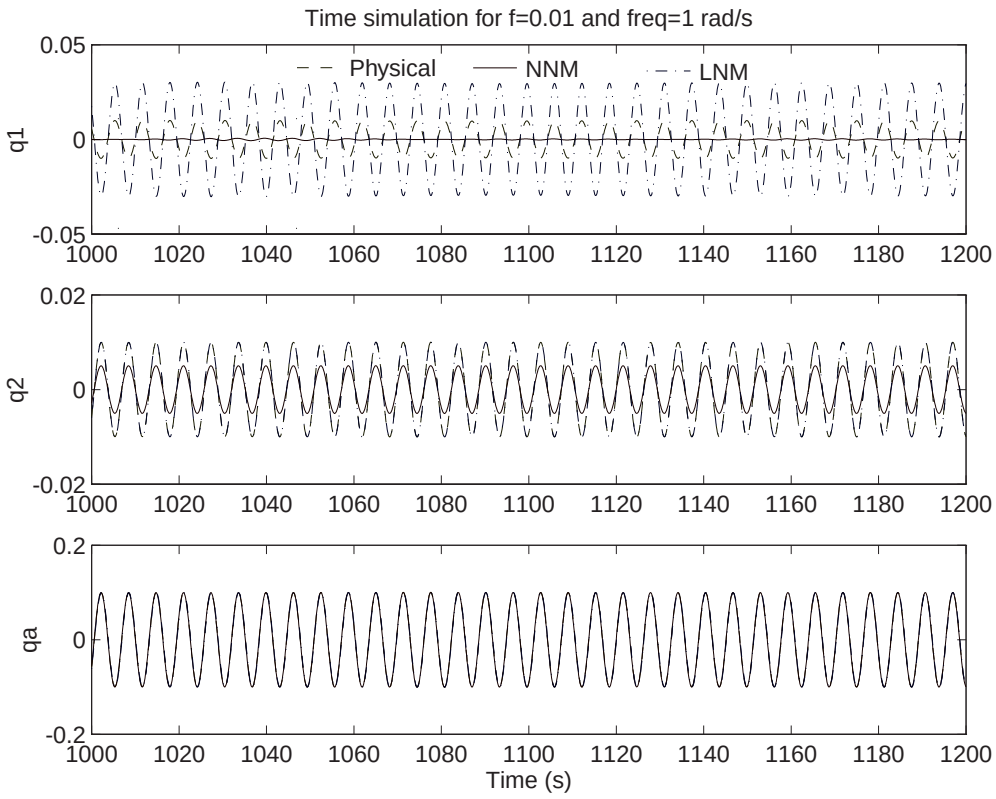

Figure 4.5: Steady-state response of the 2DOF system in modal coordinates for $f = 0.01$ and $\sigma = 0$.

responses for all three cases agree well for both q_1 and q_a, but the present nonlinear normal mode response is off. This makes physical sense since the present approach considers the solution only within the manifold of the first mode. The initial conditions are not on that manifold since on the manifold the system is at rest only if $f = 0$. As time progresses, the three responses deviate. This results from the approximations made. Recall that the slower time scales in the application of the method of multiple scales were not present in this order of analysis. The transient results for the physical coordinates demonstrate similar results, except the motion of X_2 is in agreement. This validates the assumption that the second mode, q_2, does not participate in the response to a large extent.

Examining the steady state results between t=1000s and 1200s, the agreement of the three models is poor. Physically, the reason for this is that the width of the suppression bandwidth is an $O(\epsilon^2)$ quantity. The nonlinear normal mode analysis predicts that the suppression bandwidth lies centered near 1 rad/s. Thus examining Figure 4.5, the NNM model predicts suppressed response. However the presence of the second mode has shifted the suppression bandwidth slightly. This is not captured by the present analysis. The present analysis therefore only provides qualitative agreement with the physical model. To achieve quantitative agreement for multi-mode systems, an $O(\epsilon^2)$ analysis would be required. Note that both the second mode and absorber displacements are in reasonable agreement. This is because these responses are not as sensitive to the slight shifting of the suppression bandwidth. The responses in physical coordinates shown in Figure 4.4 display similar information.

Increasing the forcing level to $f = 0.1$, the agreement between the present model and the physical model improves as shown in Figures 4.6-4.9. Again, the absorber response is in excellent agreement while the system response, although in better agreement, shows some improvement. Recall that as the excitation level increases, the suppression region shifts higher in frequency away from the 1 rad/s forcing responses plotted. The sensitivity of the system decreases with increased distance from this region, so improved results can be expected. Otherwise, similar observations can be made from these plots. Note that the

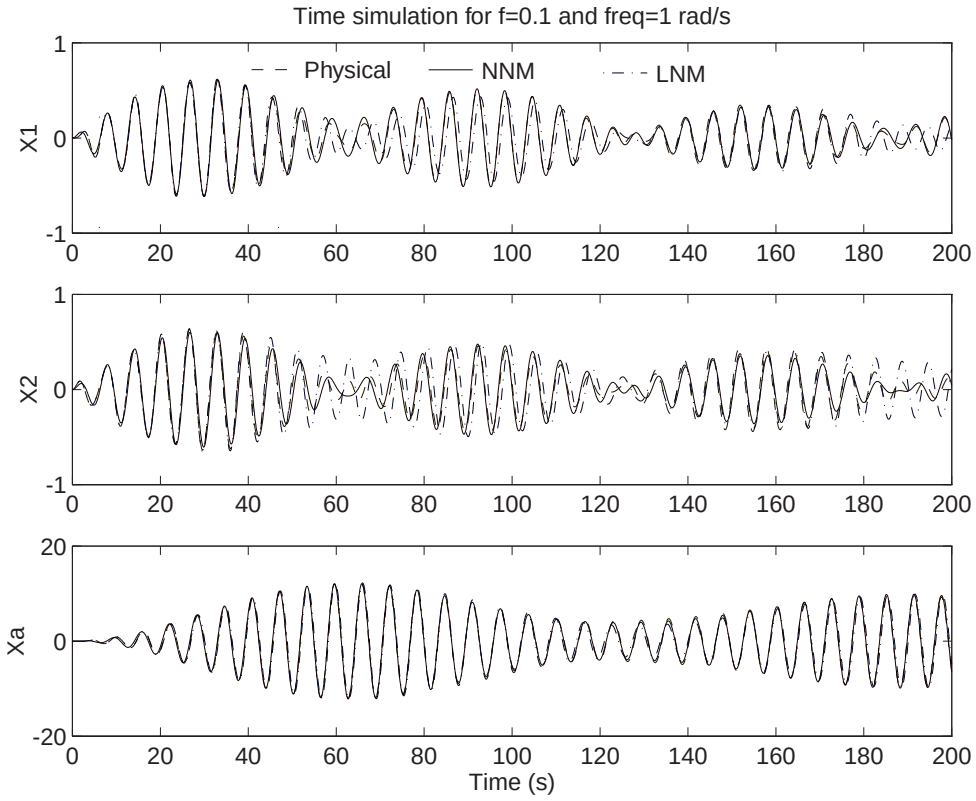

Figure 4.6: Transient response of the 2DOF system in physical coordinates for $f = 0.1$ and $\sigma = 0$.

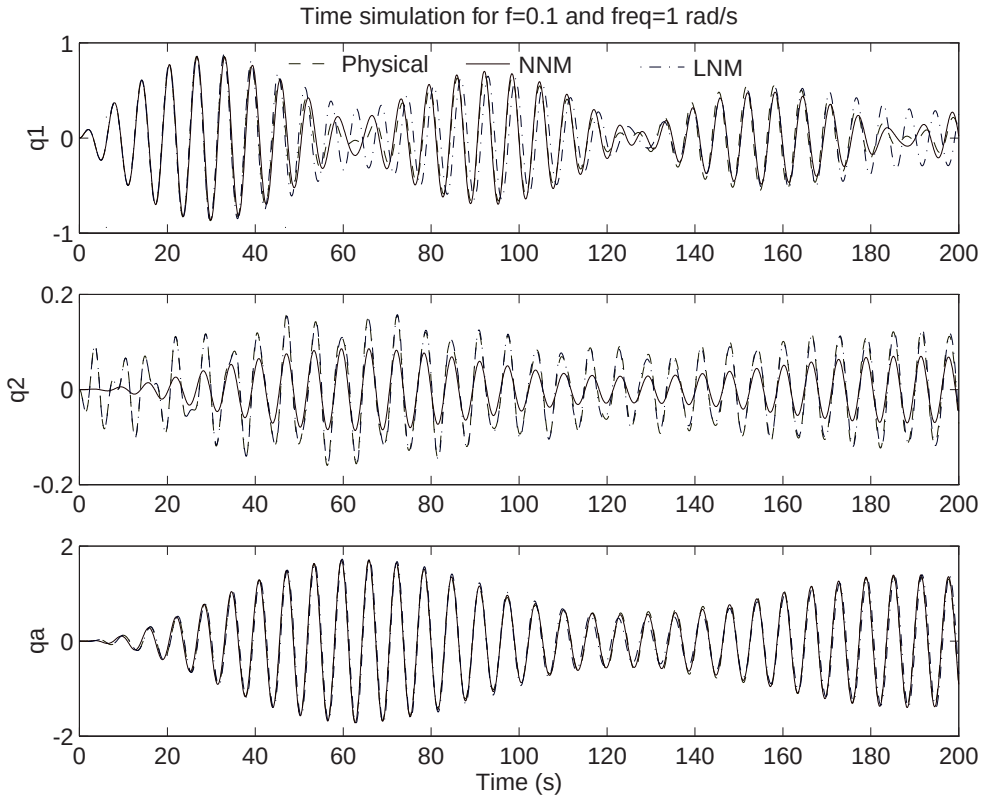

Figure 4.7: Transient response of the 2DOF system in modal coordinates for $f = 0.1$ and $\sigma = 0$.

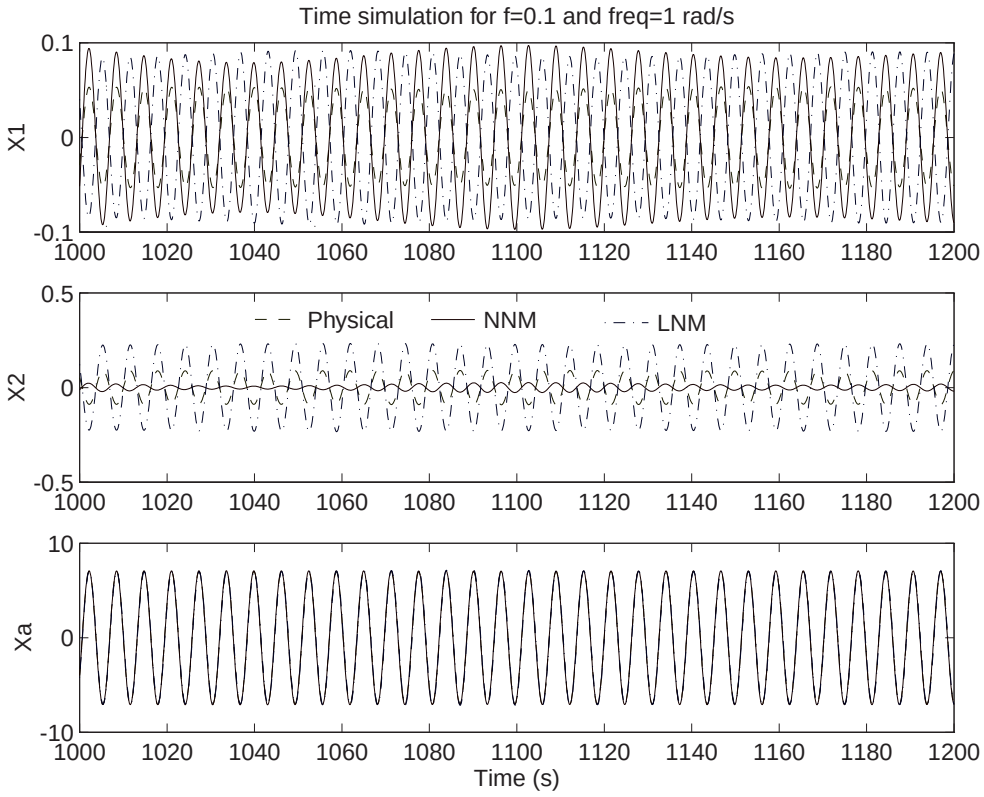

Figure 4.8: Steady-state response of the 2DOF system in physical coordinates for $f = 0.1$ and $\sigma = 0$.

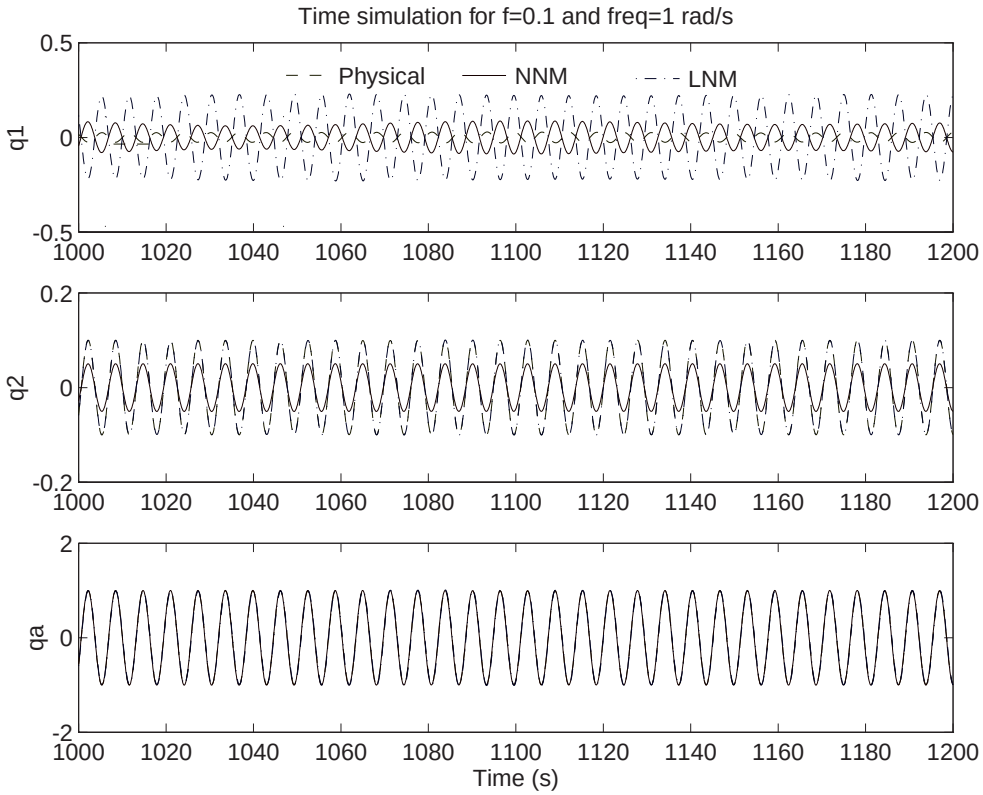

Figure 4.9: Steady-state response of the 2DOF system in modal coordinates for $f = 0.1$ and $\sigma = 0$.

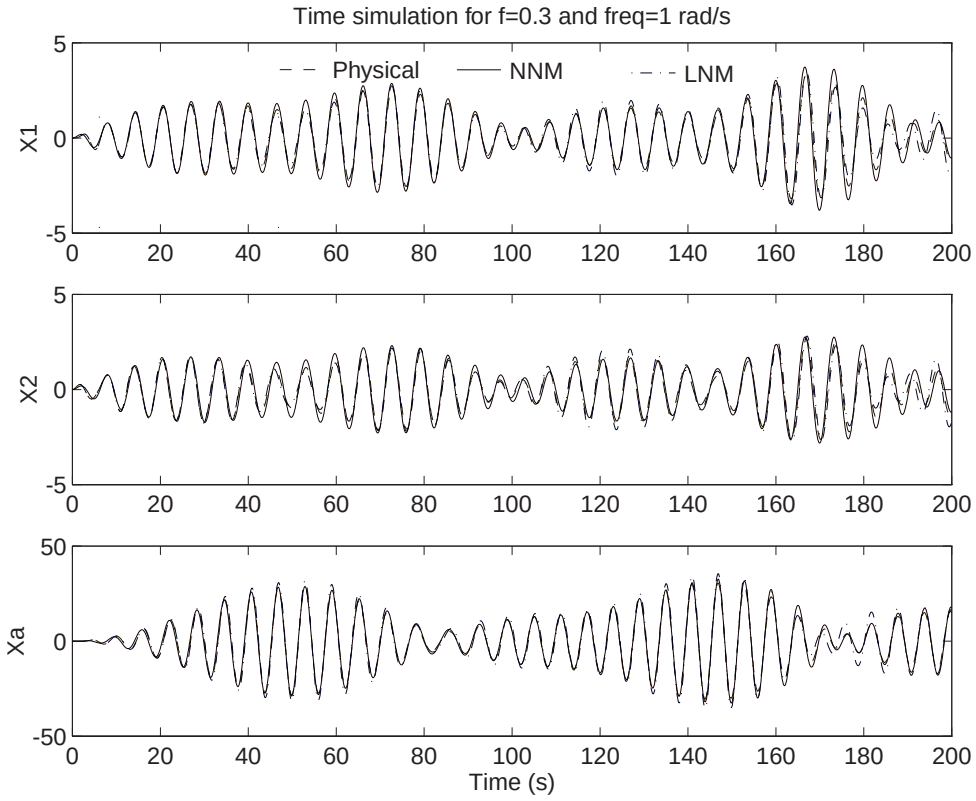

Figure 4.10: Transient response of the 2DOF system in physical coordinates for $f = 0.1$ and $\sigma = 0$.

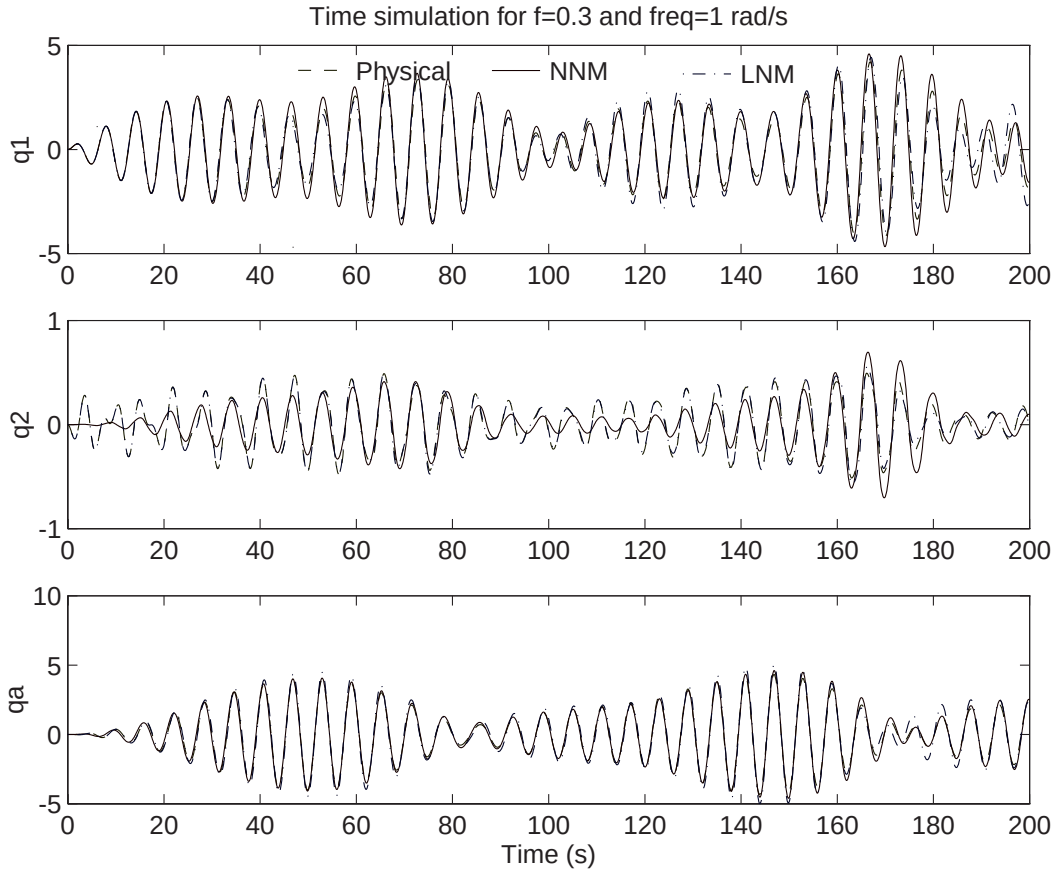

Figure 4.11: Transient response of the 2DOF system in modal coordinates for $f = 0.1$ and $\sigma = 0$.

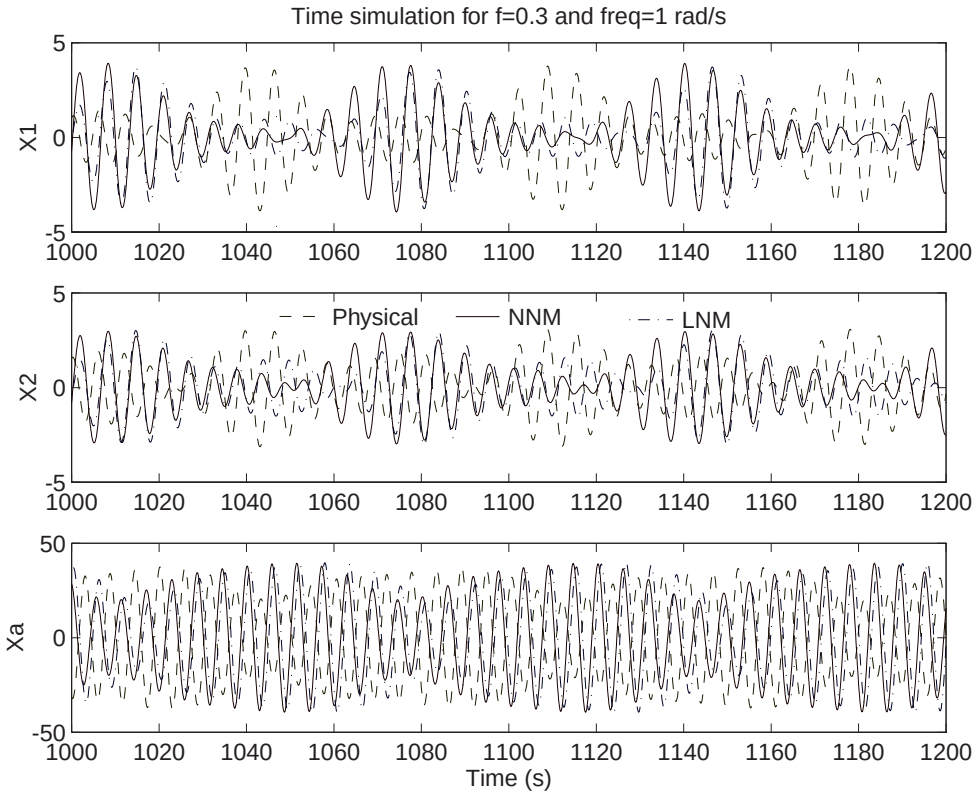

Figure 4.12: Steady-state response of the 2DOF system in physical coordinates for $f = 0.1$ and $\sigma = 0$.

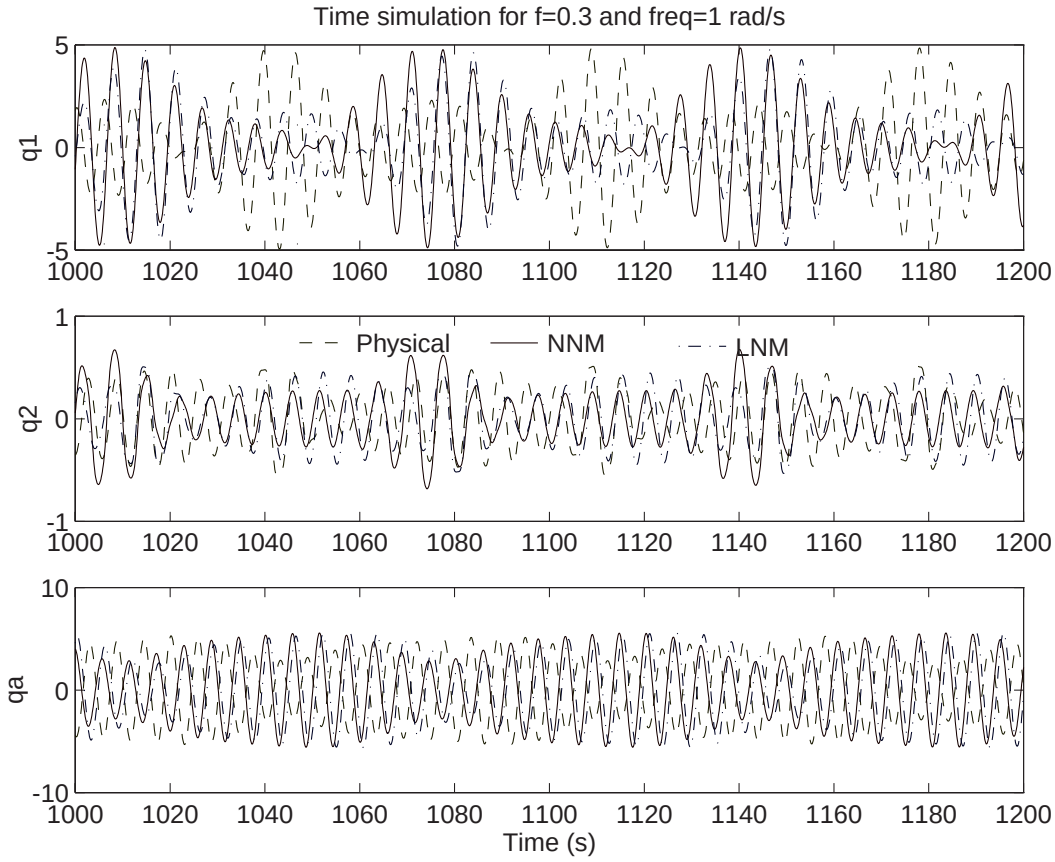

Figure 4.13: Steady-state response of the 2DOF system in modal coordinates for $f = 0.1$ and $\sigma = 0$.

steady state is periodic in all three models.

Increasing the forcing level further to $f = 0.3$ shows even better agreement as plotted in Figures 4.10-4.13. The agreement between the physical coordinates for both transient and modal coordinates is improved. Examining the steady state responses, the response in all three cases is quasiperiodic. Some phase difference is observed, but is expected due to the approximations made by the method of multiple scales. The steady state magnitudes are in agreement. Thus qualitative agreement between the nonlinear normal mode solution and direct integration of the newtonian equations of motion is achieved. Quantitative agreement is lacking due to $O(\epsilon^2)$ shifts in the location of the suppression bandwidth not captured by the $O(\epsilon)$ approximations used.

4.4 Summary

In this chapter, the equations of motion for the N-degree-of-freedom system with a vibration absorber were shown to reduce to the 2-degree-of-freedom absorber model through the application of nonlinear normal mode theory. First the theory of nonlinear normal modes was briefly reviewed. Then the theory was extended to allow small linear coupling. Finally, the theory of nonlinear normal modes for internally resonant systems was extended to model the forced and damped N-degree-of-freedom system with an attached vibration absorber. This theory was then applied to an example commonly used in the nonlinear normal mode literature.

The example has verified the qualitative correctness of the nonlinear mode approximation to the dynamics of an N-degree-of-freedom system with a vibration absorber. It has also, however, highlighted the limitations of the model near the suppression region. These limitations are due to $O(\epsilon^2)$ shifts in the location of the suppression bandwidth not captured by the $O(\epsilon)$ approximations in the model. Improvement should be possible via higher order approximations.

Chapter 5

Experimental Validation

Having developed the model in Chapter 2 and both analytically and numerically investigated the performance of nonlinear vibration absorbers in Chapter 3, experimental validation was undertaken. As noted in the literature review, little experimental investigation of nonlinear vibration absorbers has been reported. Two experimental setups were used. First, an analog computer was programmed with Equations (2.21a)-(2.21b) and the effect of the nonlinear parameters investigated. The analog computer was then wired with the two-degree-of-freedom system presented as an example in Section 4.3. In the second experimental setup, a continuous screw-mounted beam (see Appendix B for geometry) was investigated using nonlinear positive position feedback (NPPF). Since only the first mode could be excited by the shaker due to frequency constraints, and no internal resonance was identified in the open-loop structure, the beam is treated as a single-degree-of-freedom structure and only the first mode was investigated. From the results of Chapter 4, the absorber should only affect this mode. Qualitative agreement between the experimental results and the Single- and N-degree-of-freedom models is therefore investigated.

5.1 Analog Computer Experiments

A Model 7000 Compudyne Analog Computer with two GP-10 units was used to investigate the effect of the nonlinear parameters, α_3 and δ_3 on system response for both a single and multiple(two)-degree-of-freedom system. Details of the experimental hardware used may be found in Appendix Chapter B. Two experiments were conducted. In the first, the analog computer was patched with Equations (2.21a)-(2.21b) to investigate the singe-degree-of-freedom model. In the second, Equations (4.39a)-(4.39c) were patched and the effects of the vibration absorber on both the first and second mode were investigated.

In the first experiment, the system was fixed with a softening nonlinear characteristic with $\alpha_3 = -0.01$. Four cases were considered: the open loop system, a linear vibration absorber, a nonlinear softening absorber, and a nonlinear hardening absorber. These cases correspond to the NSLA and NSNA systems modeled in Chapter 3. Other system parameters were fixed as follows: $\alpha_1 = 0.1$, $\delta_1 = 0$, $\zeta_1 = \zeta_2 = 0.001$. Time scaling was used, increasing the characteristic time by a factor of 100. The open-loop system natural frequency is therefore expected to be 100 rad/s or approximately 15.9 Hz. Two types of experiments were performed. First, swept sine tests with both positive and negative frequency sweeps were performed at two forcing amplitudes, $f = 0.01$ and $f = 0.1$. The sweeps were conducted with a zoom fft bandwidth of 0.4 Hz and a step size of 1 Hz from 1-10 Hz, 0.05 Hz from 10-20 Hz, and 1 Hz from 20-30 Hz. Each sweeps takes approximately 1 hour to complete. Next, the frequency was fixed at 15.85 Hz and the force slowly increased to observe system response. Time histories were collected to evaluate the response. From the analytical models, a Hopf bifurcation is expected with quasiperiodic response.

5.1.1 Swept Frequency Tests

The swept sine results are plotted in Figure 5.1. The system (Channel (3)) and absorber response (Channel(5)) are plotted in the left and right column, respectively. All four cases are plotted. In the first row, the open loop response is shown for $f = 0.01$ (the lower

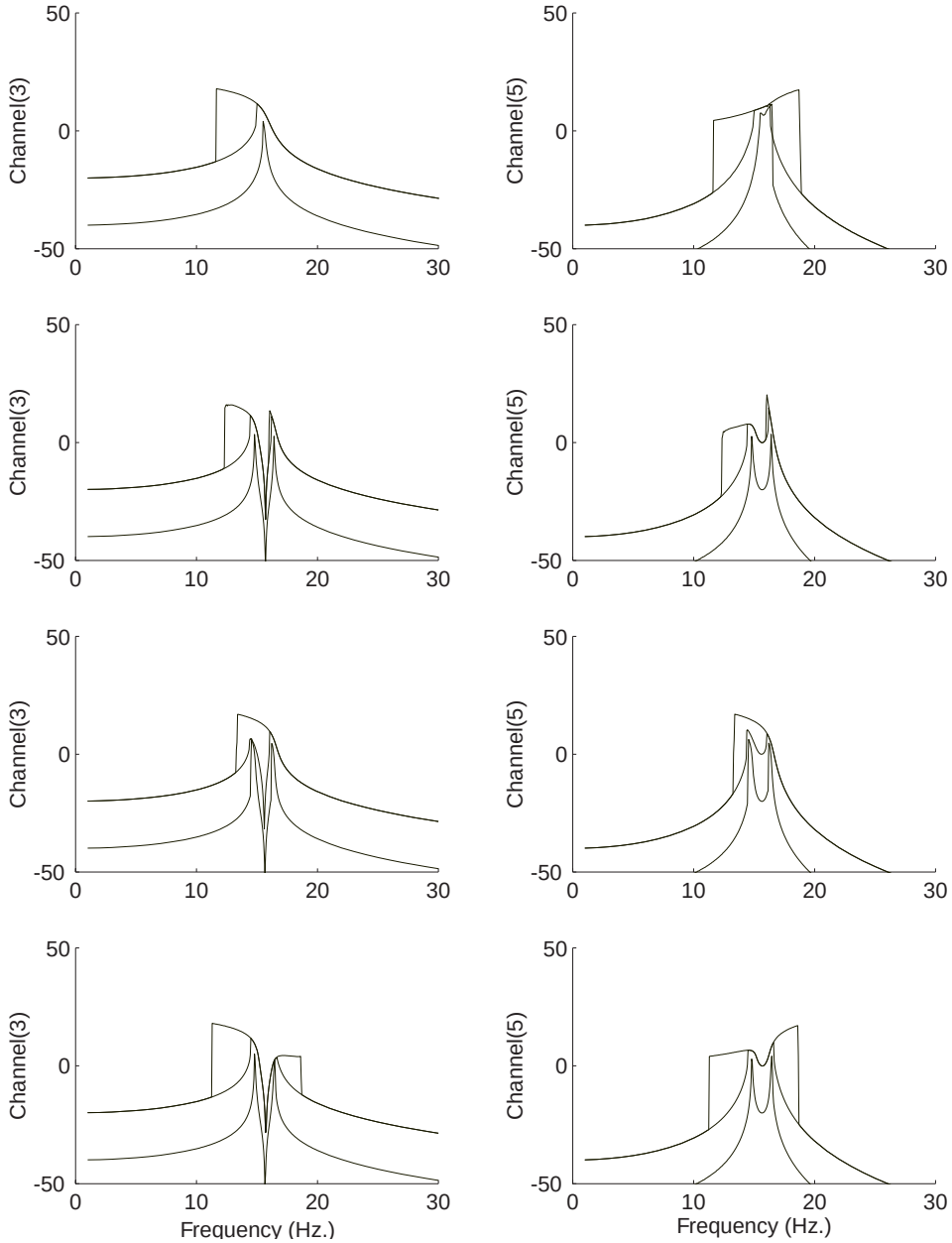

Figure 5.1: Experimental Swept Sine response of the single-degree-of-freedom analog computer experiment. The system (Channel (3)) and absorber response (Channel(5)) are plotted for the open loop, linear absorber, softening absorber, and hardening absorber in rows 1-4.

line) and $f = 0.1$. Both the forward and backward sweeps are plotted. The vertical line near 12 Hz (and 18 Hz for the absorber) results from the well-known jump phenomenon. The open-loop absorber consists of the hardening nonlinearity absorber which is excited by the system, but does not force the system degree of freedom. This cannot be realized for a mechanical or piezoelectric absorber, but is possible with PPF control. Essentially, the controller is excited by the system, but the feedback is turned off. From these plots, the damping of the open-loop system was approximately $\zeta_1 = 0.01$. This increase in damping is a result of experimental hardware and cannot be reduced. Resonance occurs near 15.65 Hz.

In the second row, the response of the softening system with linear absorber is plotted. For $f = 0.01$, the response appears linear. When the forcing level is increased to $f = 0.1$, the resonant peaks begin to bend lower in frequency. This is expected for a softening system. Jump phenomena are also visible. Resonant response is begining to coexist with suppressed response. Thus the performance of the vibration absorber is compromised, as predicted by the model for a nonlinear system with a linear absorber (NSLA).

Row three depicts the response of the softening system ($\alpha_3 = -0.02$) with a softening absorber ($\delta_3 = -0.01$). For $f = 0.01$, the response is similar to the linear system. When the sweep is performed at $f = 0.1$, the forward sweep from 1 Hz to 30 Hz indicates good performance. The suppression frequency has shifted negative as predicted by the SDOF model and although the upper resonance has shifted, it does not overlie the suppression region. This is misleading since the negative sweep from 30 Hz to 1 Hz indicates that the resonance extends from the upper frequency past the lower frequency. Although not visible on the plot, it was observed that the response was quasiperiodic near the tip of the resonance curve. This agrees well with the model predictions.

In the final row (row four), the response of a softening system with a hardening absorber is shown. For $f = 0.01$, the response again appears linear. For $f = 0.1$, the sweeps indicate acceptable absorber performance. The resonant peaks bend outwards, away from the suppression region. The suppression region shifts upward in frequency and slightly

broadens, as predicted theoretically. Jump phenomena and multi-valued solutions exist, but outside of the absorber suppression region. As in the three previous cases, the experimental results qualitatively match those of the model developed in Chapter 2 and explored in Chapter 3. Quantitative agreement would only be expected to $O(\epsilon)$ effects and as discussed in the previous chapter, the location of the suppression region is sensitive to $O(\epsilon^2)$ effects.

5.1.2 Swept Excitation Magnitude Tests

Having qualitatively verified the frequency response curves of the model, the existence of the Hopf bifurcations was next investigated. For this, the frequency was fixed at 15.85 Hz and the force level varied. The model and numerical simulations predict that as the force level is increased, the response will shift from periodic to quasiperiodic and absorber performance will deteriorate.

Time responses for $f = 0.01$, 0.03, 0.1, and 0.164 are plotted in Figure 5.2. As the force is increased, the ratio of system response to forcing magnitude decreases, indicating that the absorption frequency is shifting upwards with increased excitation as predicted. The DC offset present in the plots is a result of the analog computer and could not be eliminated. It was constant in the test for various forcing levels. When the forcing increased from 0.1 to 0.164 volts, a change in response occurred. The system lost its periodic nature and began to oscillate with a multi-frequency response. Examining the spectrum of the response in Figure 5.3, this response is quasiperiodic.

Further increases in the forcing level to $f = 0.175$, 0.19, 0.25, and 0.3 volts is shown in Figure 5.4. Examining the responses and their corresponding spectrums in Figure 5.5, the transition of the system response from a quasiperiodic to a chaotically modulated response are presented in Figure 5.6. As the forcing level is increased from 0.164 to 0.175 volts, the character of the response changes and the closed periodic curve on the Poincare section shown in Figure 5.7 begins to break into segments. This indicates that synchronization of the response is nearly occurring. Increasing the forcing level further, the response appears to become chaotically modulated. The spectrum of the response seen in the lowest plot in

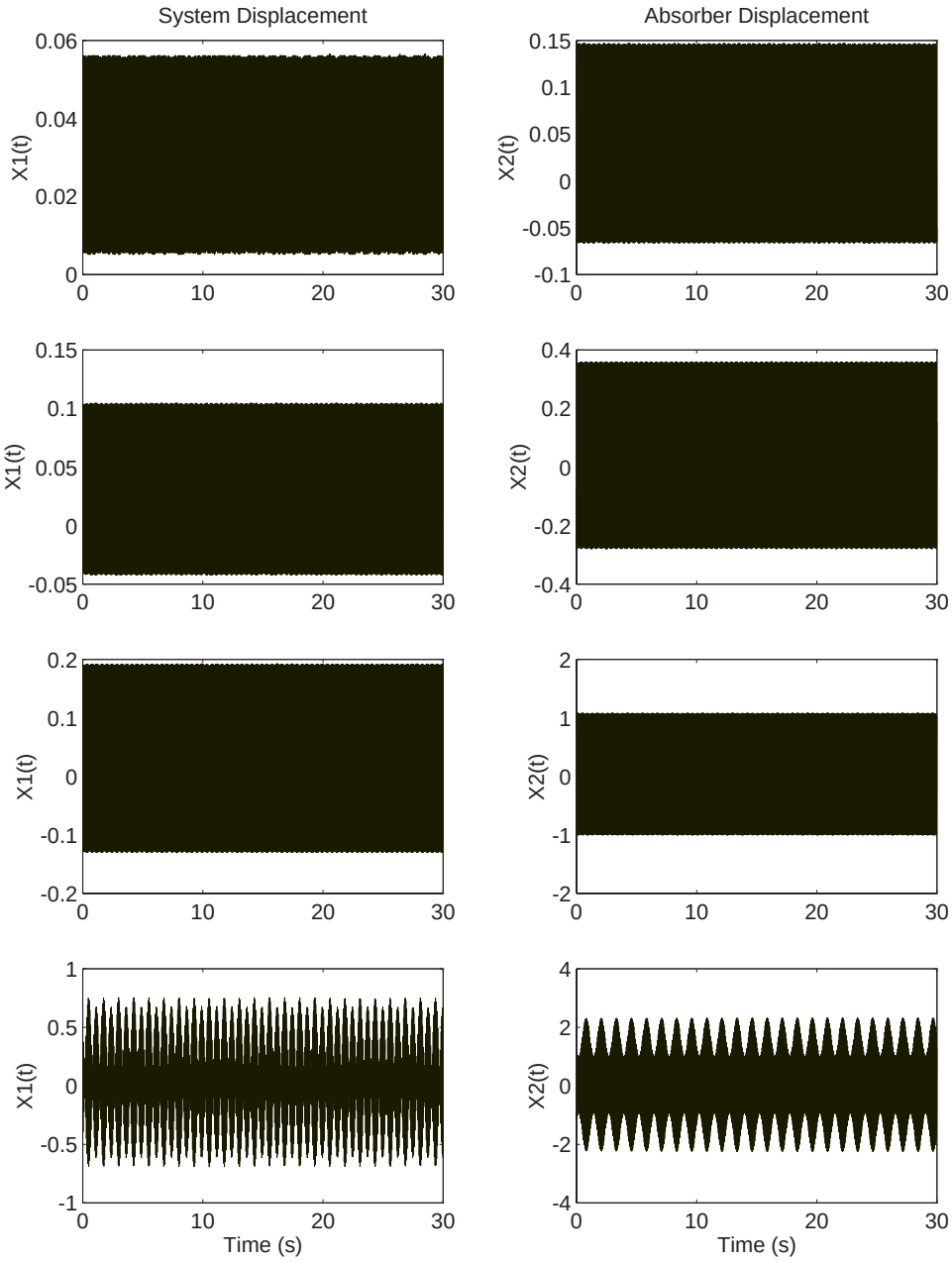

Figure 5.2: Experimental time responses of the single-degree-of-freedom analog computer experiment for $f = 0.01$, 0.03, 0.1, and 0.164. The system and absorber displacements are plotted in the first and second columns, respectively.

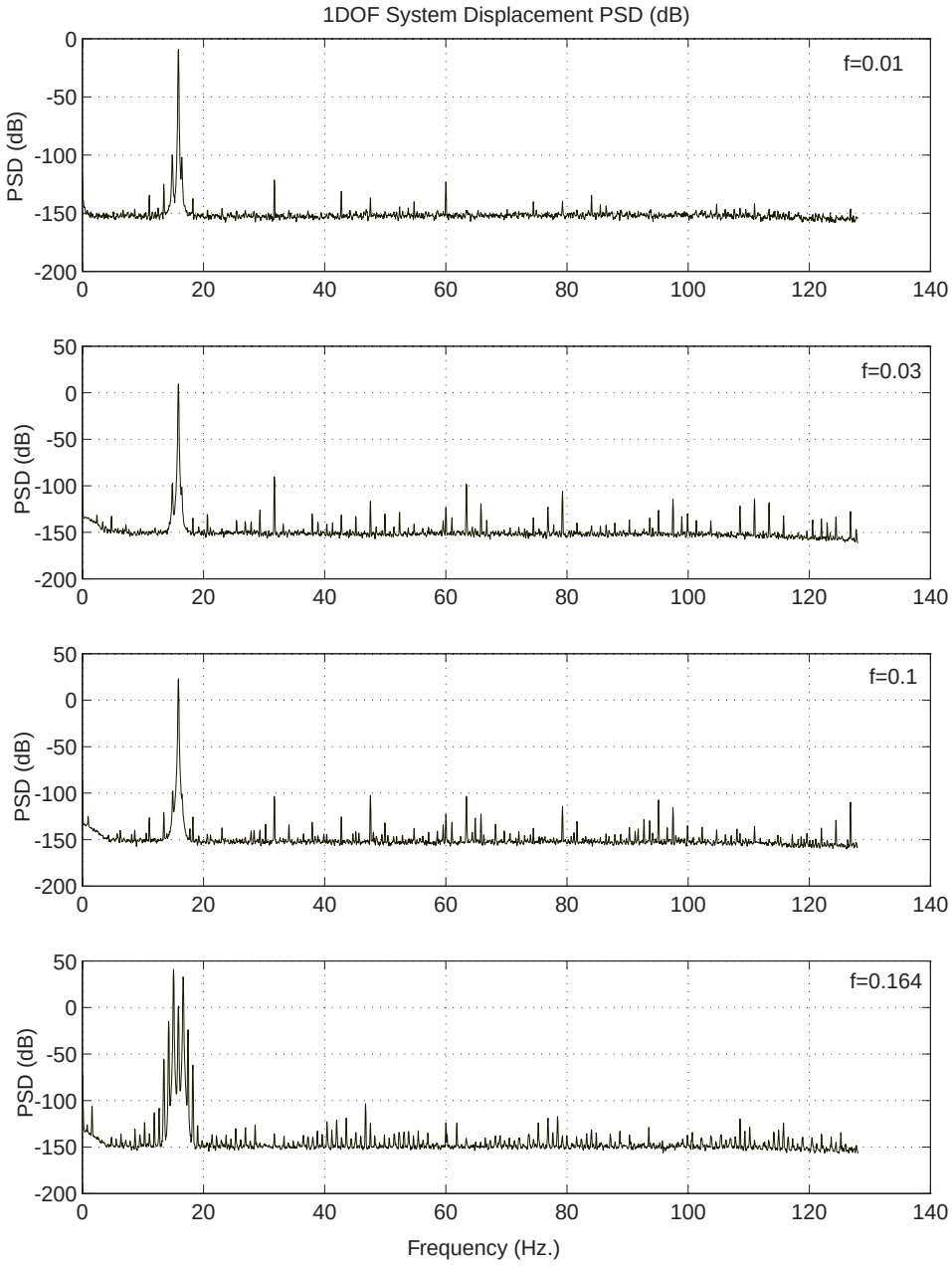

Figure 5.3: Experimental spectrums of the single-degree-of-freedom analog computer experiment for $f = 0.01$, 0.03, 0.1, and 0.164. The power spectral density of the system displacement is plotted.

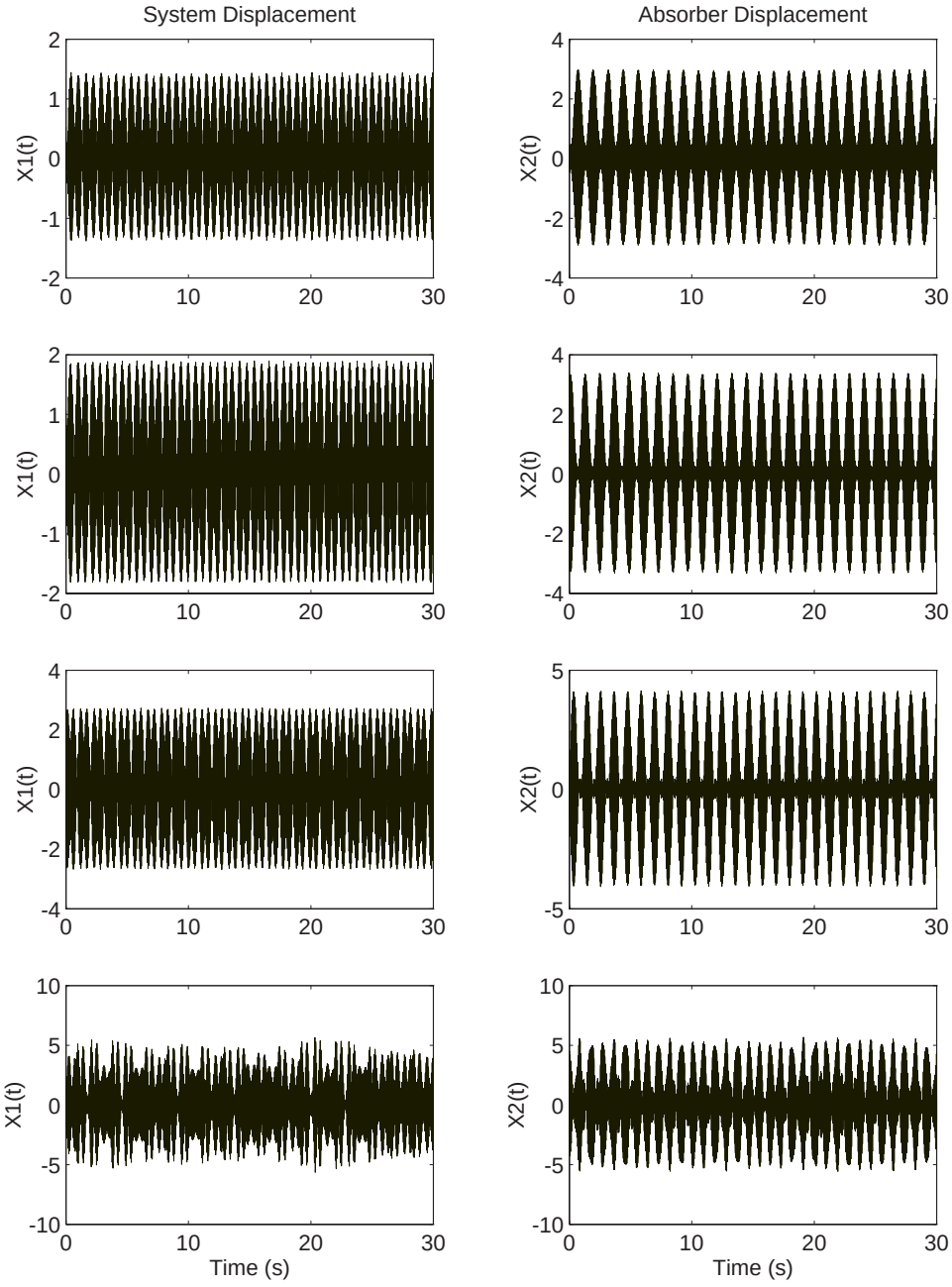

Figure 5.4: Experimental time responses of the single-degree-of-freedom analog computer experiment for $f = 0.175$, 0.19, 0.25, and 0.3. The system and absorber displacements are plotted in the first and second columns, respectively.

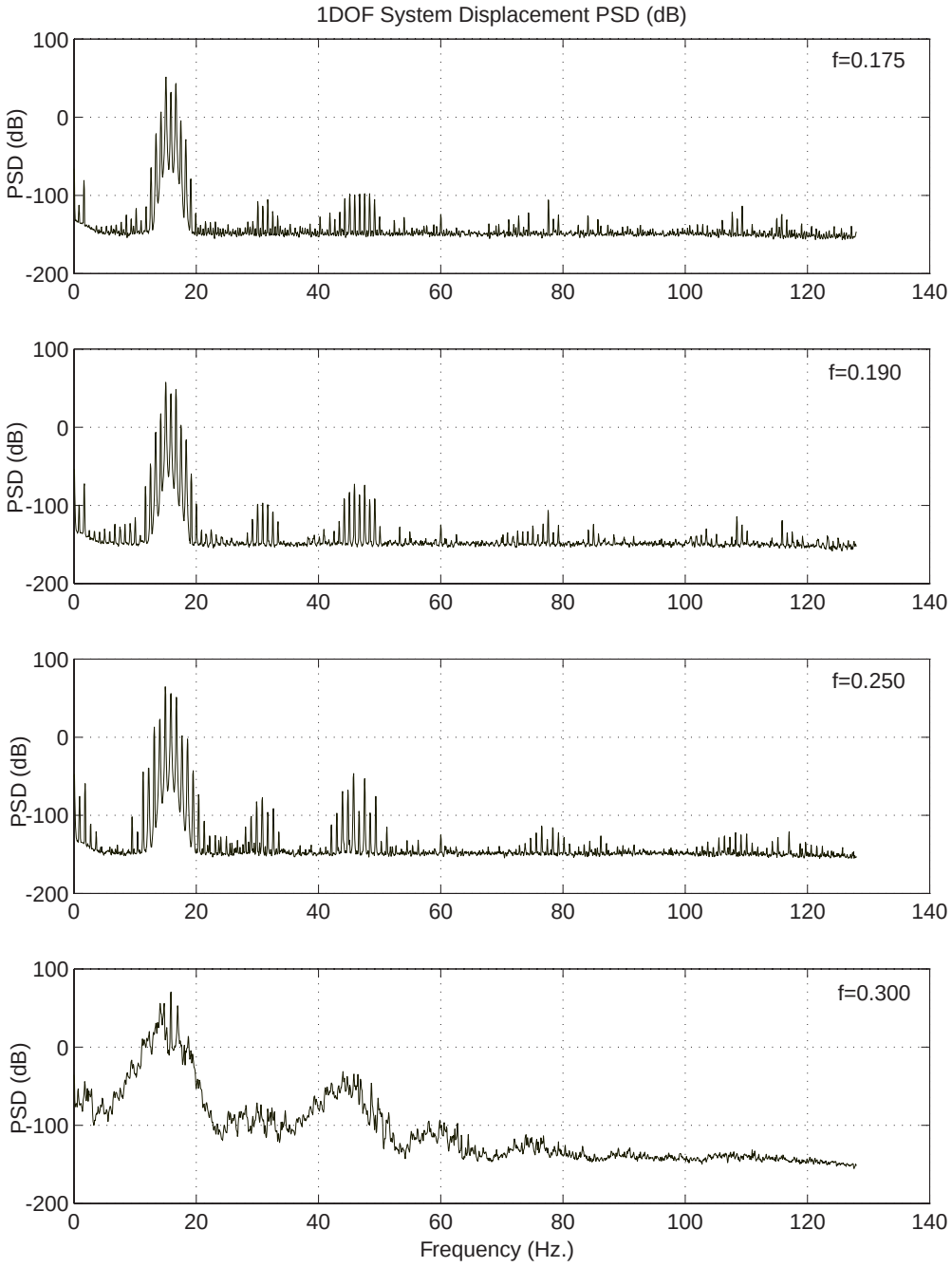

Figure 5.5: Experimental spectrums of the single-degree-of-freedom analog computer experiment for $f = 0.175$, 0.19, 0.25, and 0.3. The power spectral density of the system displacement is plotted.

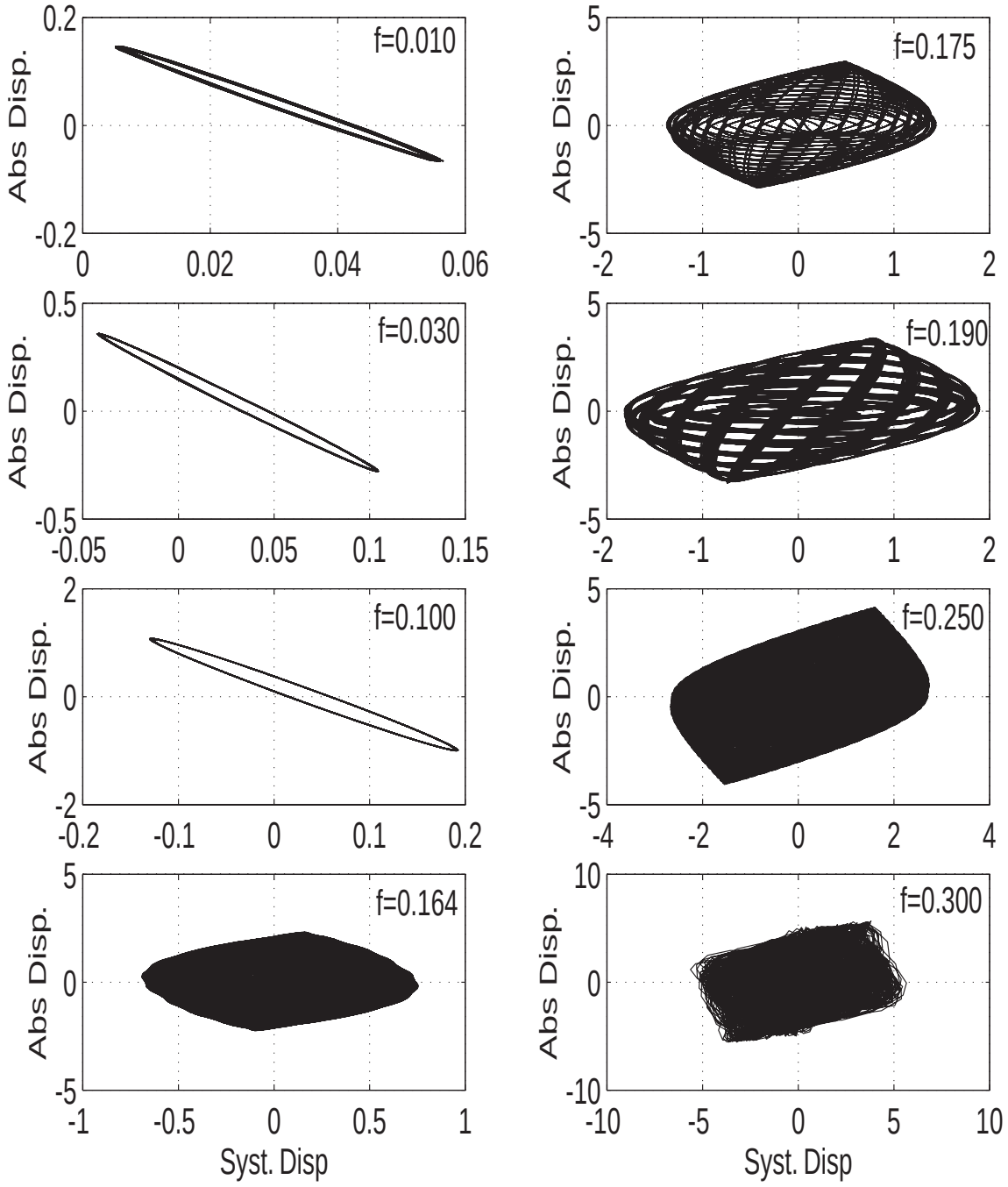

Figure 5.6: Experimental time responses of the single-degree-of-freedom analog computer experiment for all eight forcing levels plotted in X-Y format. The forcing level increases down the first and then the second column, sequentially.

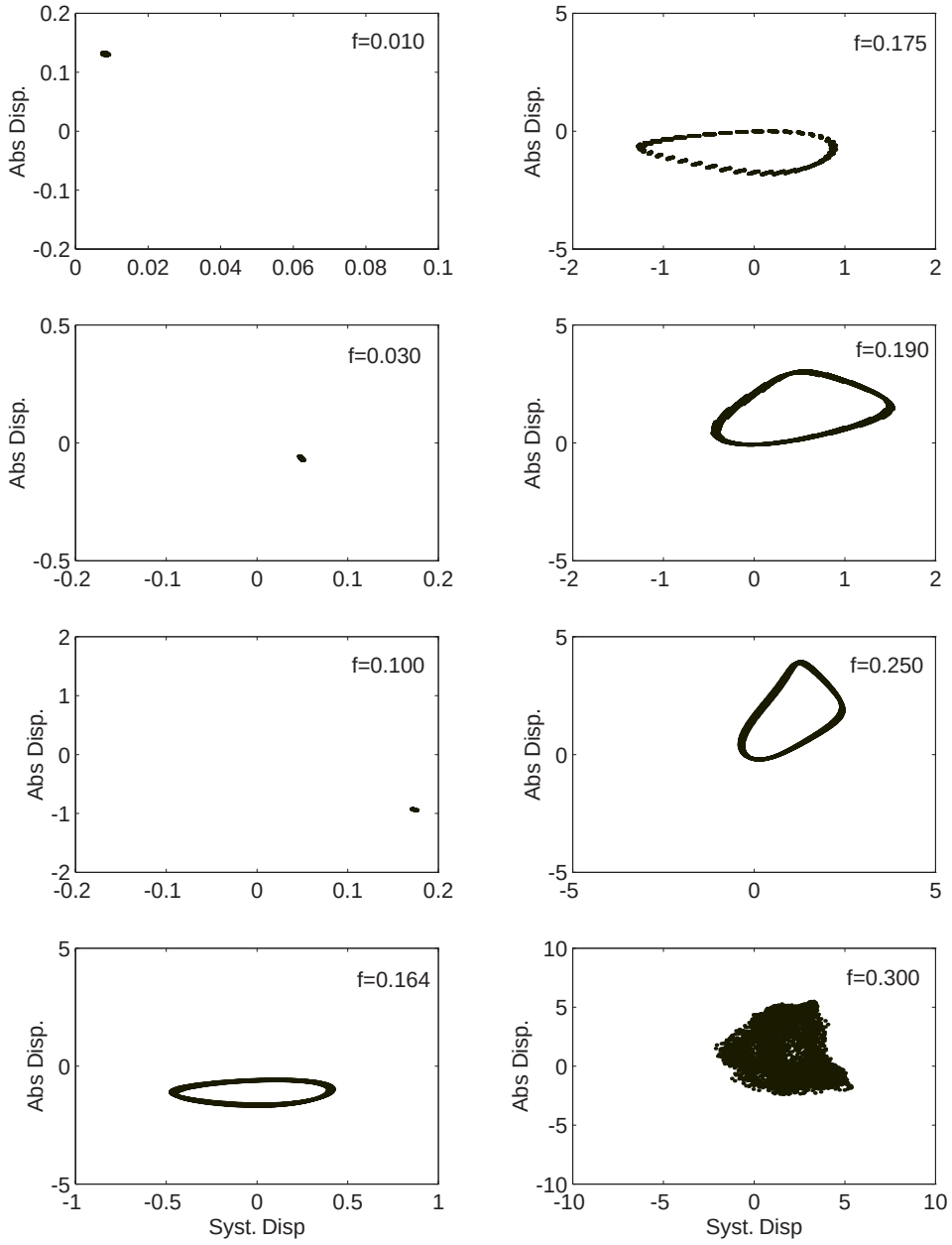

Figure 5.7: Experimental Poincare sections of the single-degree-of-freedom analog computer experiment for all eight forcing levels. The forcing level increases down the first and then the second column, sequentially.

Figure 5.5 is broadband–its corresponding Poincare section is space-filling. Note that only two of the four dimensions of the Poincare section are plotted; however, given the nature of the time signal, its spectrum, and its Poincare section, the response is, in all probability, chaotic.

Experimental investigation of a single-degree-of-freedom system with a vibration absorber therefore agrees qualitatively with the model derived in Chapter 2 to $O(\epsilon)$ effects. The quasiperiodic response of the system and its transition to chaos is shown experimentally, a novel result.

5.1.3 Swept Frequency Testing of a 2DOF System

The final experiment performed on the analog computer setup was to patch the system with the equations of motion for the example of Shaw and Pierre [10] presented in Chapter 4. The purpose of the experiment was to qualitatively evaluate the effect of the vibration absorber on the modes of the system. The parameters used were identical to those of the last chapter with the exception of $\alpha_3 = -0.02$ instead of -0.01. This corresponds to doubling the nonlinearity, N, from -0.04 to -0.08. This was done to facilitate patching three dynamic systems on the limited amplifiers of the analog computer. The open-loop and closed-loop results for swept-sine test conducted at two forcing levels, $f = 0.01$ and 0.1, are shown in Figure 5.8. The open-loop response is plotted in row one, the closed-loop in row two. The results are more easily examined by zooming the plots near the two modal frequencies near 15.6 and 27.5 Hz. Examining the first mode in Figure 5.9, the effect of the vibration absorber is identical to that presented in Figure 5.1 for the hardening absorber. In the second plot, Figure 5.10, the effect of the vibration absorber tuned to the first mode on the second mode can be seen. Perhaps the lack of effect would be a better description. Both the open-loop and closed loop results are overlaid for a forcing level of $f = 0.1$. These results thus qualitatively verify the model presented in Chapter 4. Again they are new to the literature. Swept forcing tests are not shown since the results duplicate those for the single-degree-of-freedom case presented in the last section.

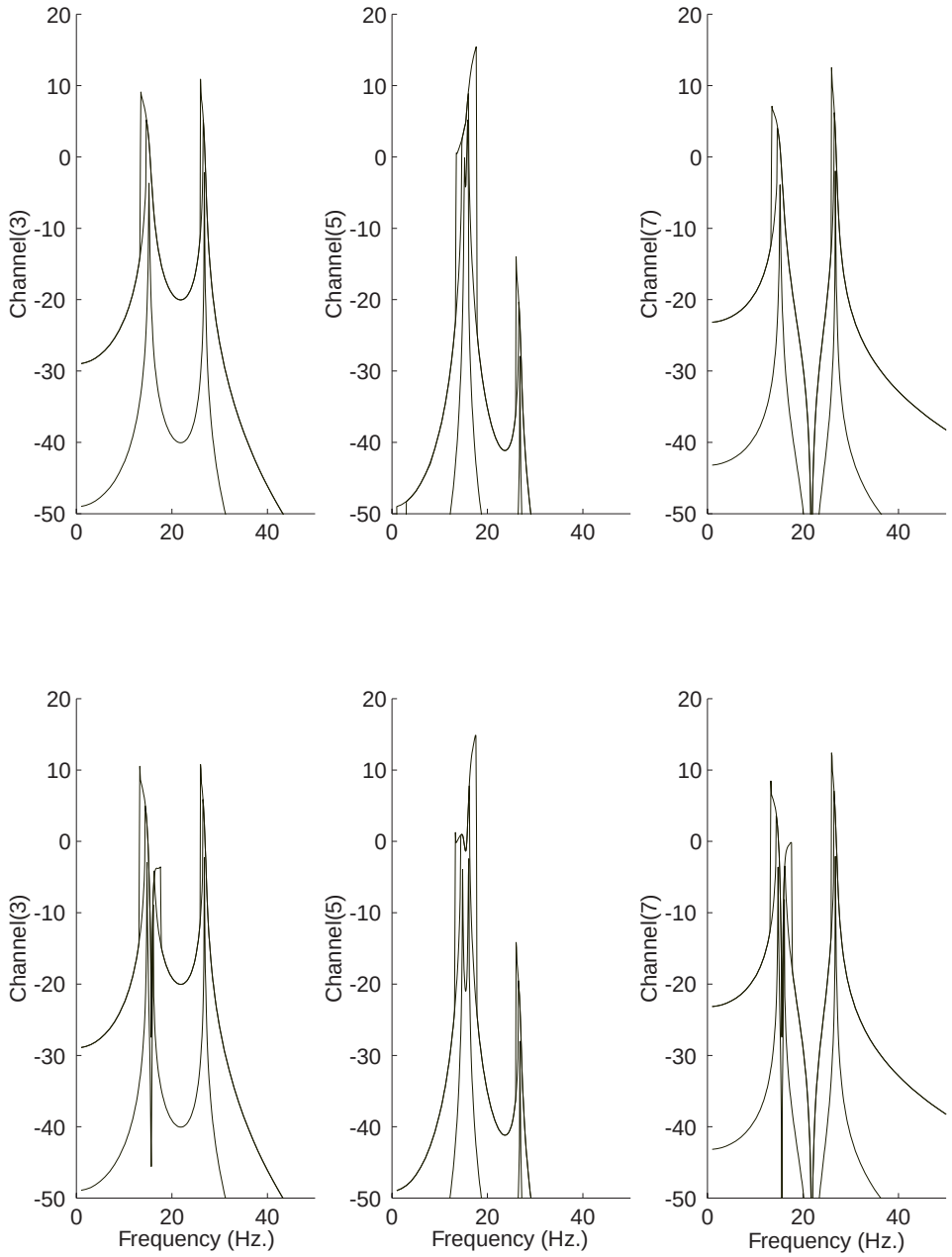

Figure 5.8: Experimental Swept Sine response of the two-degree-of-freedom analog computer experiment. The system (Channels (3) and (7)) and absorber (Channel(5)) responses are plotted for the open loop, and hardening absorber in rows 1-2.

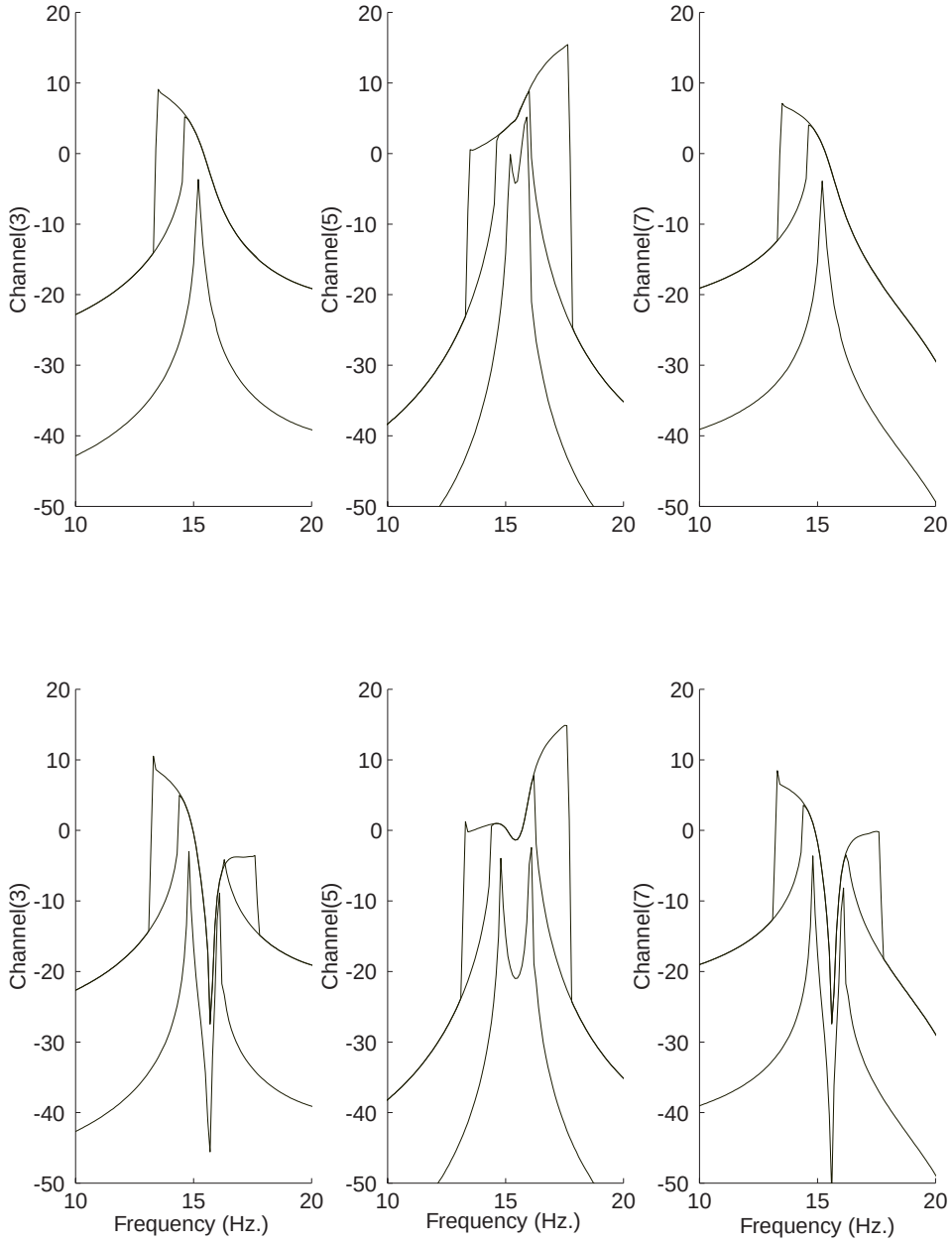

Figure 5.9: Experimental Swept Sine response of the two-degree-of-freedom analog computer experiment near the first mode. The system (Channels (3) and (7)) and absorber (Channel(5)) responses are over-plotted for the open loop and hardening absorber, but due to their agreement, only one curve is visible.

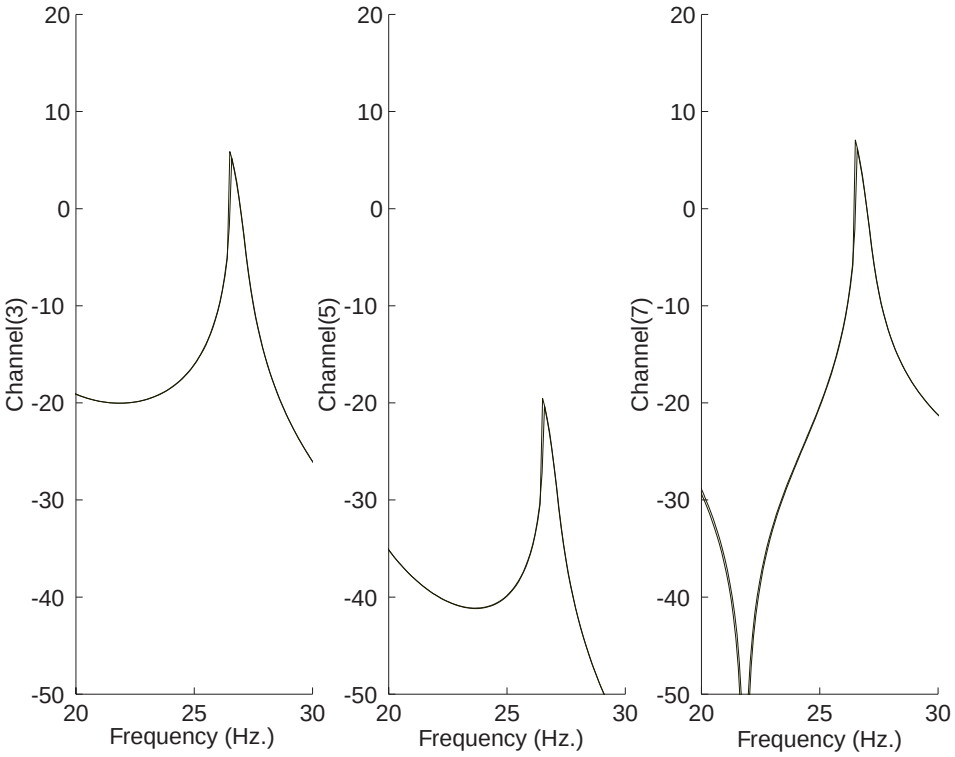

Figure 5.10: Experimental Swept Sine response of the two-degree-of-freedom analog computer experiment near the second mode. The system (Channels (3) and (7)) and absorber (Channel(5)) responses are plotted for the open loop, and hardening absorber in rows 1-2.

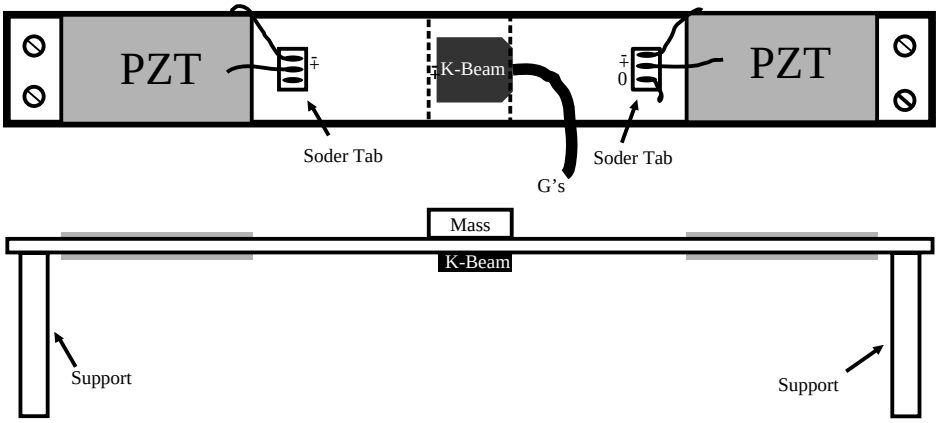

Figure 5.11: Screw Mounted Beam. See Appendix B for dimensions.

5.2 Screw Mounted Beam Experiment

The second experimental setup consists of a beam mounted by screws on posts and actuated by piezoelectric patches surface bonded to the aluminum beam. Details on construction and hardware used in the experiment may be found in Appendix B. A diagram of the beam is shown in Figure 5.11. Experimental data is presented first for the open loop (uncontrolled) case, then for two closed loop cases with both linear and nonlinear vibration absorbers implemented as positive position feedback control using a dSpace DSP based real-time controller. Several types of tests were run for a variety of forcing levels to investigate the linear and nonlinear behavior of the system. Before PPF control was implemented, open loop results were obtained to identify the system under test.

5.2.1 Open Loop Results

Three types of tests were run to establish the baseline model of the screw-mounted beam. First, random base excitation of the structure was used to determine the linear model. Excitation rms levels were varied over several orders of magnitude to check for linearity. The frequency response transfer functions for both acceleration and displacement can be seen in Figure 5.12. Examining the region of resonance in more detail in Figure 5.13, softening of the response with increasing forcing is visible. As the base excitation was increased, resonance tended to shift lower in frequency.

Since the random response showed indications of nonlinear behavior, swept sine tests were conducted to more accurately measure the system behavior. Frequency steps of 0.1 Hz were taken between 60 and 80 Hz with a zoom fft bandwidth of 0.4 Hz. Four averages of the zoomed transfer function response were computed at each point. A two second (approx. 140 cycles) delay was taken between frequency steps to minimize transient effects. Auto-ranging was utilized to ensure accurate data acquisition since the response levels varied over several orders of magnitude. Each sweep took approximately 1 hr., although some of the nonlinear PPF sweeps presented below took as long as 4 hrs. due to auto-ranging. The

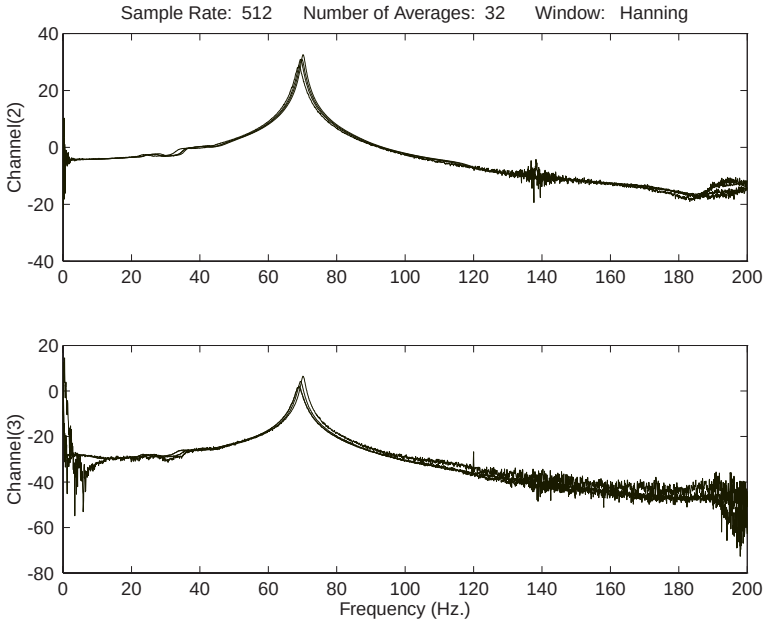

Figure 5.12: Screw Mounted Beam open-loop transfer functions for various base acceleration levels of 0.025, 0.08, 0.25 and 0.8 g_{rms}. Transfer functions are shown between base acceleration and beam acceleration (upper subplot) or beam displacement (lower subplot).

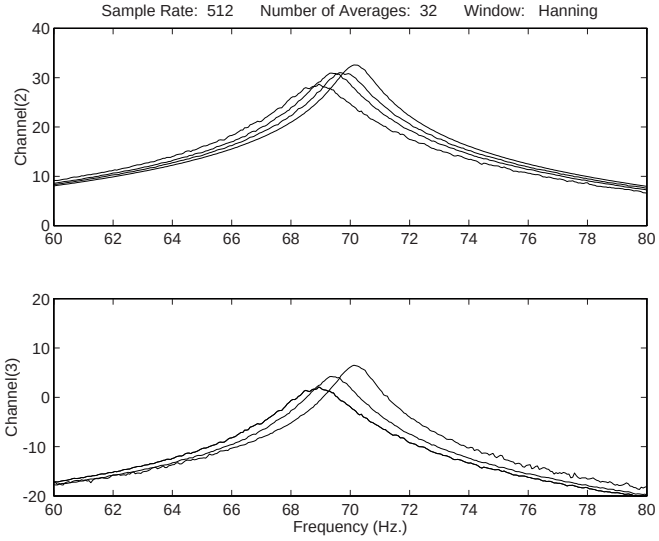

Figure 5.13: Screw Mounted Beam open-loop transfer functions for various base acceleration levels as indicated on the curves. Transfer functions are shown between base acceleration and beam acceleration (upper subplot) or beam displacement (lower subplot).

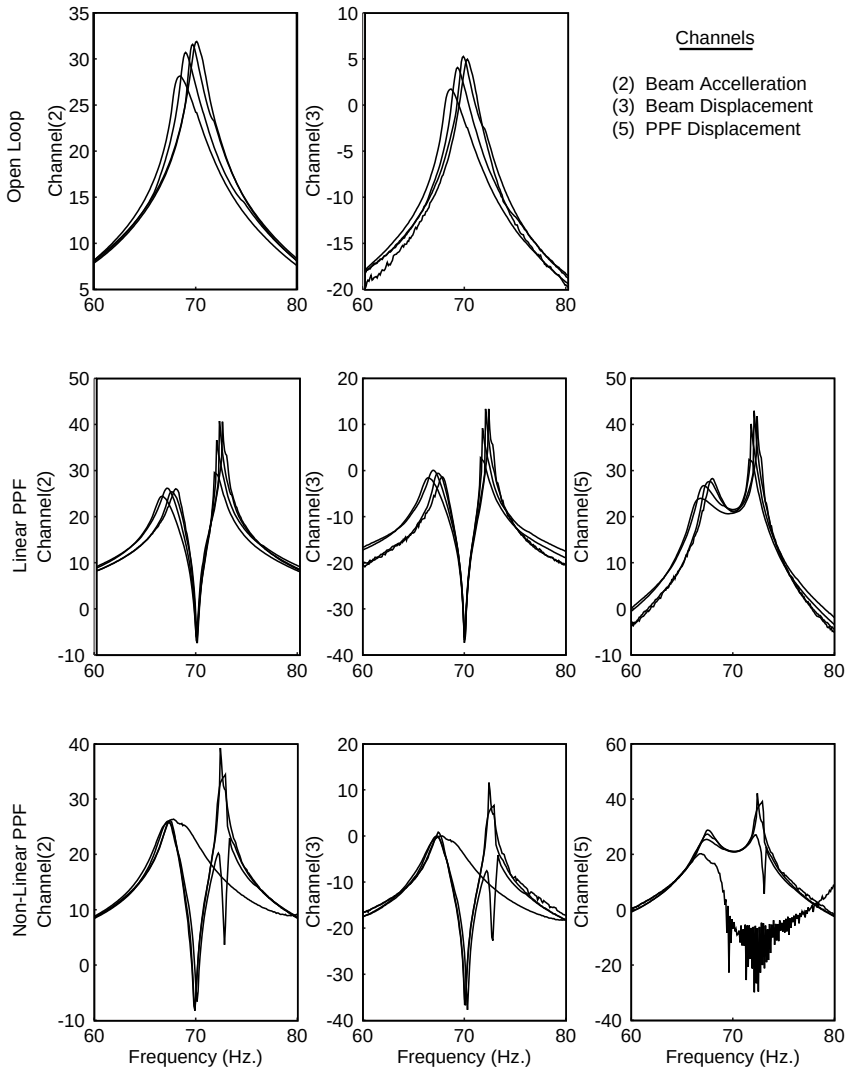

Figure 5.14: Screw Mounted Beam transfer functions for base acceleration levels of 0.01, 0.03, 0.1 and 0.3 g's. Transfer functions between base acceleration and the indicated channels are shown for the open loop, linear PPF and nonlinear PPF controller. Note that the responses are plotted in volts/volt. See Appendix B for sensor sensitivities.

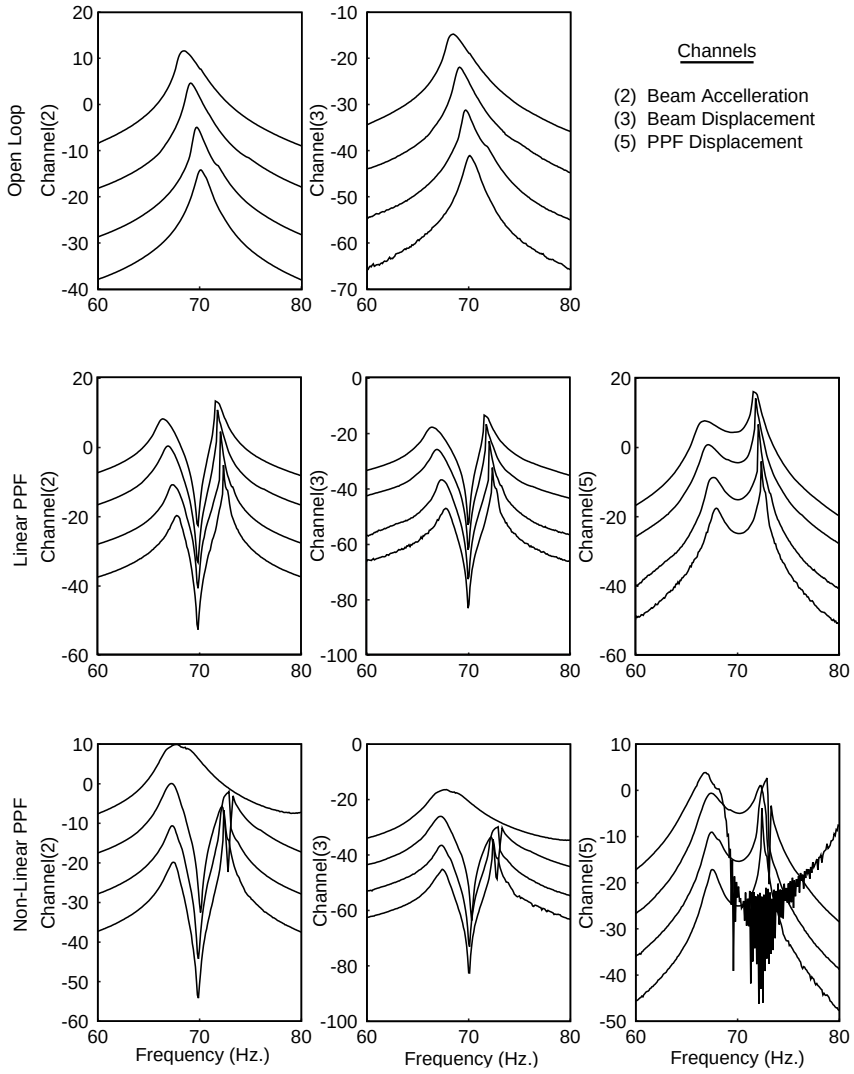

Figure 5.15: Screw Mounted Beam frequency response functions for various base acceleration levels as indicated on the curves. Responses are plotted for four excitation levels: 0.01, 0.03, 0.1 and 0.3 g's. Note that the responses are plotted in volts. See Appendix B for sensor sensitivities.

open loop responses are plotted as transfer functions (Figure 5.14) and absolute response (Figure 5.15) in the first row of each figure. Both the center acceleration and displacement are shown. Again similar observations were made. As the base excitation increased, the resonant response shifts lower in frequency. This indicates that a softening cubic stiffness or either a stiffening or softening quadratic stiffness of the beam was present.

Time responses to a fixed frequency excitation at various forcing levels are shown in Figures 5.16-5.19. Several plots are shown in each figure for different forcing levels. First, portions of the time responses on two channels are shown in Figure 5.16. Both the system displacement and absorber displacement are plotted. For the open-loop case, the absorber displacement is not fed back to the piezoelectric actuators. Next, the spectrum of the beam center displacement is shown in Figure 5.17. As the forcing level is increased, the influence of the second and third harmonics varies. The response is generally clean, although some noise is noted especially in at 120 Hz due to the optical displacement sensors. All tests were conducted with a shield to minimize this noise which comes from the fluorescent light fixtures. X-Y plots for the time responses (Figure 5.16) are shown in the first column of Figure 5.18. In Figure 5.19 in the first column, the Poincare section, obtained by resampling the data at the forcing frequency, is plotted. These figures illustrate the noise indicated by the spread of the beam displacement signal and the size of the Poincare section. Instead of a single point, a filled area is seen, especially at lower levels. This is due to noise inherent in experimental work. For larger forcing levels, the X-Y plot is an oval, indicating that the system and the absorber are not in perfect phase due to damping in the beam.

Examination of the response spectrum for 70.5 Hz forcing frequency shows that both even and odd harmonics are present in the system response. However, examination of the base acceleration also showed the presence of even and odd harmonics. The results were thus inconclusive as to the exact nature of the nonlinearity of the beam although a combination of quadratic and cubic behavior is suspected. However, as shown in Chapter 3, the presence of nonlinearity in the system only slightly affects linear absorber performance. A linear vibration absorber was next implemented using positive-position-feedback control

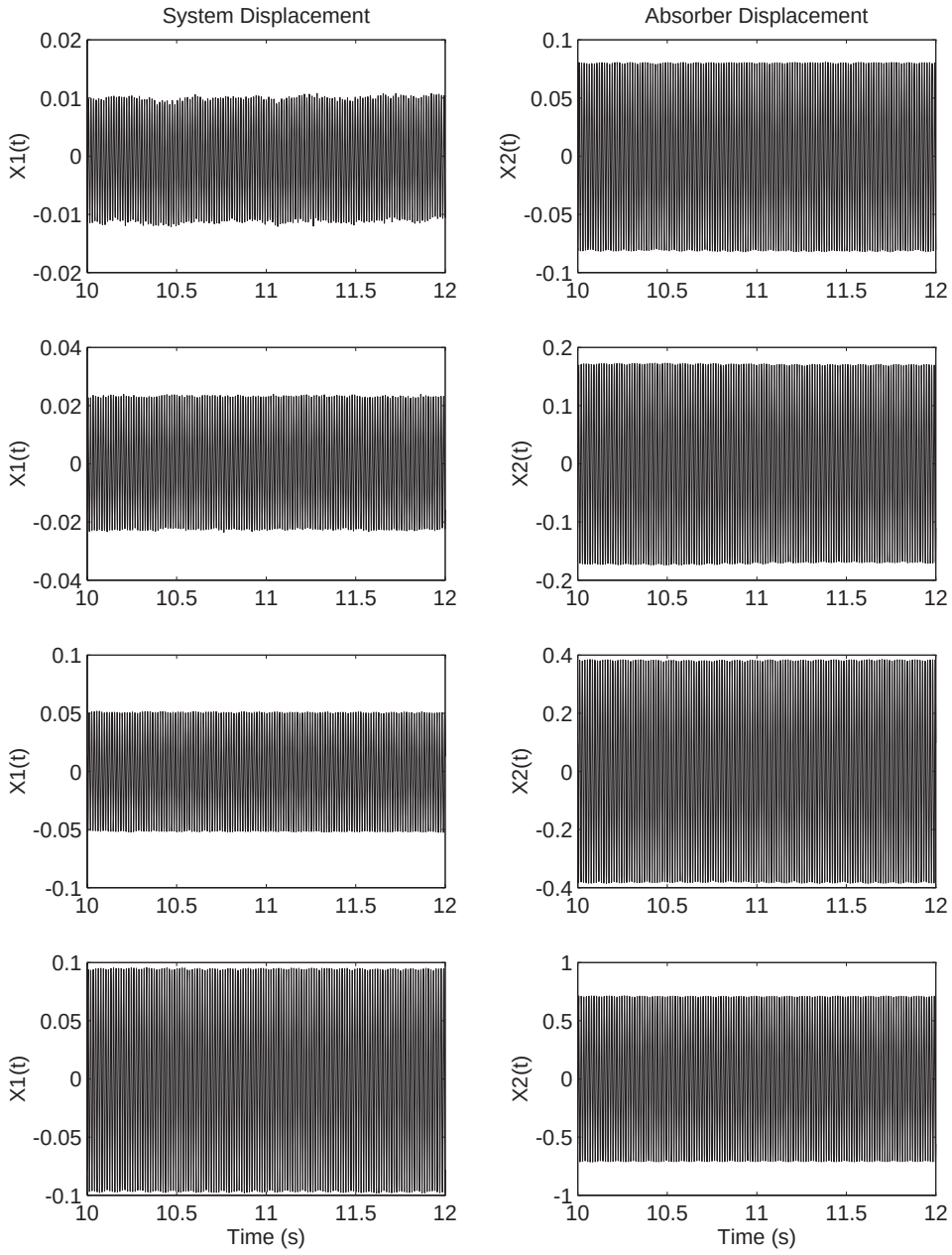

Figure 5.16: Screw Mounted Beam open-loop time response in volts (from top to bottom) for $\ddot{x_0} = 0.005$, 0.015, 0.05, and 0.15 g. X(1) is beam displacement and X(2) is PPF controller displacement. See Appendix B for sensor sensitivities.

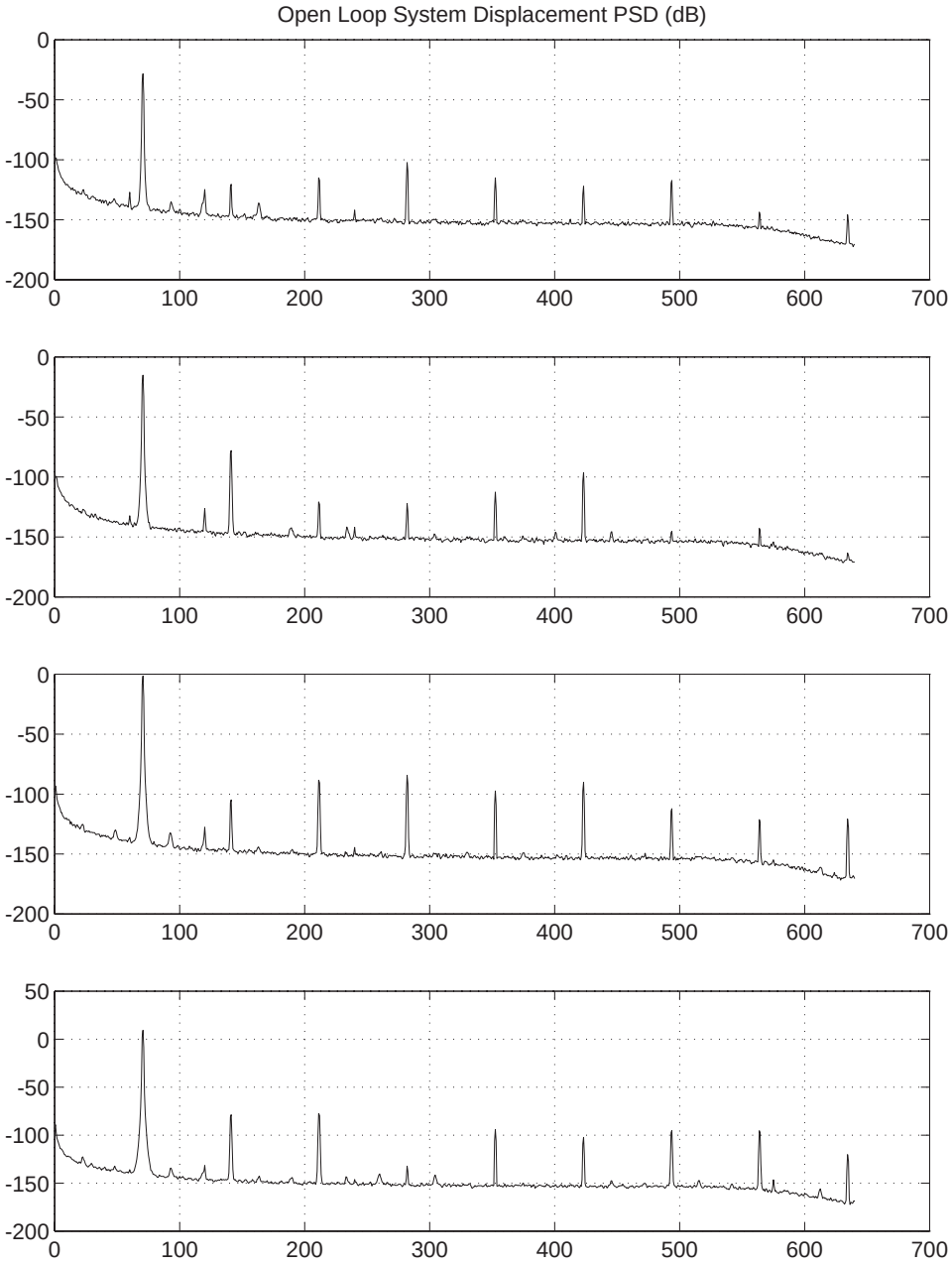

Figure 5.17: Screw Mounted Beam open-loop response spectrum for $\ddot{x}_0 = 0.005$, 0.015, 0.05, and 0.15 g.

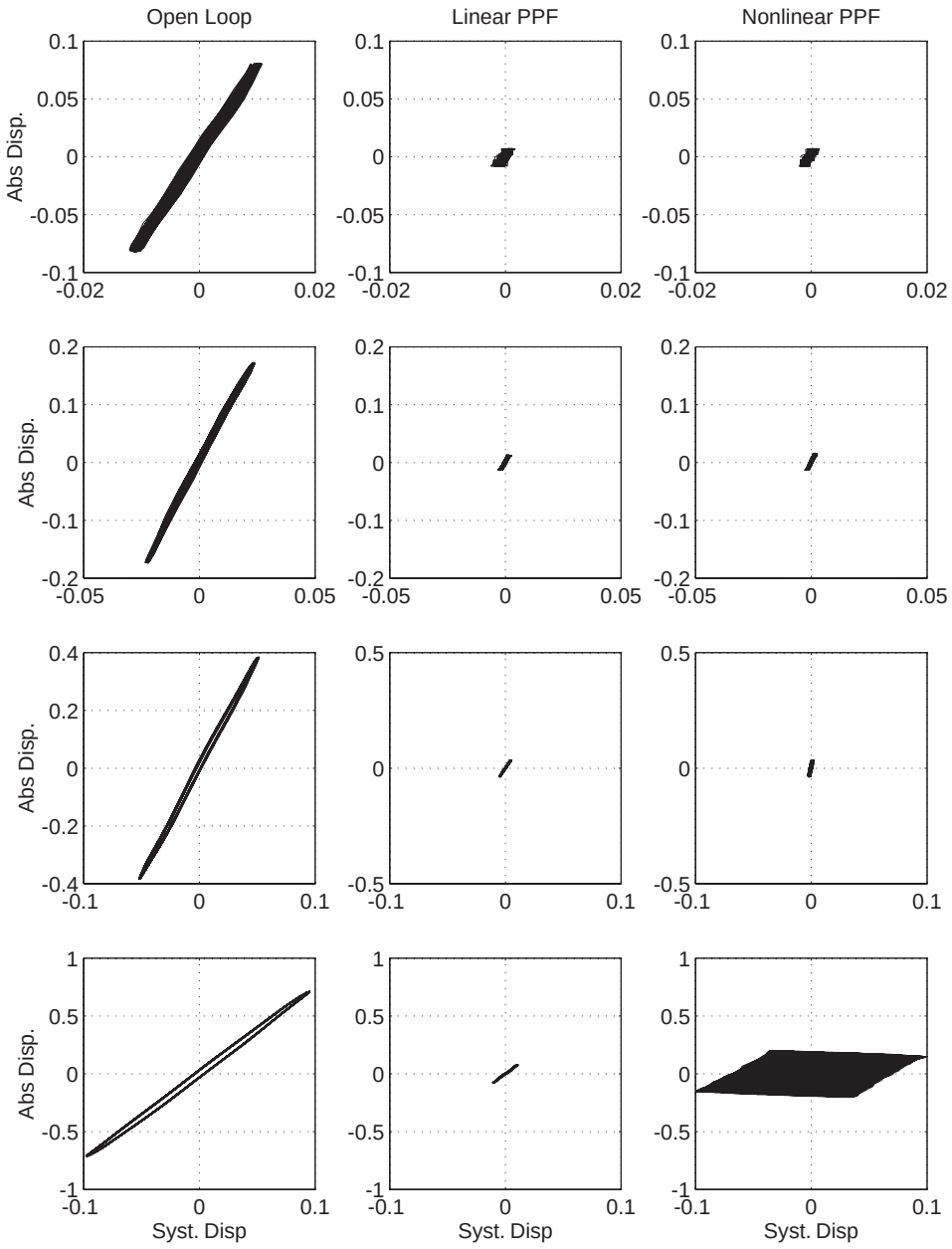

Figure 5.18: Screw Mounted Beam X-Y time response in volts for open-loop, linear and nonlinear PPF controllers. $\ddot{x_0}$ = 0.005, 0.015, 0.05, and 0.15 g, respectively. X(1) is beam displacement and X(2) is PPF controller displacement. See Appendix B for sensor sensitivities.

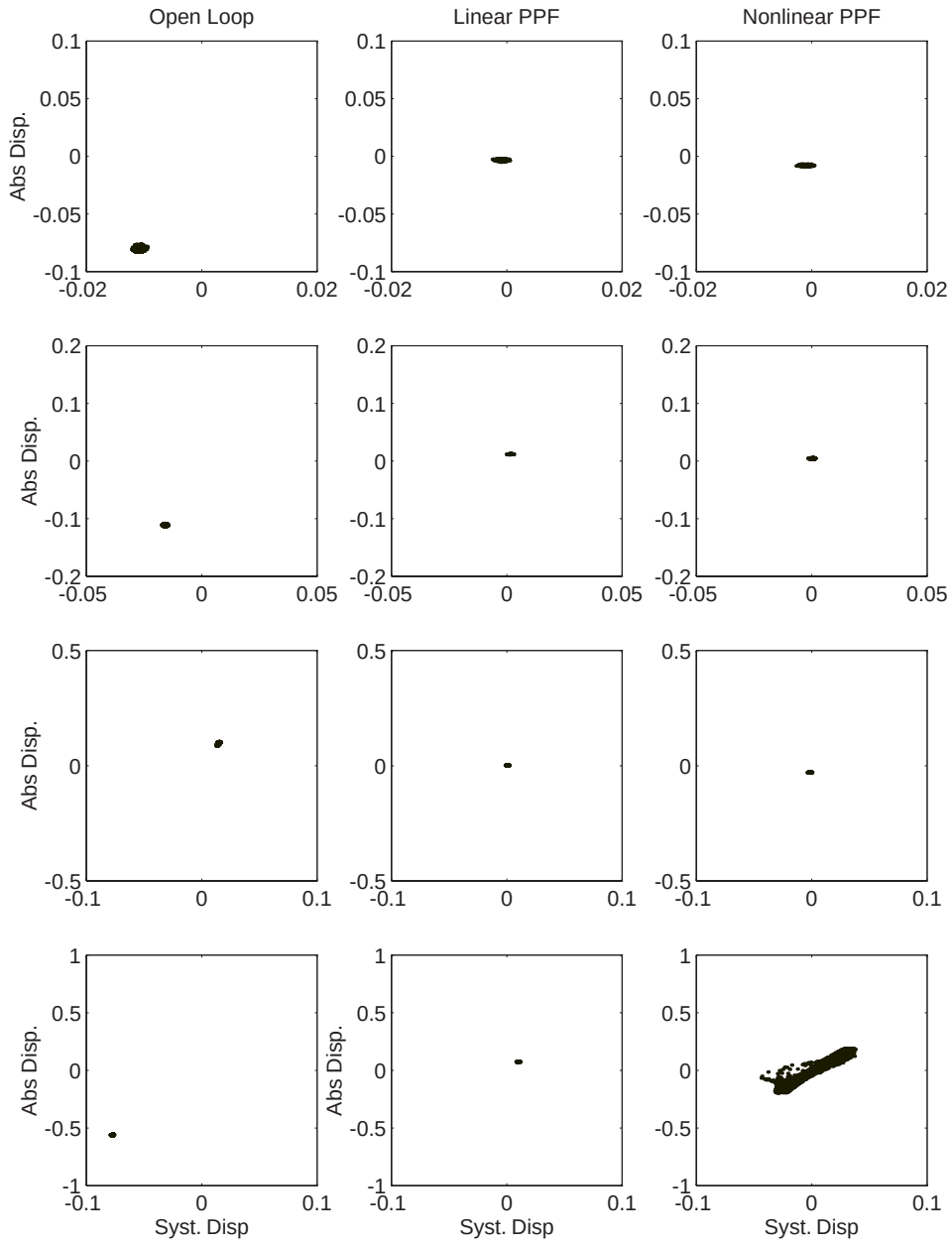

Figure 5.19: Screw Mounted Beam Poincare sections in volts for open-loop, linear and nonlinear PPF controllers. $\ddot{x_0}$ = 0.005, 0.015, 0.05, and 0.15 g, respectively. X(1) is beam displacement and X(2) is PPF controller displacement. See Appendix B for sensor sensitivities.

to verify this analytical result.

5.2.2 Linear PPF

The PPF control was implemented using a dSpace real-time controller as detailed in Appendix B. Gains on the controller were set using a trial and error approach to maximize absorber performance. Since the piezoceramic elements on the beam will respond over a large frequency range, filtering of the control signal was needed to prevent excitation due to the digital signal. The filter was tuned to 2500 Hz which was half of the 5000 Hz sampling rate. Additionally, an AC filter was used on the beam displacement signal since the Philtec optical probes have a DC bias in their output and played no role in the dynamics. The control signal filter however causes a constant phase shift which did not affect the first mode, but destabilizes higher modes at high control gains. Since the piezoceramic actuators excite the odd modes, the third mode would become unstable if the gain is too high. This limitation in gain was due to the digital control, not to limitations of the PPF algorithm. To prevent this problem in future work, an analog PPF filter should be implemented or a piezoelectric vibration absorber shunt used instead.

With the gain set, linear control was implemented on the system. As with the open loop case three types of tests were performed: random, swept sine, and fixed frequency excitation. Results from the random excitation tests are shown in Figures 5.20-5.21. The response is slightly different from the models of Chapter 3, but generally in good qualitative agreement. The asymmetry in the response is due to nonlinearity in the system, agreeing with the NSLA results presented in the Section 3.4.

Again steady state responses to 70.5 forcing at 0.005, 0.015, 0.05, and 0.15 g were recorded. The sensor noise is evident in Figure 5.22 for the responses corresponding to the lower two forcing levels. As the forcing level is increased, the effect of noise lessens due to increased system response. The spectrum, Figure 5.23, shows some harmonic effects, although less influence of the nonlinearity is seen than in the open loop response (Figures 5.16-5.17). This is due to reduced beam displacement as predicted by the theo-

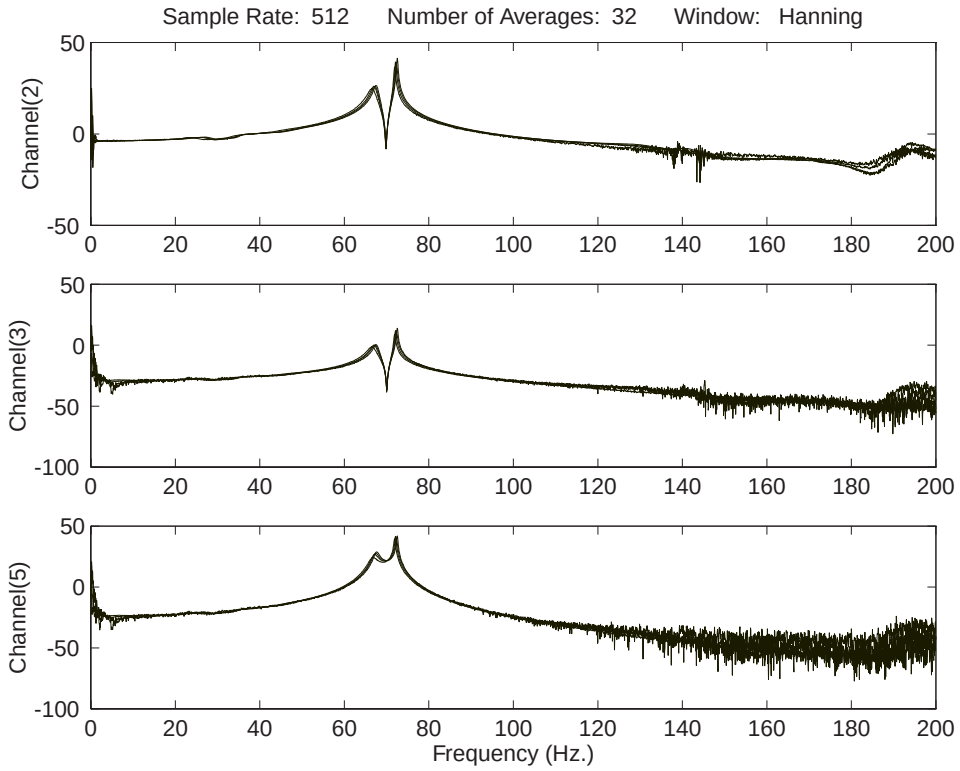

Figure 5.20: Screw Mounted Beam linear closed-loop transfer functions between base acceleration and the indicated channels for base acceleration levels of 0.025, 0.08, 0.25 and 0.8 g_{rms}. Channel(2) is beam acceleration, Channel (3) is beam displacement, and Channel (5) is PPF filter displacement.

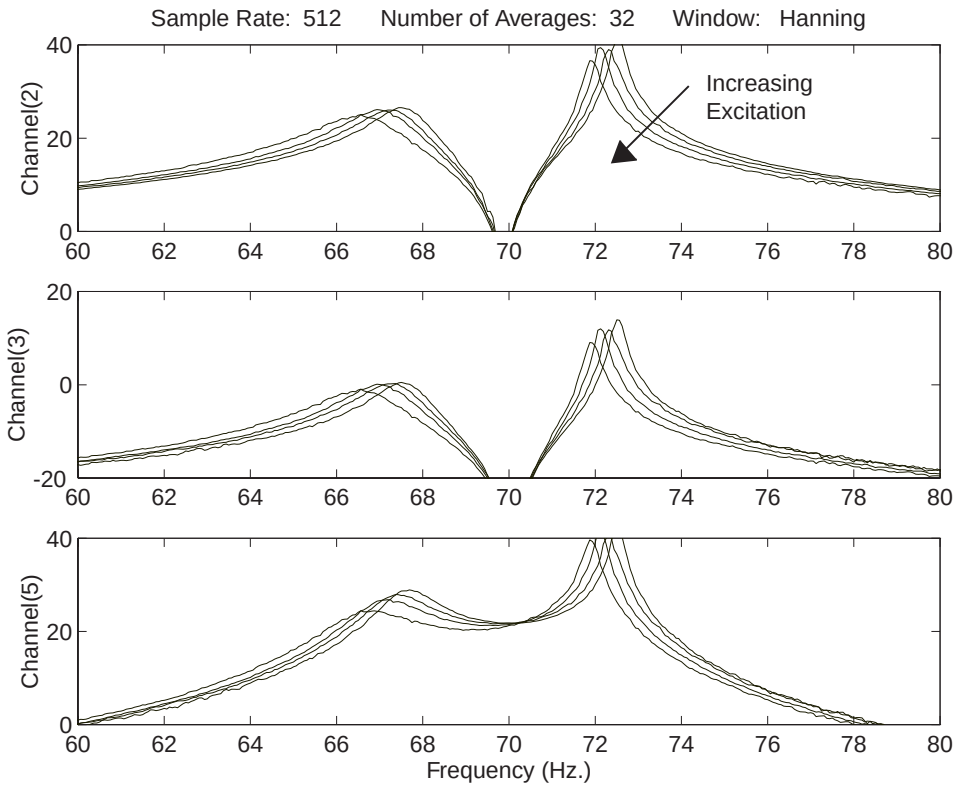

Figure 5.21: Screw Mounted Beam linear closed-loop transfer functions for base acceleration levels of 0.025, 0.08, 0.25 and 0.8 g_{rms}. Channel(2) is beam acceleration, Channel (3) is beam displacement, and Channel (5) is PPF filter displacement.

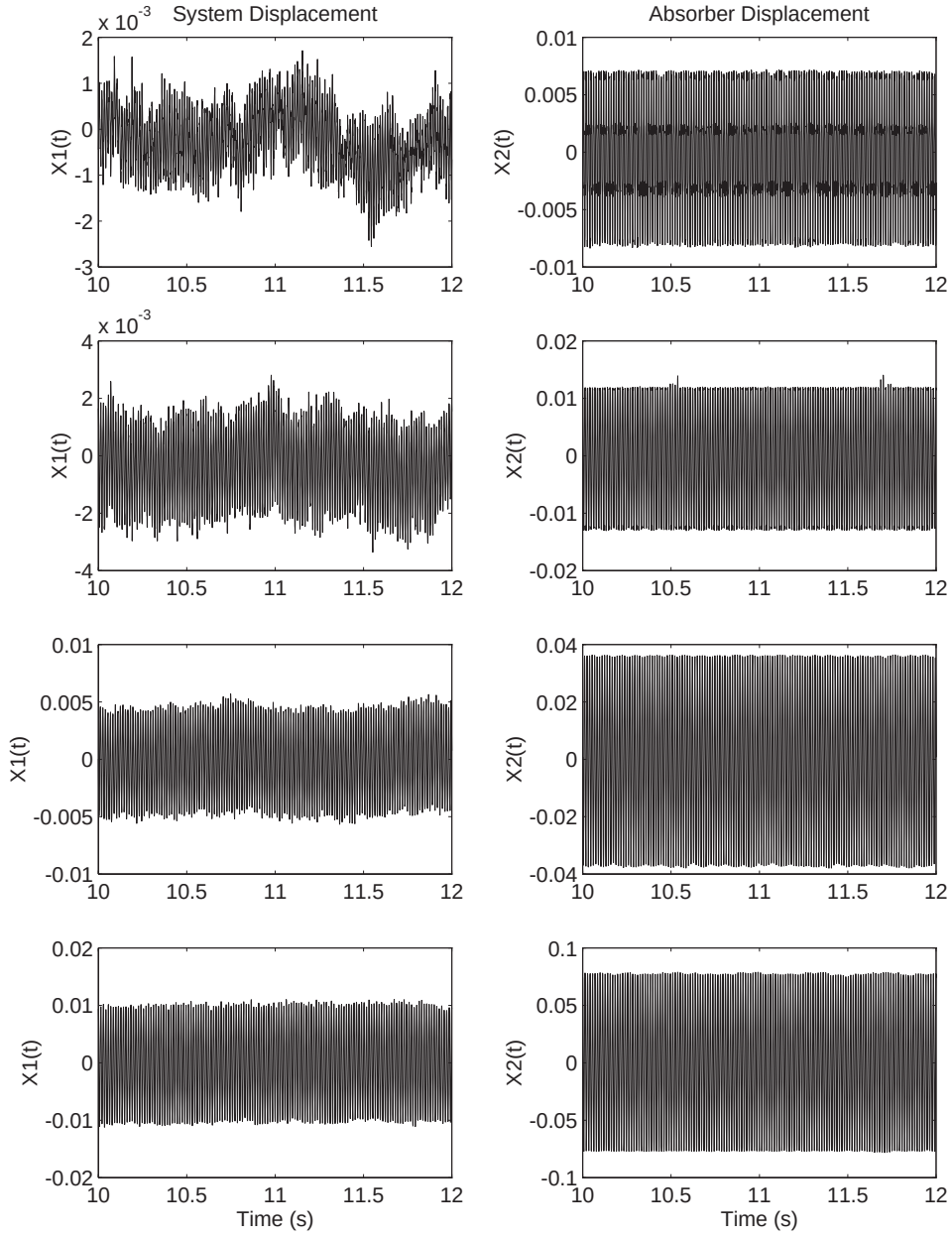

Figure 5.22: Screw Mounted Beam open-loop time response in volts for $\ddot{x_0} = 0.005$, 0.015, 0.05, and 0.15 g. X(1) is beam displacement and X(2) is PPF controller displacement. See Appendix B for sensor sensitivities.

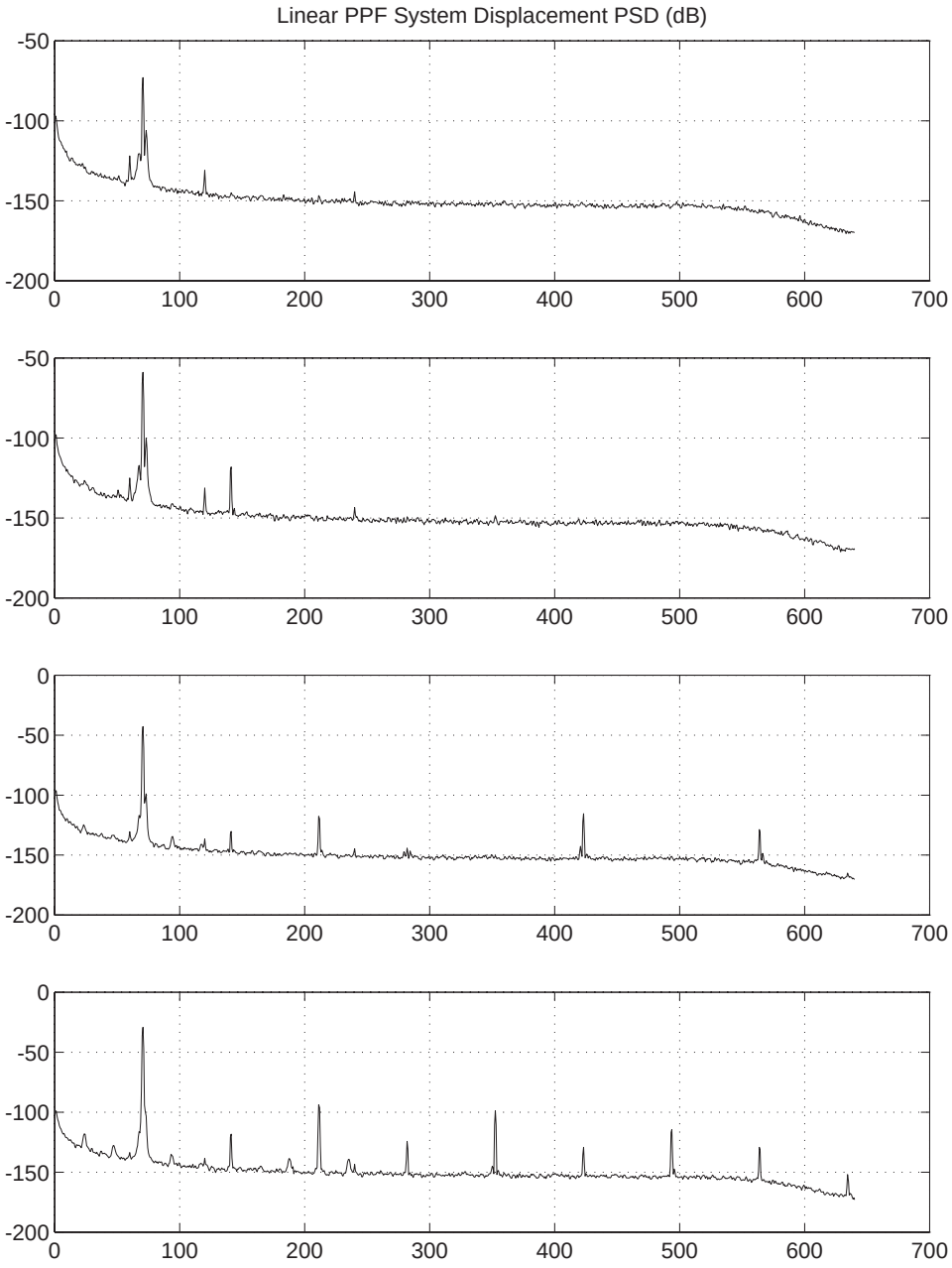

Figure 5.23: Screw Mounted Beam with linear PPF response spectrum for $\ddot{x_0} = 0.005$, 0.015, 0.05, and 0.15 g (from top to bottom).

retical results. The X-Y results and Poincare sections can be seen in the second column of Figures 5.18-5.19. For a given forcing level, the system response is reduced due to the action of the absorber within the narrow absorber bandwidth. The linear PPF results thus agree with the single-degree-of-freedom model presented in Chapter 3.

5.2.3 Nonlinear PPF

The experimental effect of a nonlinear absorber was next investigated. A nonlinear hardening term was added to the linear PPF filter. Its level was set to maximize the nonlinear influence without destabilizing higher modes in the beam. The reason for destabilization is unclear but similar to increasing the system gain. The loss of stability was for zero input force and it is hypothesized that the shifting of phase due to the nonlinear term caused the third mode to destabilize. Since the linear gain was set near the stability boundary, the nonlinear phase shift would cause the higher mode to destabilize. This is an influence of the required low-pass filter and not an effect of the PPF vibration absorber per se. As before, analog implementation is recommended to avoid this problem in future investigations. If the linear gain was reduced, greater nonlinearity was possible. However, to maintain consistent results, this was not done. Instead, the nonlinear stiffness was set as high as possible without destabilizing the third mode, since this was sufficient to demonstrate the influence of nonlinearity on the absorber performance.

Swept sine tests were conducted and the results are shown in the third row of Figures 5.14-5.15. Initially, the nonlinear absorber performs better than the linear absorber; system response is reduced with less absorber stroke. However, when the forcing level is increased to 0.15 g, absorber performance is degraded and the system response is quasiperiodic. Note that the apparent "noisy" absorber response is due to the zoom frf's used in swept sine testing. Only the response around the driving frequency is plotted, not the total rms of the system. As the excitation frequency changes, the response at that frequency varies, giving the "noisy" appearance. Also note that the "dip" in system and absorber performance on the 0.05 g response curves corresponds to quasiperiodic response at reso-

nance. Again, the narrowband rms may decrease, but the magnitude of system response actually increases. The response simply is in other frequencies. The screw beam swept sine testing thus agrees with the analytical models. As the forcing level was increased, quasiperiodic system response occurs due to a Hopf bifurcation and causes a breakdown in absorber performance.

To further investigate this phenomenon, time responses were measured at 70.5 Hz for various forcing levels. The results are presented in Figure 5.24. As the forcing is increased from 0.005 to 0.015 to 0.05 g's, absorber performance is excellent. However when the force is increased to 0.15 g, the response appears quasiperiodic. Examining the spectrum in Figure 5.25, the quasiperiodic nature of the response is evident. This is also confirmed by the X-Y plots and Poincare sections plotted in Figure 5.18 and Figure 5.19, respectively.

These results thus indicate that the analytical model for a single-degree-of-freedom system with a vibration absorber is capable of qualitatively modelling the behavior of the screw-mounted beam. As predicted, the nonlinearities present in the beam did not significantly affect the performance of the linear PPF algorithm. However, the introduction of absorber nonlinearity, while widening the suppression bandwidth, also introduced Hopf bifurcations resulting in quasiperiodic response and poor absorber behavior. The nonlinearity in the absorber is thus insignificant for low excitation amplitude, beneficial for moderate excitation amplitude, and detrimental for large excitation amplitude.

5.3 Summary

Experimental investigation was conducted on a single-degree-of-freedom, a two-degree-of-freedom, and a continuous system with vibration absorbers tuned to the first linear natural frequency. The results quantitatively validate the models presented in the previous chapters. As the excitation level increases, experimental verification of the predicted quasiperiodic and chaotic response was obtained. Additionally, the need to tune the sign of the nonlinearity of the absorber opposite to that of the system was observed.

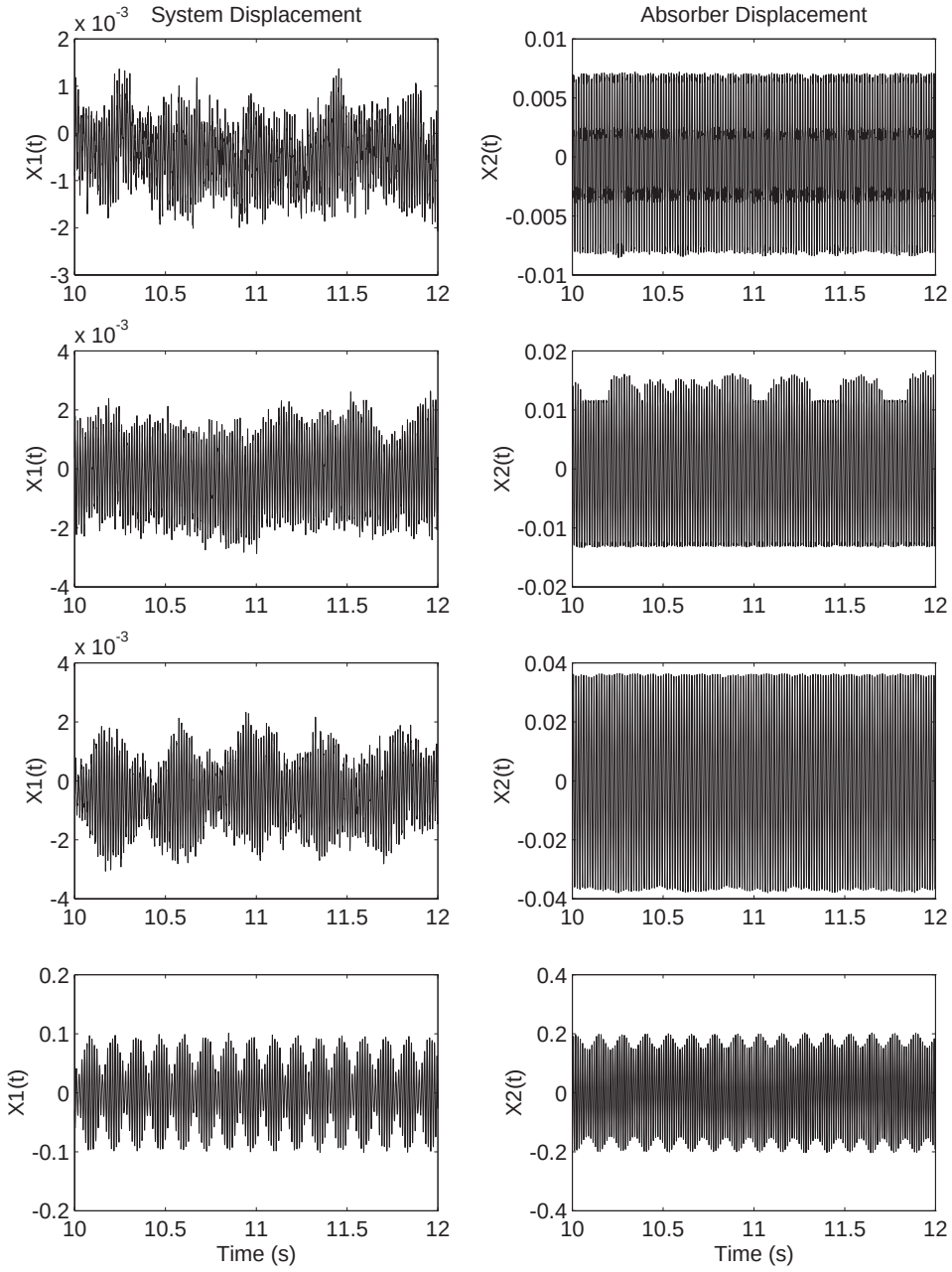

Figure 5.24: Screw Mounted Beam nonlinear PPF time response in volts for $\ddot{x}_0 = 0.005$, 0.015, 0.05, and 0.15 g. X(1) is beam displacement and X(2) is PPF controller displacement. See Appendix B for sensor sensitivities.

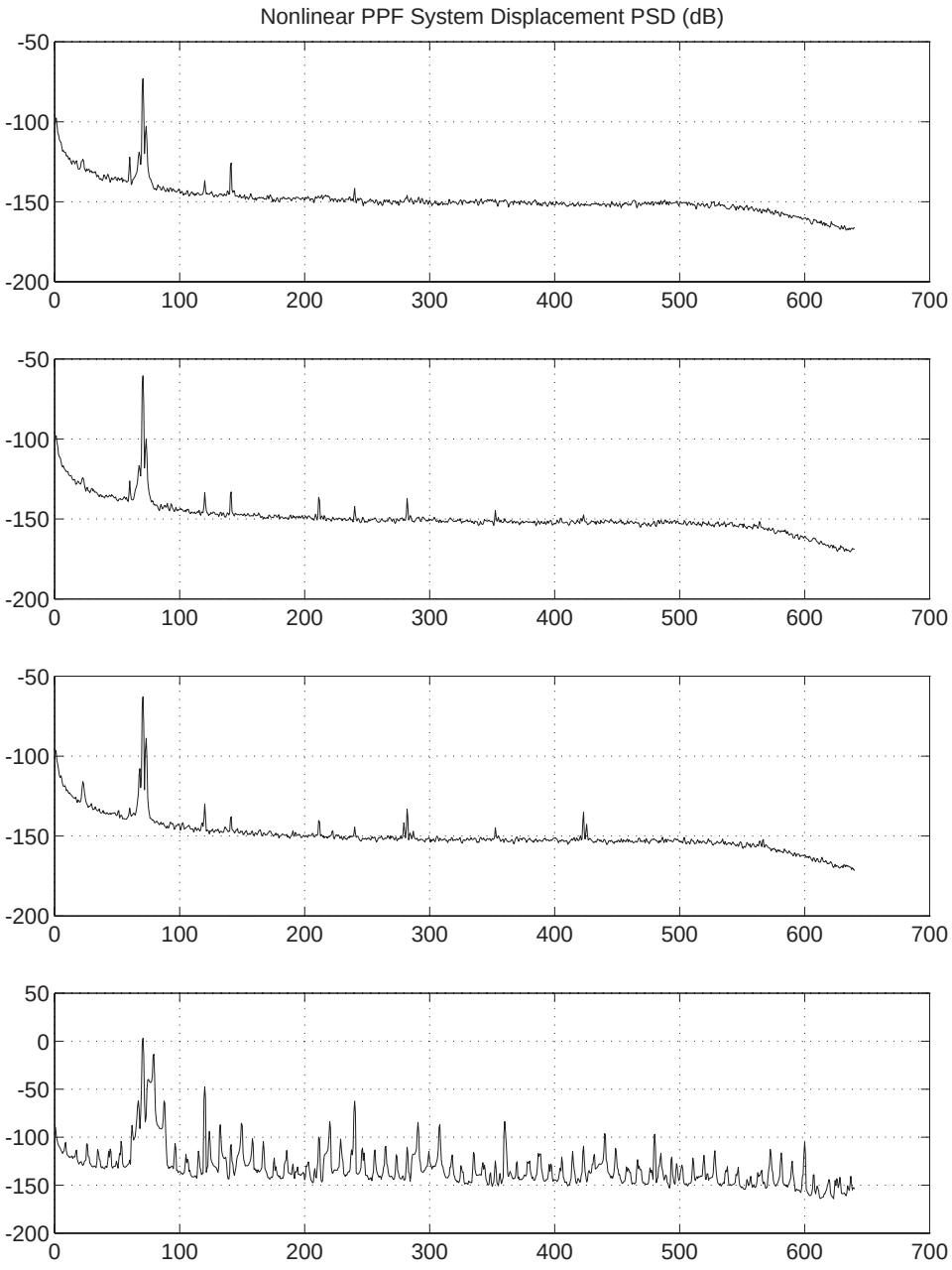

Figure 5.25: Screw Mounted Beam with nonlinear PPF response spectrum for $\ddot{x_0} = 0.005$, 0.015, 0.05, and 0.15 g.

Chapter 6

Conclusions and Future Work

The focus of this work was to investigate the performance of nonlinear vibration absorbers for lightly damped multi-degree-of-freedom discrete structures. The objectives were to:

- Demonstrate the equivalence, to first-order nonlinear effects, of the mechanical vibration absorber, the piezoelectric vibration absorber, and positive position feedback.
- Utilize perturbation methods to find the general nonlinear response of the aforementioned systems.
- Develop guidelines for tuning the linear and nonlinear parameters for vibration absorbers for nonlinear single-degree-of-freedom systems.
- Demonstrate the use of nonlinear normal modes to allow modal design of absorbers for N-degree-of-freedom nonlinear structures using these guidelines.
- Qualitatively verify the models through experimental investigations for both single and multiple degree-of-freedom systems.

Each of these objectives has been addressed.

6.1 Conclusions

In Chapter 2, a general model for the mechanical vibration absorber, the Inductive-Resistive Shunted piezoelectric vibration absorber, and the electronic (Positive Position Feedback) vibration absorber was derived. The model allows a single set of equations to investigate the effects of nonlinearity on absorber performance using a single dynamic model. Furthermore, this model was consistent between systems with its degrees of freedom maintaining a consistent physical meaning, a feature unique in the literature. By deriving this model, the effect of nonlinearity on the piezoelectric and electronic vibration absorber, an effect unexplored in the literature heretofore, as well as those for the mechanical vibration absorber could be examined using perturbation, numerical and experimental methods and the results applied to all three physical implementations.

In Chapter 3, the general model developed in Chapter 2 for the single-degree-of-freedom system with a vibration absorber were investigated using both perturbation and numerical methods. Parameter studies were performed on four systems, the linear system with a linear absorber, the linear system with a nonlinear absorber, the nonlinear system with a linear absorber, and the nonlinear system with a nonlinear absorber. Three key performance qualities were identified: suppression bandwidth, stability and robustness.

The size of the suppression bandwidth was found to depend not only on the coupling parameter (either mass ratio, piezoelectric coupling coefficient, or gain) but also on the force and absorber nonlinearity as a function of the $\frac{\delta_3 f^2}{\alpha_1^2}$ parameter group and the linear frequency mistuning parameter, δ_1. The identification of these groups and the effect of frequency mistuning is a novel result and shows that for an absorber tuned above the open-loop modal frequency, a hardening absorber is superior whereas below the modal frequency, a softening absorber is required. The location in frequency of the suppression region was found to depend on the tuning frequency of the absorber as well as the nondimensional nonlinear parameter discussed above. The combination of these show that the maximum achievable bandwidth increases as the tuning frequency deviates from the open-loop modal frequency.

Moreover, it was determined that system nonlinearity did not affect the suppression region at the level of approximation considered in this study.

This does not imply that system nonlinearity is unimportant: it affects the second parameter, robustness. Robustness, defined in this study as the absence of multiple solutions, one of low and the other of high magnitude, in the absorber suppression region. If the system nonlinearity is of the same type (hardening or softening), the resonant peaks will overlie the suppression region, eliminating system robustness. Additionally, even for a linear absorber, robustness is a concern when coupled with the linear mistuning. If the absorber is tuned to a frequency less than the modal frequency, robustness is an issue for hardening systems. The contrary is also true. The end result is that for softening systems, a hardening nonlinear absorber tuned to a frequency above the open-loop modal frequency is desirable; whereas, for a hardening system, a softening absorber should be tuned to frequencies below the modal frequency. This result clarifies conflicting reports of hardening or softening absorber preference in the literature.

The third and perhaps most troubling performance characteristic is stability of the periodic solutions in the suppression region. As the excitation level increased, a Hopf bifurcation was found to occur, resulting in quasiperiodic response of the system. This response was determined detrimental to absorber performance for lightly damped systems. In the literature, the presence of higher harmonic behavior has in some cases been beneficial. However, most of those investigations concerned highly damped systems. For the lightly damped systems considered herein, the quasiperiodic response always resulted in poor performance. For modal frequencies between the locations of linear resonance (i.e. between the dual natural frequencies of the undamped linear vibration absorber) these quasiperiodic responses seem to limit the benefit of the nonlinearity to low forcing levels only. For higher forcing levels, increased damping is required to suppress this effect, trading suppression performance for stability. At present, no analytic solution for the location of the Hopf bifurcations within the suppression bandwidth is available for lightly coupled absorbers.

Having considered the performance of the vibration absorber on lightly damped single-

degree-of-freedom systems in Chapter 3, multiple-degree-of-freedom systems were considered in Chapter 4. The theory of nonlinear normal modes was extended in this work to include harmonic forcing near the linear resonance, linear modal damping, and the presence of small linear coupling. Using these results, the effect of vibration absorbers tuned near a structural mode was shown to reduce to the response on a single four dimensional manifold. The dynamics of this manifold were exactly of the form investigated in Chapters 2 and 3. Numerical integration demonstrated some limitations to the $O(\epsilon)$ models derived in this investigation. Since the size of the suppression region is $O(\epsilon^2)$, the models derived, while sufficient for qualitative analysis, are insufficient for quantitative analysis. Essentially, since the size of the suppression region is zero at the level of the analysis, small shifts in the location of this region can result from unmodeled effects in the next level of analysis. Qualitatively, the model is accurate and allows important insight into absorber performance. More importantly, the application of nonlinear normal mode theory simplifies the dynamics required for preliminary analysis, even if final performance considerations would require a more detailed analysis.

Finally, the accuracy of the qualitative aspects of the model were verified through experimental investigations presented in Chapter 5. Little experimental investigation of nonlinear vibration absorbers was found in the literature. Through the analog computer investigations, the effects predicted in Chapters 2-4 were verified. The nonlinearity shifted the suppression bandwidth as predicted. The quasiperiodic responses predicted in the literature were observed experimentally for the first time to the author's knowledge. Furthermore, the transition of the response to chaotically modulated motion was observed. The beam experiment again verified the model on a real-world structure. Quasiperiodic response was again observed, although chaotic response was not, perhaps due to limitations in forcing level and/or feedback gains. Additionally, the effect of the filtering on the stability of higher modes was also noted. Finally, the quasiperiodic response was not a gradual transition, but instead an abrupt jump phenomenon. This discovery emphasizes the need to avoid this region since, if the force was increased to the point where quasiperiodic response occurred,

a significant reduction in the forcing level was required to regain periodic performance.

All of the goals for this research have thus been accomplished. A consistent model for the three common implementations of the vibration absorber has been derived. This performance of the nonlinear vibration absorber has been investigated and qualitative agreement was found between the analytical model and both numerical and experimental results. The performance of nonlinear vibration absorbers for multi-degree-of-freedom discrete structure has been explored and via the application of nonlinear normal modes shown to reduce to the dynamics of the single-degree-of-freedom model. Experimental results have been performed and demonstrate the presence of quasiperiodic and chaotically-modulated response.

6.2 Future Work

This work would be incomplete without some discussion on the practicality and applicability of the nonlinear vibration absorber for engineering applications. In the author's opinion, the benefits of the nonlinear absorber are outweighed by the limitations imposed by stability concerns for linear systems at this time. If possible, a larger coupling should be sought rather than resorting to a nonlinear absorber. For a nonlinear structure, the utility of the nonlinear absorber may be to create a more robust system by bending the resonant responses away from the suppression region. If a nonlinear absorber is required, the natural frequency of the system should be shifted so that the absorber is operating away from the open-loop resonance for best performance. System damping should also be increased since the quasiperiodic response can be delayed. Under these circumstances, it is possible to design a vibration absorber capable of significantly increasing the suppresion bandwidth for a moderate excitation level as shown in Chapter 3. Further investigation is required before nonlinear vibration absorbers enter the vibration engineer's toolbox. Future work on the nonlinear vibration absorber can be divided into three sections: additional investigations with the current $O(\epsilon)$ analysis, extension of this analysis, and further experimental work.

Using the current model, several more investigations should be undertaken. First, the

results of this study have been limited to light damping since this case was least investigated in the literature. The damped nonlinear vibration absorber should be examined. The application of damped vibration absorbers is generally to broadband, randomly excited structures, but they can and are used to suppress harmonic excitation as well. In the numerical investigation of the piezoelectric vibration absorber reported in [46], the presence of undamped resonant response in damped vibration absorbers was seen. This should be further investigated. Additionally, more investigation on the relationship between damping and the minimum excitation level of the Hopf bifurcations is required to establish design guidelines. The results of this analysis could be used to determine optimal designs though the application of optimization techniques. Such an analysis should consider the effects of using (static) added mass or stiffness to shift system frequencies and allow larger suppression bandwidths. Any optimization effort must also consider the robustness and stability of the final design, something lacking in the current literature.

To allow better quantitative analysis required to verify performance and fine-tune designs, the $O(\epsilon)$ analysis presented herein should be extended to the next level. This will allow more accurate determination of the suppression region's location and width. Additionally, the next level of analysis would allow analytical evaluation of preliminary designs determined using the current analysis. A useful result would be an analytical determination of the Hopf bifurcation points for lightly coupled systems such a more detailed analysis might provide. A second extension of the analysis would be to examine the performance of vibration absorbers coupled to a set of internally resonant modes. Since periodic and symmetric structures are common in engineering design, such an analysis would be required to handle internally resonant modes.

Further experimental investigation of the application of nonlinear normal modes to real-world structures is required. The accuracy of the predicted responses must be quantitatively established by using structures with analytical models such as clamped-clamped beams. Although nonlinear, the screw-mounted beam did not exhibit large nonlinearities at the forcing levels obtainable with available equipment. Additionally, although nonlinear Positive Po-

sition Feedback controllers or inductive-resistive piezoelectric shunts can be implemented, a robust mechanical absorber with controllable nonlinear properties must be identified for those situations where the electronic or piezoelectric vibration absorber is impractical. Additionally, the nonlinear properties of piezoelectric materials must to determined to allow a proper nonlinear design. Through the pursuit of these experimental investigations along with the analytical investigations suggested above, the nonlinear vibration absorber may be able to achieve the level of practicality required to join the engineer's toolchest.

Bibliography

[1] A. D. Nashif, D. I. G. Jones, *et al. Vibration Damping.* John Wiley & Sons, New York, NY, 1985.

[2] D. J. Inman. *Engineering Vibration.* Prentice Hall, Englewood Cliffs, NJ, revised edn., 1996.

[3] L. Meirovitch. *Elements of Vibration Analysis.* McGraw-Hill, New York, NY, second edn., 1986.

[4] A. H. Nayfeh and D. T. Mook. *Nonlinear Oscillations.* John Wiley & Sons, New York, NY, 1979.

[5] R. M. Rosenberg. The normal modes of nonlinear n-degree-of-freedom systems. *Journal of Applied Mechanics*, **30**:7–14, 1962.

[6] R. M. Rosenberg and J. K. Kuo. Nonsimilar normal mode vibrations of nonlinear systems having two degrees of freedom. *Journal of Applied Mechanics*, **31**:283–290, 1964.

[7] R. M. Rosenberg. On nonlinear vibrations of systems with many degrees of freedom. In G. Kuerti, ed., *Advances in Applied Mechanics*, vol. 9, pp. 155–242. Academic, New York, NY, 1966.

[8] A. H. Nayfeh and B. Balachandran. *Nonlinear Interaction.* John Wiley & Sons, New York, NY, 1997.

[9] A. F. Vakakis, L. I. Manevitch, *et al. Normal Modes and Localization in Nonlinear Systems*. John Wiley & Sons, New York, NY, 1996.

[10] S. W. Shaw and C. Pierre. Non-linear normal modes and invariant manifolds. *Journal of Sound and Vibration*, **150**:170–173, 1991.

[11] S. W. Shaw and C. Pierre. Normal modes for non-linear vibratory systems. *Journal of Sound and Vibration*, **164**:85–124, 1993.

[12] J. C. Slater and D. J. Inman. Nonlinear modal control method. *Journal of Guidance, Control and Dynamics*, **18**:433–440, 1995.

[13] A. H. Nayfeh, S. A. Nayfeh, *et al.* On nonlinear normal modes of systems with internal resonance. *Journal of Vibration and Acoustics*, **118**:340–345, 1996.

[14] J. C. Slater. *Nonlinear Modal Control*. Ph.D. thesis, State University of New York at Buffalo, 1993.

[15] D. Sciulli. *Dynamics and Control for Vibration Isolation*. Ph.D. thesis, Virginia Polytechnic Inst. and State Univ., 1997.

[16] J. P. DenHartog and J. Ormondroyd. The theory of the dynamic vibration absorber. *Transactions of the ASME*, **50**:A9–A22, 1928.

[17] J. Q. Sun, M. R. Jolly, *et al.* Passive, adaptive, and active tuned vibration absorbers. *Trans. ASME Combined Anniversary Issue Journal of Mechanical Design and Journal of Vibration and Acoustics*, **117(B)**:234–42, 1995.

[18] A. H. VonFlotow, A. Beard, *et al.* Adaptive tuned vibration absorbers: Tuning laws, tracking agility, sizing, and physical implementations. *Proc. Noise-Con 94*, 1994.

[19] R. L. Forward. Electronic damping of vibrations in optical structures. *Journal of Applied Optics*, **18**:690–7, 1979.

[20] N. W. Hagood and A. VonFlotow. Damping of structural vibrations with piezoelectric materials and passive electrical networks. *Journal of Sound and Vibration*, **146**:243–68, 1991.

[21] D. L. Edberg, A. S. Bicos, *et al.* On piezoelectric energy conversion for electronic passive damping enhancement. In *Proc. Damping '91*, pp. GBA–1. U. S. Air Force, San Diego, CA, 1991.

[22] J. J. Hollkamp. Multimodal passive vibration suppression with piezoelectric materials and resonant shunts. *Journal of Intelligent Materials Systems and Structures*, **5**:49–57, 1994.

[23] J. J. Hollkamp and T. F. Starchville. A self-tuning piezoelectric vibration absorber. In *Proc. 35th AIAA/ASME/ASCE/AHS/ACS Structures, Structural Dynamics and Materials Conf.*, pp. 94–1790. American Institute of Aeronautics and Astronautics, Hilton Head, SC, April 1994.

[24] G. S. Agnes. Active/passive piezoelectric vibration suppression. *Journal of Intelligent Materials, Systems, and Structures*, **6**:482–7, 1995.

[25] S. N. Joshi. Nonlinear constitutive relations for piezoelectric materials. *Smart Materials and Structures*, **1**:80–3, 1992.

[26] R. E. Roberson. Synthesis of a nonlinear vibration absorber. *Journal of the Franklin Institute*, **254**:205–20, 1952.

[27] F. R. Arnold. Steady-state behavior of systems provided with nonlinear dynamic vibration absorbers. *Journal of Applied Mechanics*, **22**:487–92, 1955.

[28] L. A. Pipes. Analysis of a nonlinear dynamic vibration absorber. *Journal of Applied Mechanics*, **20**:515–8, 1953.

[29] H. M. Miller and J. R. Gartner. Tunable, non-linear vibration absorber. *ASME Paper*, **75-DET-9**, 1975.

[30] J. B. Hunt and J. C. Nissen. The broadband dynamic vibration absorber. *Journal of Sound and Vibration*, **83**:573–8, 1982.

[31] H. Kojima and H. Saito. Forced vibrations of a beam with a non-linear dynamic vibration absorber. *Journal of Sound and Vibration*, **88**:559–568, 1983.

[32] I. N. Jordanov and B. I. Cheshankov. Optimal design of linear and non-linear dynamic vibration absorbers. *Journal of Sound and Vibration*, **123**:157–170, 1988.

[33] J.-C. Nissen, K. Popp, *et al.* Optimization of a non-linear dynamic vibration absorber. *Journal of Sound and Vibration*, **99**:149–154, 1985.

[34] J. Shaw, S. W. Shaw, *et al.* On the response of the nonlinear vibration absorber. *International Journal of Nonlinear Mechanics*, **24**:281–93, 1989.

[35] H. J. Rice and J. R. McCraith. Practical non-linear vibration absorber design. *Journal of Sound and Vibration*, **116**:545–559, 1987.

[36] S. Natsiavas. Steady state oscillations and stability of non-linear vibration absorbers. *Journal of Sound and Vibration*, **156**:227–245, 1992.

[37] M. F. Golnaraghi. Regulation of flexible structures via nonlinear coupling. In *Dynamics and Control I*, pp. 405–28. Kluwer Academic, Boston, MA, 1991.

[38] S. S. Oueini, A. H. Nayfeh, *et al.* Control of flexible structures using the saturation phenomenon. *Nonlinear Dynamics*, **Submitted**, 1996.

[39] C. J. Goh and T. K. Caughey. On the stability problem caused by finite actuator dynamics in the collocated control of large space structures. *International Journal of Control*, **41**:787–802, 1985.

[40] J. L. Fanson and T. K. Caughey. Positive position feedback control for large space structures. In *Proc. 28th AIAA/ASME/ASCE/AHS/ACS Structures, Structural Dynamics*

and Materials Conf., pp. 87–0902. American Institute of Aeronautics and Astronautics, Monterey, CA, April 1987.

[41] J. L. Fanson and T. K. Caughey. Positive position feedback control for large space structures. *AIAA Journal*, **28**, 1990.

[42] L. Meirovitch and H. Baruh. Control of self-adjoint distributed-parameter systems. *Journal of Guidance and Control*, **5**:59–66, 1982.

[43] L. Meirovitch, H. Baruh, *et al.* Comparison of control techniques for large flexible systems. *Journal of Guidance and Control*, **6**:302–310, 1983.

[44] T. K. Caughey. Dynamic response of structures constructed from smart materials. *Smart Materials and Structures*, **4**:A101–A106, 1995.

[45] J. J. Dosch. *Active Vibration Suppression: Stability and Design in Second Order Form.* Ph.D. thesis, S.U.N.Y at Buffalo, 1995.

[46] G. S. Agnes and D. J. Inman. Nonlinear piezoelectric vibration absorbers. *Smart Materials and Structures*, **5**:704–714, 1996.

[47] B. Jaffe, R. Cook, *et al. Piezoelectric Ceramics.* Academic, New York, NY, 1971.

[48] A. H. Nayfeh. *Introduction to Perturbation Techniques.* John Wiley & Sons, New York, NY, 1981.

[49] The MathWorks, Inc. *MATLAB© High-Performance Numeric Computation and Visualization Software Reference Guide Ver. 4.2c.* http://www.mathworks.com, 1992.

[50] J. P. DenHartog. *Mechanical Vibrations.* Dover Books, New York, NY, 1985.

[51] A. H. Nayfeh and B. Balachandran. *Applied Nonlinear Dynamics.* John Wiley & Sons, New York, NY, 1995.

[52] A. F. Vakakis. Nonlinear normal modes (nnms) and their applications in vibration theory: An overview. *Mechanical Systems and Signal Processing*, **11**:3–22, 1997.

[53] R. Seydel. *From Equilibrium to Chaos. Practical Bifurcation and Stability Analysis.* Elsevier, New York, 1988.

[54] R. Seydel. Tutorial on continuation. *International Journal of Bifurcation and Chaos*, **1**, 1990.

[55] E. Doedel, H. B. Keller, *et al.* Numerical analysis and control of bifurcation problems (i) bifurcation in finite dimensions. *International Journal of Bifurcation and Chaos*, **1**:493–520, 1991.

[56] U. Feudel and W. Jansen. Candys/qa–a software system for qualitative analysis of nonlinear dynamical systems. *International Journal of Bifurcatin and Chaos*, **2**:773–794, 1992.

[57] H. B. Keller. Numerical solution of bifurcation and nonlinear eigenvalue problems. In P. H. Rabinowitz, ed., *Applications of Bifurcation Theory*, pp. 359–389. Academic Press, New York, 1977.

[58] dsp Technology, Inc. *dspT Siglab Version 2.13 User's Guide.* siglab@dspt.com, 1996.

Appendix A

PSAL Overview

PSAL performs pseudo-arclength continuation to find solutions to a system of nonlinear equations, $\{\mathbf{F}\}(\{\mathbf{x}\};\{\lambda\}) = \{\mathbf{0}\}$. It is a robust code with the following key capabilities.

- Determination of fixed points with or without time integration of the equations $\{\mathbf{x}\}' = \{\mathbf{F}\}(\{\mathbf{x}\};\{\lambda\}_0)$ from a user supplied initial guess $\{\mathbf{x_0}\}$.
- User function $\{\mathbf{F}\}(\{\mathbf{x}\};\{\lambda\})$ is input along with its Jacobian in a single MATLAB function.
- Continuation is performed within a user specified parameter range with adaptive step-size using pseudo-arclength continuation.
- Bifurcation points are identified using efficient indirect methods and then solved for using direct methods if desired. Turning Point, Hopf, and Branch points are supported. Branch switching is not yet implemented.
- Newton-Raphson methods are employed throughout. Second order differentials are thus required for direct solution of bifurcation points. Numerical computation of these derivatives is supported.

This combination of features combined with MATLAB's flexible programing environment allow PSAL to serve as an excellent tool for parameter study, especially for small to

medium size problems. The source code may be obtained by emailing the author at `greg.agnes@iname.com`.

The goal of continuation methods is to determine a set of solutions to the n equations $F(x;\lambda) = 0$ such that $x \in \Re^n$ and $\lambda \in \Re^m$ as one (or more) of the parameters, λ_i varies from an initial solution $\{x_0, \lambda_0\}$. Some basic references used in constructing the code are [51, 53–57]. The algorithm for constructing a continuation scheme consists of three key portions: first, a robust root finder for systems of nonlinear equations to find the initial solution, $\{x_0, \lambda_0\}$; next, a prediction method to step from the initial solution to an adjoining solution; and finally, since he predicted solution won't usually be an actual point in the solution set, a correction method to find the actual solution. The algorithm continues stepping from solution to solution until a stopping point is encountered. As it steps, bifurcation points must be identified and the stability of the solution tracked. The algorithm followed must therefore look as follows:

i. Find a starting ($k = 0$) solution, $\{x_0; \lambda_0\}$, to $F(x;\lambda) = 0$.

ii. Evaluate the stability of this solution.

   (a) If a bifurcation occurred between x_k and x_{k-1}, determine the type and use a direct method to find it.

iii. Set $k = k + 1$ and Predict the next solution, $\{x_k^0; \lambda_k^0\}$

iv. Correct the solution with p iterations and set $x_k = x_k^p$ and $\lambda_k = \lambda_k^p$.

v. If $\{x_k, \lambda_k\}$ is out of bounds, terminate; otherwise repeat from step 2.

The theory of each of the first four steps is briefly explained in the next four subsections. The Fifth step consists of checking if λ_k is within user set bounds. For efficiency and data structure limitations in MATLAB, the code actually performs a user set block of iterations before termination. This allows a matrix of fixed size to be returned and stored. The results are then stored in a large Matrix with an index identifying the run (which starting point it

began from). The actual code does not terminate, but allows the user to begin the process again from a new starting point. Additionally, plotting commands are used to post-process and plot the data.

A.1 Initial Solution

The initial solution to the equations $F(x;\lambda) = 0$ is accomplished using a Newton-Raphson iteration scheme:

$$\lambda = \lambda_0 \tag{A.1}$$

$$x_k^{j+1} = x_k^j + r\Delta x^j \tag{A.2}$$

$$F_x(x_k^j;\lambda_0)\Delta x^j = -F(x_k^j;\lambda_0) \tag{A.3}$$

where F_x is shorthand notation for the matrix $\frac{\partial F(x;\lambda)}{\partial x}$. The parameter r is a relaxation parameter used to ensure $||F(x_{k+1},\lambda_0)|| < ||F(x_k,\lambda_0)||$. If not, r is reduced until this relation is satisfied. The iteration is repeated until

$$||F(x_k,\lambda_0)|| < E_a \tag{A.4}$$

where E_a indicates how close to zero the norm of F must be.

In addition to the Newton-Raphson approach, the implementation also allows numerical integration in time of the equations since often one is looking for the steady state response to $x' = F(x,\lambda)$. If this is the case, time integration can reduce the initial estimate of the solution before Newton-Raphson iteration is used, improving the chance of convergence. Note that the Newton-Raphson algorithm is quadratically convergent so it usually is faster to use it as opposed to time integration.

A.2 Predictor

Once a solution is found, a prediction to the next fixed point in $\{x,\lambda\}$ state-control space is needed. It is tempting to just increment λ and repeat the Newton-Raphson process.

This approach will not yield successful results near turning or branch bifurcation points as explained in [51, 53], for example. Instead a tangent predictor is used in a scheme known as arclength continuation [51]. Thus, we consider the arclength s along the fixed-point solution curve and have $x = x(s)$ and $\lambda = \lambda(s)$. Differentiating the fixed point equation, $F(x, \lambda) = 0$, with respect to s

$$F_x(x;\lambda)x' + F_\lambda(x;\lambda)\lambda' = 0 \tag{A.5}$$

a system of n equations in $n+1$ unknowns. To find a solution we set

$$x'^T x' + \lambda'^2 = \Delta s^2 \tag{A.6}$$

which allows solution for the predicted step using an Euler step:

$$x^0_{k+1} = x_k + x'\Delta s \tag{A.7}$$

$$\lambda^0_{k+1} = \lambda_k + \lambda'\Delta s \tag{A.8}$$

This predicted solution will not usually be an exact solution, but will require correction. The size of the step, Δs, is adapted in the code using a method suggested in [53]. The length of the step is based upon the number of corrections needed to converge. The Euler step is slightly modified to

$$x^0_{k+1} = x_k + x'||x_k, \lambda_k||\Delta s_k \tag{A.9}$$

$$\lambda^0_{k+1} = \lambda_k + \lambda'||x_k, \lambda_k||\Delta s_k \tag{A.10}$$

$$\Delta s_k = \Delta s_k \left(\frac{j_k}{j_{des}}\right)^{\frac{1}{2}} \tag{A.11}$$

where p_k is the number of correction steps needed to converge to x_k, λ_k. The number of desired correction steps j_{des} was set to twelve, but can be adjusted if desired.

A.3 Corrector

Once a prediction $\{x^0_{k+1}, \lambda^0_{k+1}\}$ is determined, it must be corrected to satisfy the fixed point equation. Again it is tempting to fix λ and use the initial solution iteration, but

this approach will face problems at either branch or turning points. To solve this problem, pseudo-arclength continuation is used. Instead of seeking a solution parametrized by $\lambda = \lambda_{k+1}^0$, one is sought which satisfies

$$g(x,\lambda) = (x - x_k)^T x_k' + (\lambda - \lambda_k)\lambda_k' - ||x_k, \lambda_k||\Delta s_k = 0 \tag{A.12}$$

This is equivalent to searching for a solution which is normal to the predicted step, thereby allowing one to move around most turning points. If small steps are taken, this also allows branch points to be included, but does not guarantee branch switching will not occur [53]. To perform the correction, an iterative Newton-Raphson algorithm is used:

$$F_x(x_{k+1}^j, \lambda_{k+1}^j)\Delta x^j + F_\lambda(x_{k+1}^j, \lambda_{k+1}^j)\Delta\lambda^j = -F(x_{k+1}^j, \lambda_{k+1}^j) \tag{A.13}$$

$$x_k'^T \Delta x^j + \lambda_k'\Delta\lambda^j = -g(x_{k+1}^j, \lambda_{k+1}^j) \tag{A.14}$$

and

$$x_{k+1}^{j+1} = x_{k+1}^j + r\Delta x^j \tag{A.15}$$

$$\lambda_{k+1}^{j+1} = \lambda_{k+1}^j + r\Delta\lambda^j \tag{A.16}$$

are repeated until convergence. Again, r is a relaxation parameter. If the equations fail to converge, the step length, Δs, is reduced and the correction is repeated. Should this procedure fail to converge, a singularity in the solution is probable. From experience, this often happens at undamped resonant peaks. Once a solution is found, the index , k, is updated and the prediction/correction cycle repeated until termination. Before beginning the next prediction cycle, the stability of the new fixed point is investigated to determine if bifurcations have occurred.

A.4 Stability and Bifurcation

Two classes of methods are available to detect and determine bifurcation points: indirect and direct. Indirect methods determine the passage of a bifurcation point by examining

data calculated at the fixed points determined by the corrector step. In general they are "cheap" to evaluate, but not accurate in determining the location of the bifurcation point. They simply determine that a bifurcation point was located between x_{k-1} and x_k. Direct methods, in contrast, are more expensive to evaluate since they rely on iterative solutions to larger systems of equations. They also require a good initial estimate of the root location and often the marginally stable eigenvector of the jacobian (Since bifurcation is marked by the passage of an eigenvalue of the jacobian into the right-half plane) for convergence.

PSAL uses a combination of indirect and direct methods. Indirect methods are used to identify the presence and type of bifurcation point as the method steps along the fixed point curve. Once a bifurcation point is identified, its corresponding direct method is used to locate the point more exactly if desired. Thus for quick initial parameter studies an approximation can be used, while for more accurate analysis, the direct solution can be found. The drawback to this approach is that bifurcations can be missed if two bifurcation points lie between the steps taken by the prediction-correction cycle. This possibility can be minimized by performing runs with smaller values of Δs, the prediction step size.

Three types of bifurcation points are detected: turning points, branch points, and Hopf points. The first two are characterized by having F_x lose stability through the origin. Thus a single real pole moves into the right-half plane. A Hopf bifurcation occurs when two complex conjugate poles move into the right-half plane. Turning points and branch points differ since for a turning point $F_\lambda \in \aleph(F_x)$ (the null space of F_x) whereas it is not for a branch point. By calculating

$$det = |F_x| \quad \text{and} \quad DET = \begin{vmatrix} F_x & F_\lambda \\ x'^T & \lambda' \end{vmatrix} \tag{A.17}$$

the presence of a turning or branch point can be detected since det changes sign for turning points while DET only changes at branch points. Since the stability of the fixed point is also of interest, the number of right-half plane eigenvalues is checked. If this increases or decreases by two, a Hopf point has occurred. Using these indirect calculations, the presence of bifurcation points is detected. For quick calculations, the points are identified

as the average of the current and previous fixed points. For more exact calculations, direct methods must be used.

To directly determine turning points, an expanded function, $T(x, p, \lambda) = 0$, is solved where

$$T(x, p, \lambda) = \begin{Bmatrix} F(x; \lambda) \\ F_x(x; \lambda)p \\ p^T p - 1 \end{Bmatrix} \tag{A.18}$$

Instead of using the Newton-Raphson method directly, a faster algorithm from [51] is used. The same algorithm will detect branch points since the equations simply state that the jacobian, $F_x(x, \lambda)$ has a real eigenvector u with a corresponding eigenvalue of zero.

For Hopf points, $H(x, p, q, \lambda, \omega) = 0$ is solved where

$$H(x, p, q, \lambda, \omega) = \begin{Bmatrix} F(x; \lambda) \\ F_x(x; \lambda)p - \omega q \\ F_x(x; \lambda)q + \omega p \\ p_k - 1 \\ q_k \end{Bmatrix} \tag{A.19}$$

In this case the F_x has an imaginary eigenvector $p \pm iq$ with a corresponding eigenvalue $\pm i\omega$. Note the last two equations simply normalize the eigenvector such that the k^{th} element is unity. Again, the algorithm for solving these equations is that in [51].

Finding the solution to Equations (A.18)-(A.19) depends on an initial guess for both the bifurcation point and its eigensolution. To determine this, the eigensolution of the jacobian at the initial guess of the bifurcation point with the largest real portion of the eigenvalue is used. Convergence is sometimes still an issue and the code resorts to taking smaller steps and using the indirect scheme.

In summary, the predictor, corrector and stability algorithms presented form a robust MATLAB toolbox for performing a single parameter study using pseudo-arclength continuation.

Appendix B

Experimental Setup

This appendix details the experimental setups used. Three sections detail the common equipment as well as the equipment used for analog computer simulations and the screw mounted beam experiment.

B.1 Common Equipment

All experiments were run with the general setup of Figure B.1. The experiment is connected to two I/O systems. One performs excitation and data acquisition while the other functioned as a Real-time DSP based controller.

Data acquisition was performed with two SigLab 20-42 units connected to an Intel PentiumPro 200 MHz. computer running Windows95. The SigLab [58] software runs as a Matlab© Virtual Instruments (VIs) which operate as an oscilloscope, function generator, spectrum analyzer, network analyzer, or swept sine analyzer. In addition, long time record capture to memory or disk is possible. All data was captured using the eight differential-ended inputs. Excitation was via the four single-ended outputs capable of producing a variety of signals including random, sine, step, and arbitrary. FFTs are performed real-time using DSP code on the SigLab unless otherwise noted. Data acquisition sampling rate, windowing, and other relevant parameters are indicated in the main text.

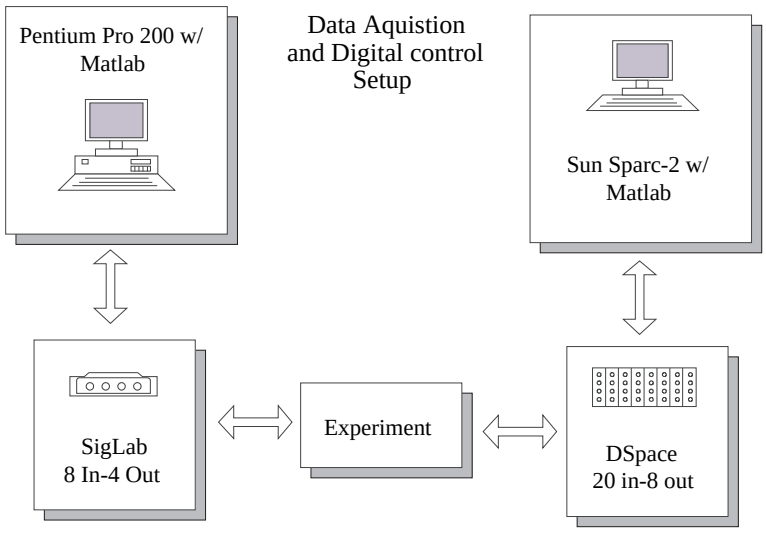

Figure B.1: General Experimental Setup.

The second I/O subsystem is a DSpacea real-time controller. Control systems are designed in Simulink and downloaded to the dsp chip for implementation via the Matlab© Real Time Workshop. This system allowed easy implementation of nonlinear real-time control, although its maximum sampling rate limitation required that a filter be used to smooth the 5 kHz discrete output of the D/A outputs. Their effect is discussed in Chapter 5.

B.2 Analog Computer

For the analog computer tests a Compdyna Model 7000/GP-10 system was used. To patch the two-degree-of-freedom system with a vibration absorber, all but one available amplifier was required. Free choice of the system parameters was therefore hampered. Additionally the limitation in maximum operating speed (time scale) imposes longer time requirements on data acquisition. Some DC offset of the amplifier channels was also present, and could not be eliminated. A benefit of the analog computer was the flexibility in adjusting system parameters in real time, allowing deeper understanding of the system dynamics in a given time than numerical integration.

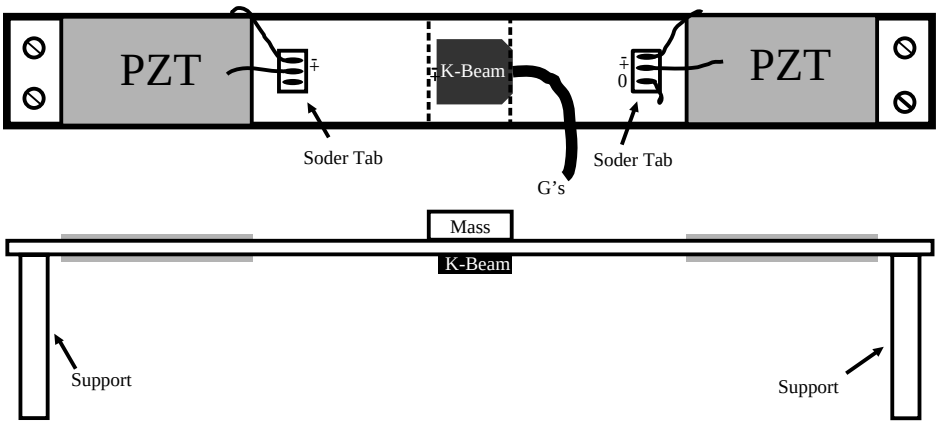

Figure B.2: Screw Mounted Beam. See text for dimensions.

B.3 Screw Mounted Beam

Experimental investigations were conducted on a screw mounted beam as seen in Figure B.2. The beam consisted of an 8.5 x 1 x 0.032 inch aluminum substrate with holes drilled at 1/4 in. from each edge at all four corners. Through these holes, the beam was mounted to 1/4 in. diameter supports typically used for spacing electronic circuit boards. A machine screw was used to connect the beam to the spacer. The boundary condition is not a classical one, but of common engineering practice with mode shapes similar to a clamped boundary condition.

To the beam, four 1.5 x 1 x 0.010 inch nickel-electroded, G1195 piezoceramic sheets were attached using MBond 2000 adhesive. Attachment was performed using the manufacturer's instructions for adhering strain gauges with the sole modification that a small drop of nickel print was placed in the center of the sheet to ensure electrical connection between the inner electrode and the beam, thereby providing a good ground plane. Polarity of the sheets on the top and bottom of the beam were flipped so a positive voltage applied to the beam resulted in a bending moment when the top sheet expands and the bottom contracts. The outer electrodes and the beam were then attached to solder tabs with fine wire. The solder tabs were then connected to an amplifier to provide a control actuator for the beam.

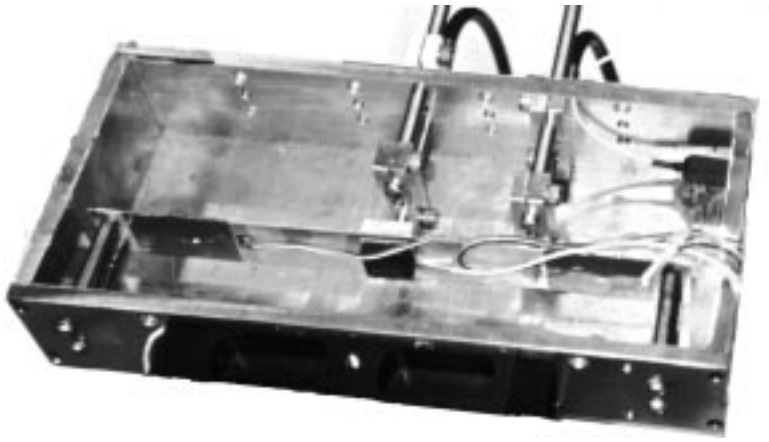

Figure B.3: Mounting of the beam.

Maximum amplifier voltage was 60 V.

To complete the beam, a Kistler K-Beam accelerometer (Type 8302A(X)S1) was attached at the center of the beam along with a 0.75 x 1.0 x 0.25 inch aluminum mass. The mass served two purposes. First, it lowered the natural frequency of the system. Second, the additional mass causes the effect of cable damping from both the piezoelectric and accelerometer leads to be reduced. The accelerometer had a sensitivity of 0.499 V/g with a maximum of 10 g's.

The beam was mounted in an aluminum frame and attached to an APS shaker as seen in Figure B.3. The aluminum frame had an additional K-Beam accelerometer attached to provide a measurement of the input motion. The sensitivity of the accelerometer was 499 mv/g with a maximum of 10 g's. Additionally, two Philtec Model D170 displacement probes were mounted to provide a measurement of the relative displacement of the beam. One was located at the center of the beam; the other varied. Only the results from the center probe are reported in this work. Its sensitivity was 125.33 μin/mV with a maximum of 0.1 in. for linear response. The center displacement signal was used in the feedback control laws implemented.

Vita

Gregory Agnes was born on June 8, 1967 in Baltimore, Maryland and is the first child of Stephen and Janet Agnes. Greg attended the Rensselear Polytechnic Institute on a U.S. Air Force 4-year scholarship where he received his Bachelor of Science in Aeronautical Engineering and was commissioned a 2nd Lt. in the U.S. Air Force in May, 1989. Greg received an educational delay to pursue a Master of Science in Aerospace Engineering which he received in August, 1991 with a thesis entitled: *Vibration Control of Composite Beams Through Strain Actuation and H_∞ Control Theory* and married Susan Carney of Rochelle Park, New Jersey. He then entered the active duty Air Force where he was stationed in the Structural Dynamics Branch of Wright Laboratory (now the Air Force Research Laboratory) in Dayton, Ohio. After a three year assignment and the birth of his daughter, Courtney Janet Agnes, Greg was selected to pursue a PhD. in Engineering Mechanics at Virginia Polytechnic Institute and State University under the watchful eye of Dr. Daniel J. Inman via the Air Force Civilian Institute Program. Upon receiving his PhD in 1997, he will pursue a follow-on assignment to the Air Force Institute of Technology in Dayton, Ohio as a faculty member.

Gregory S. Agnes